NORM FASTENERS
AR-GE MERKEZİ YAYINLARI
R&D CENTER PUBLICATIONS

2020

VOLUME 6

NORM
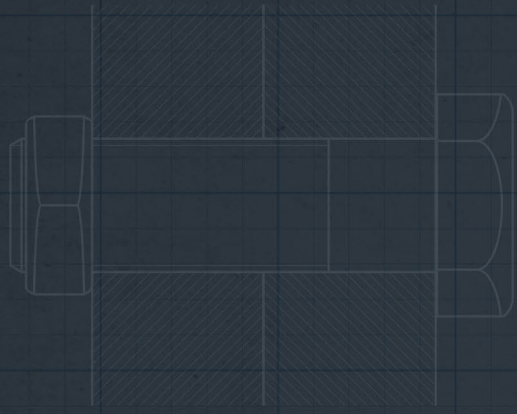FASTENERS

NORM FASTENERS
AR-GE MERKEZİ YAYINLARI
R&D CENTER PUBLICATIONS

FATIGUE LIFE PREDICTION MODEL OF WC-CO COLD FORGING DIES BASED ON EXPERIMENTAL AND NUMERICAL STUDIES

Barış TANRIKULU
Ramazan KARAKUZU
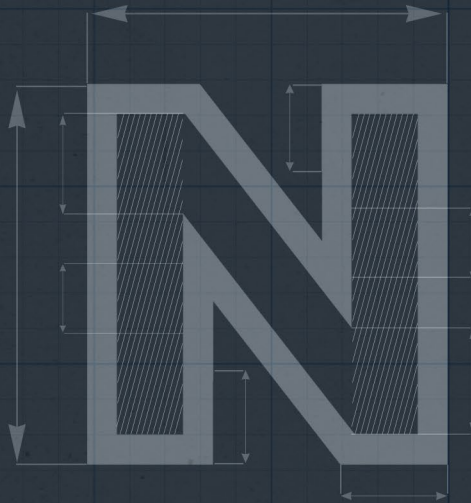
FATIGUE LIFE PREDICTION MODEL OF WC-Co COLD FORGING DIES BASED ON EXPERIMENTAL AND NUMERICAL STUDIES

*Baris Tanrikulu (a,b) *, Ramazan Karakuzu (c)*

(a) *Dokuz Eylül University, Graduate School of Natural and Applied Sciences, Izmir, Turkey*
(b) *Norm Civata San. ve Tic. A.Ş., A.O.S.B., Izmir, Turkey*
(c) *Dokuz Eylül University, Department of Mechanical Engineering, Izmir, Turkey*

https://orcid.org/0000-0001-8149-4871

Abstract

This study presents experimental and numerical studies to predict fatigue life of WC-Co 20% cold forging die. In order to determine the fatigue behavior of the material, three-point bending fatigue tests were performed and Morrow-Haigh diagrams were constructed. The analytical formulation was established by means of Basquin correlation obtained from the experimental results and die life was estimated according to the stress amplitude and mean stress values obtained from the finite element analysis. Verification of the analytical formulation was also carried out by obtaining the fatigue life cycle of the die from production line. The findings obtained showed that the life estimation method made the correct prediction with a deviation of 5.6%.

Keywords: *WC-Co, fatigue life, finite element analysis, three-point bending test*

1. Introduction

Cold forging is one of the most preferred production methods in fastener production. Particularly suitable for mass production, it provides a direct advantage over cost and is more economical compared to hot forging and other material processing methods like machining. Developments in the field of materials industry directly affect production efficiencies and more effective production options are emerging every day with a low-cost option. Technological studies in the field of materials has led to the production of dies used in cold forging industry from WC-Co material. High compressive strength, abrasion resistance and very low elastic deformation abilities directly affect the desired tolerance and the formability of the product. Tool life has always been an important research area in cold forging industry. The need for a reliable and easy-to-use prediction model for die life in the industry increases day by day due to productivity pressure. With the possibility of predicting fatigue-induced fractures, measures on the production line can be taken precisely before the failure of the tool. Due to the complex failure mechanics of cemented carbide material that is mainly used in die inserts, life prediction methods can vary widely. Nowadays, various studies are carried out on WC-Co materials produced by powder metallurgy. The cobalt content in the material and the dimensions of the Tungsten particles directly affect the mechanical properties of the material. Studies show that the cobalt content in WC-Co directly influences the brittle and ductile behavior of the material.

It has been determined that the tendency to ductility of the materials increases and the transverse fracture strength values decrease with the increase of cobalt ratio [1]. Although many studies have been carried out to examine the fracture behavior of WC-Co materials, two different approaches are generally considered; Llanes et al. [2] and Torres et al. [3] examined the behavior of WC-Co materials in terms of crack propagation and K factors. Schleinkofer et al. [4,5] examined the fatigue behavior of materials by means of S-N curves. The findings of both studies have concluded that the fracture mechanism has a complex structure and that the fatigue strength of the materials found to be very low compared to their static strengths.

Some of the studies on the mechanical behavior of WC-Co materials focus on the effect of particle size and microstructure. In the study of Klünsner et al. [6], the effects of microstructure on fatigue behavior were examined by subtracting the S-N curves and the inhomogeneity of the material microstructure was found to play an effective role at the early stage of fatigue fracture phenomena. In the studies that were carried out on the material characteristic in the microstructure of WC, the material exhibits ductile behavior if the grain size changes between 20 and 30 microns, brittle behavior in the case of lower particle sizes [7]. In the studies conducted on the mechanical behavior of WC-Co materials, it was found that the transverse fracture strength was an effective parameter for explaining the material behavior compared to the tensile and compression criteria, and standards were established for the detection of three-point and four-point transverse fracture strengths [8,9]. When the studies in the literature are examined, it has been seen that the transverse fracture strength is also taken as a reference for the understanding of the fatigue behavior of WC-Co materials. In the related study, the effects of different cobalt ratio and particle size of WC-Co materials on fatigue mechanism of the material were examined by considering transverse fracture strength and fatigue strength of the materials. It is concluded that transverse fracture strength is more dominant on the fatigue behavior of the material especially in low cobalt ratio while fracture toughness has a higher effect in high cobalt ratio [10]. The effect of surface treatment processes, which is another parameter affecting the mechanical properties of WC-Co materials, was examined by Yang et al. [11] and the effect of residual stress on the surface to transverse fracture strength was revealed. Similarly, in another study, the effects of grinding process with different grinding parameters on transverse rupture fatigue strength were investigated [12] .The findings show that micro-cracks and white layer formation on the surface during EDM processing of WC-Co die material have a significant effect on fatigue life [13,14]. Tanrikulu [15] also investigated the fatigue behavior of WC-Co material with a point of three point fatigue bending.

The use of high-strength special forging steels in the forging industry has led to an increase in the studies on die life. Many different approaches have been followed in these studies that aim to determine die life especially in forging processes. It was found that two main factors cause fatigue failure in forging die. First of all, it has been shown that the maximum stresses in the radius area change their direction under forging load from the compression to the tension and originate fracture [16]. In the studies on forging tools where the failure mechanism is mainly fatigue, researchers have carried out tests to prevent stress concentration in the radius areas that cause fracture and prevent early failures with design improvements [17]. Findings on tool failure also show that premature failure can be prevented with optimizing design stage of the forging operation which can cause stress concentration [18].

In the studies conducted to investigate tool failure, it was mentioned that pre-stressing operation has a serious effect on the die life and this factor should be taken into consideration in fatigue life calculations [19]. Shrink-fit operation can be described as the process of driving the inner core within a certain tolerance range into the outer die with a lower diameter which will cause additional pre-stresses on the die [20]. Different studies have been carried out in order to examine the effect of shrink fitting ratios and fatigue life of forging dies [21,22]. With the development of composite material technology, the studies on the effects of shrink fitting with carbon fiber material were also investigated [23]. High cycle fatigue life estimation using Basquin equation in tungsten carbide tool steels based on the workpiece material properties was also investigated. The findings shows that life obtained from Morrow equations were more realistic [24].

Falk et al. [25] studied the estimation of the service life of the cold forging dies by taking into account the parameters affecting the service life. In another study on the fatigue life of cold forging dies, the fatigue lives of four different die materials with different hardness values were compared with each other. As a result of the study, a theory has been developed to determine the life of cold forging dies by using material hardness and total strain parameters. Fatigue behavior of the materials was studied by using S-N curves and the life expectancy can be made by means of stress values.

In the present study, fatigue life of the cold forging die was estimated by using finite element method and analytical formulation which was obtained by experimental three-point bending tests results of coarse grain WC-Co 20%. In order to reflect better the surface conditions of the dies, three-point bending tests were carried out after grinding and polishing processes. The samples are prepared as b type samples with dimensions of 5.5 x 6.5 x 20 (width (h), depth (b), length, respectively) in mm according to the ISO 3327 standard [8]. Within the scope of the fatigue tests, three-point bending test system has been used and Goodman diagrams have been developed by obtaining Wöhler curves of materials at R=0.1 loading. Because of the compression load on the die after pre-stressing process used especially in forging dies, the fatigue curves were iterated to the compression zone after three-point bending tests and fatigue results and a better prediction mechanism was established. In the second section of the study, the forming and die analysis were carried out by using Simufact Forming software. Based on the maximum and minimum principle stress values obtained, the mean stresses (σm) and stress amplitudes (σa) were determined for cyclic stroke. Life estimation was realized by using improved Morrow diagram obtained by the experimental method and fatigue lives were compared with the data obtained from the production.

2. Material and Methods

2.1 Experimental procedure

In this study, Tungsten Carbide material with coarse grain size structures was used. The properties of the used cemented carbide material are given in Table 1 and microscopic examination of grain sizes is presented in Figure 1.

Table 1. Material catalogue values of coarse grain WC-Co 20% [26].

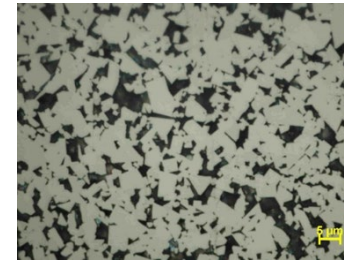| Material	Hardness (HV10)	Average Grain Size (μm)	Transvers Rupture Strength (MPa)	Fracture Toughness (MPa.m $^{1/2}$)
WC-Co 20% Coarse Grain	850	2.5-<6.0	2900	24.0

Figure 1. Microstructural investigation of WC-Co 20% coarse grain specimens in 150x magnification.

Grinding and polishing processes were carried out on the surfaces of the samples for better reflecting the die conditions. Paste with 5-15-30-60 μm values used in cold forging dies during polishing process were preferred for test specimens and polishing time of three minutes was applied to each surface with different paste values, so that the total polishing time was 12 minutes. The surface roughness values of the materials were measured after the polishing processes and the samples were obtained with the same surface conditions. Measured average surface roughness values and of the specimens are given in Table 2. Within the scope of material characterization tests, the transverse fracture strength and fatigue limits were determined by using a three-point bending test device with 16 mm support range. A schematic representation of the test device is given in Figure 2. All the stress values for the fatigue tests are summarized in Table 3. Mean stresses were chosen as 700 MPa, 750 MPa, 800 MPa and 850 MPa. Minimum-maximum stresses on the lower surface of the specimens were calculated by using formula given in Eq. 1 with the force values applied on the fatigue tests. Fatigue tests were performed by using Zwick Roell 250 kN testing machine with an average frequency of 85 Hz and a stress ratio (R=0.1) was used. As a result of the experimental tests, the number of cycles were obtained for different stress amplitudes and fatigue curves were drawn. SEM analyses were also performed on the fracture surface of the material and the failure phenomena were investigated.

Table 2. Surface roughness and standard deviation values of the specimens.

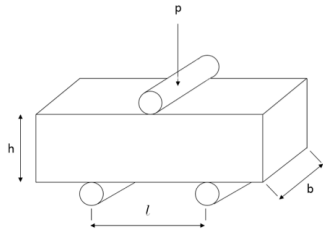| Material	Surface condition	Ra (μm)	Rz (μm)	Rq (μm)
WC-Co 20% Coarse Grain	Polished	0.06 (±0.02)	0.57 (±0.03)	0.08(±0.02)
WC-Co 20% Coarse Grain	Unpolished	0.73 (±0.04)	3.2 (±0.2)	0.9 (±0.04)

Figure 2. *Schematic representation of the three-point bending test.*

$$\text{Flexural Stress} = \frac{3.P.l}{2.b.h^2} \qquad (1)$$

Table 3. *Loading condition for fatigue testing.*

R ($\sigma_{min}/\sigma_{max}$)	P_m (kN)	P_a (kN)	σ_a (MPa)	σ_{min} (MPa)	σ_{max} (MPa)	σ_m (MPa)
0.1	7.8	6.3	850	188.9	1888.9	1038.9
0.1	7.3	6.0	800	177.8	1777.8	977.8
0.1	6.8	5.6	750	166.7	1666.7	916.7
0.1	6.4	5.2	700	155.6	1555.6	855.6

2.2. Finite element modelling

Within the scope of the numerical simulation studies, the forming simulation of the bolts was carried out by Simufact Forming finite element software. The required stage designs for the forming analyses were obtained by equalizing the volumes of material at each stage and the numerical simulation were carried out. Table 4 shows the chemical composition of 23MnB4 material, which was used as a bolt material according to the DIN EN 10263-4 standard [27].

Table 4. *Chemical composition of 23MnB4 (DIN EN 10263-4) [27].*

C%	Si%	Mn%	P%	S%	Cr%	Cu%	B%
0.20-0.25	0.30	0.90-.20	0.025	0.025	0.30	0.25	0.0008

Cold forming simulation was conducted with a hexahedral mesh structure and an element size of 0.3 mm in the forming analyses of the workpiece. For the die load analysis, tetrahedral mesh structure type was used with 102,030 elements for the insert and 25,581 elements for the shrink ring. With the realization of the forming process which is given in Figure 3, the die analysis was carried out and the effective plastic strain distribution of the last stage (ST4), which is expected to be critical for fatigue fracture, was obtained.

Tangential stress values on the die surface were read from the analysis results to obtain the mean stress and the stress amplitude values for the related process. Die analysis of the forging die, which is given in Figure 4, was carried out on the last stage stationary dies that is the most critical one for fatigue failure. The shrink fitting step is also included in the finite element model for better estimation. 0.5% shrink fitting between the core and the shrink ring was applied and the formation of compressive stress in the core region was ensured. Within the scope of the die analysis, the core material was chosen as WC-Co and the shrink ring material as H13 (DIN 1.2344). For meshing structure, tetrahedral mesh with element size 0.3 mm was used. The modulus of elasticity and Poisson's ratio were taken as 470 GPa and 0.27 for the WC-Co 20% material and 270 GPa and 0.29 for the H13 material, respectively.
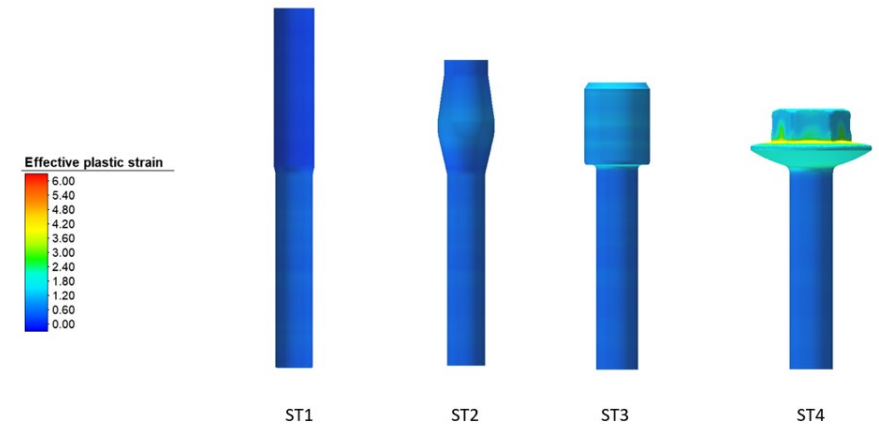
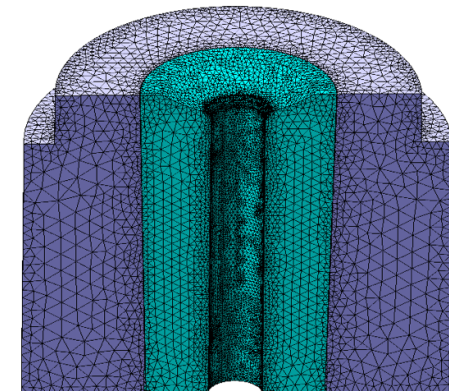**Figure 3.** *Cold forging simulation of the product.*

Figure 4. *Die model with insert and shrink ring in FEM.*

3. Results and Discussion

3.1. Fatigue tests and life maps

Fatigue tests were performed at a stress ratio value of R=0.1. Both polished and unpolished specimens were subjected to cyclic loading by using three-point bend test fixture. Fatigue lives obtained from fatigue tests are shown in Table 5 for different surface conditions and stress amplitudes. The representation of the results as S-N curves is given in Figure 5 in the form of log-log plot for polished and unpolished specimens. When the results obtained were examined, it was determined that the samples with polished coarse grain size were failed in longer cycle under same loading conditions. It is clearly seen from Table 5 and Figure 5 that polishing affects the number of cycles significantly until failure, as expected. So subsequent studies are carried out for only polished coarse grain WC-Co 20% specimens.

The stress amplitude vs mean stress diagram was drawn by using Morrow's equations in order to estimate the fatigue life. Due to the fact that fatigue tests could not be carried out at R=-1 stress ratio for the three point bend specimens , transverse fracture strength of the material was used instead of the ultimate tensile stress value of the Morrow graph. The lines of the life band were drawn in Figure 6 by using the number of fatigue cycles obtained. The life bands were obtained by fitting fatigue lifes and transverse rupture strength value, which are obtained by using stress amplitude and mean stress values. Morrow equation was also extended to the compression zone in order to adapt the obtained lines to the compression zone of the material. With the shrink fitting process in cold forging dies, a combined fatigue life map is needed due to the compressive stresses in the core material of WC-Co. As a result of the tests carried out with the samples passing through the same steps in the production stage of the cold forging dies, a means to predict the fatigue life of dies with the correlation of the experimental tests has been opened.

Table 5. Fatigue test results for polished and unpolished coarse grain WC-Co 20%.

Surface condition	R	σ_a (MPa)	Test 1 (cycle)	Test 2 (cycle)	Test 3 (cycle)	Test 4 (cycle)	Test 5 (cycle)	Mean (cycle)	STD
Unpolished	0.1	850	5084	7858	7143	6719	7192	7228	471
Unpolished	0.1	800	8439	7000	12651	8314	9373	9155	2129
Unpolished	0.1	750	11028	18706	29062	13451	17627	17975	6934
Unpolished	0.1	700	36734	31994	25778	29628	30931	31013	3969
Polished	0.1	850	36964	42295	32345	39830	41867	38660	4112
Polished	0.1	800	57933	75222	68394	71237	59608	66479	7466
Polished	0.1	750	97264	84367	204604	95937	136284	123691	49296
Polished	0.1	700	157945	203472	287613	187692	211731	209691	48157

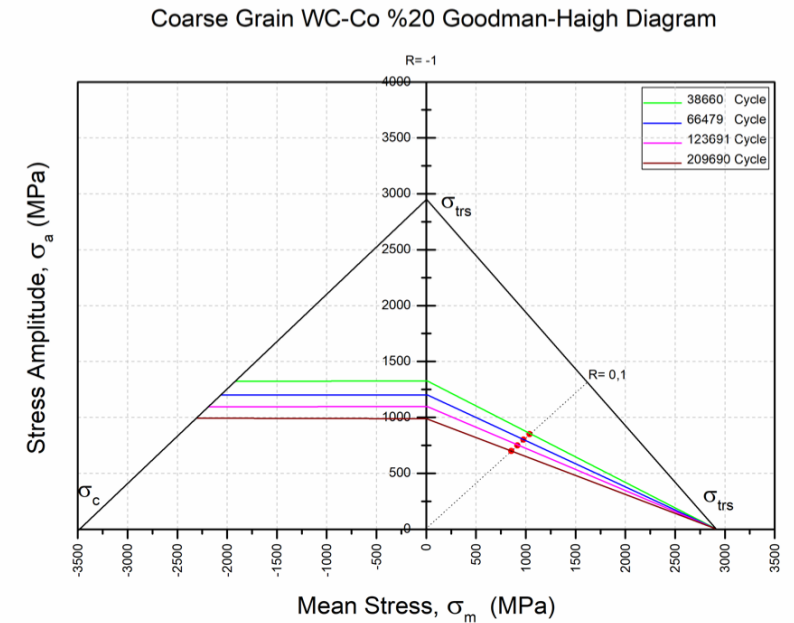*Figure 5. Fatigue test results of unpolished (a) and polished (b) coarse grain WC-Co 20% in log-log scale.*

Figure 6. Fatigue life map for experimental results of coarse grain polished WC-Co 20%.

Stress amplitude values for R = 0.1 loading ratio and for 1000; 10,000; 50,000; 100,000; 200,000; 400,000 and 1,000,000 cycles were calculated through the Basquin relation in the high and low cycle regions using fatigue data obtained for polished coarse-grained WC-Co 20% material from experimental studies. The values determined by Equation 1 were used for Morrow-Haigh diagram formation and linear fit was made based on the transverse fracture strength of the material. Thus, life bands were obtained and drawn (Figure 7). With the formation of the fatigue curves, the endurance limit of WC-Co 20% material in R = -1 loading condition was found to be 775 MPa. It has been seen from the literature that similar material endurance limit in fully reversed condition for 106 cycle shows a good agreement with obtained values. These findings show the consistency of the experimental results compared to literature [28].
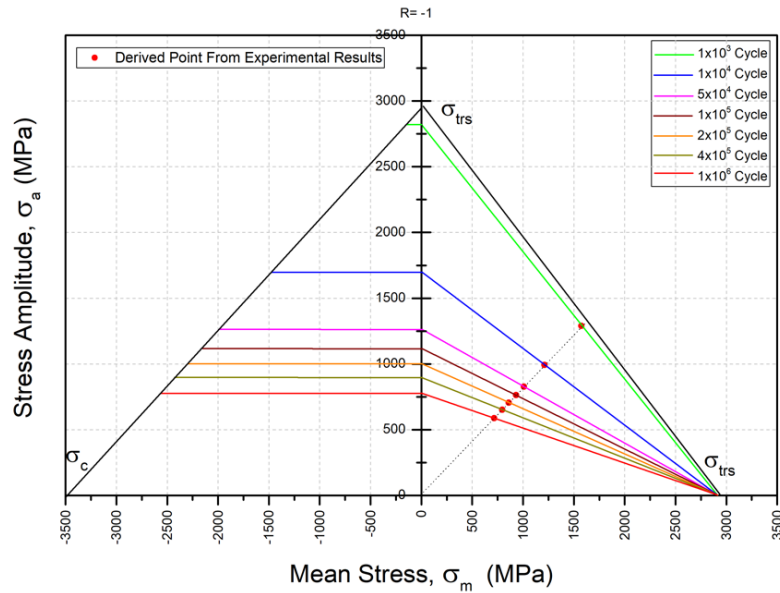
Figure 7. Generalized fatigue life map of coarse grain WC-Co 20%.

3.2. Finite element results

In order to make die life estimation, firstly, FEA studies were performed on the existing dies for obtaining σm and σa values. Due to the shrink fitting effect, tangential stresses have to be considered for a better estimation of the fatigue life [16]. From the results, tangential stress change on the critical section of the die in one stroke was taken into account and shown in Figure 8.
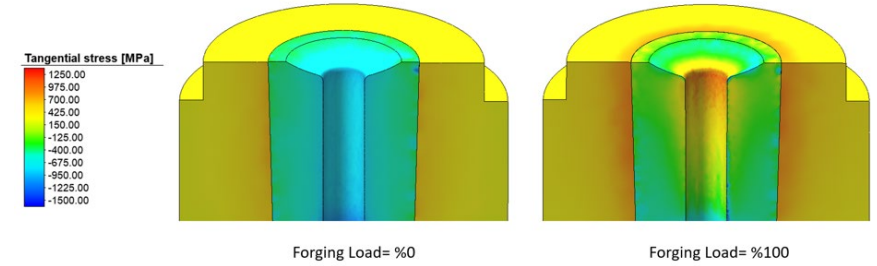
Figure 8. Tangential Stresses distribution before and after forging operation.

The stroke-based tangential stress change of the expected region of fracture is given in Figure 9. Stroke-based stress graphs were used to determine the mean stress and stress amplitude values for fatigue estimation. According to the FEA results stresses were obtained as σ_{max}=1122 MPa, σ_{min}= -954 MPa and σ_m= 84 MPa.
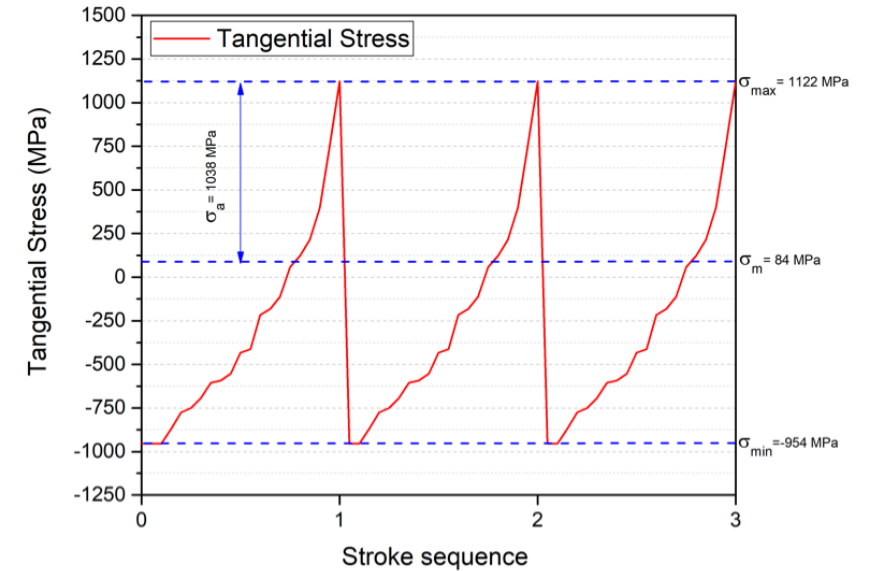
Figure 9. Stroke based tangential stress distribution in die surface.

3.3. Fatigue life prediction

With the help of generalized Morrow-Haigh diagrams plotted for WC-Co 20%, the life interval during which the die can work under current conditions was determined by placing the data obtained from the simulations on the graph in Figure 10. Accordingly, the life of the die under current conditions is between 100,000 and 200,000 cycles. In order to reduce the estimated value to a more specific range, firstly the mathematical relations given in Eq.2 are extracted. Accordingly, with the help of the Wöhler curve performed under the loading of R= 0.1, the approximate number of cycles of the die can be calculated with the known tensile amplitude and average stress value.
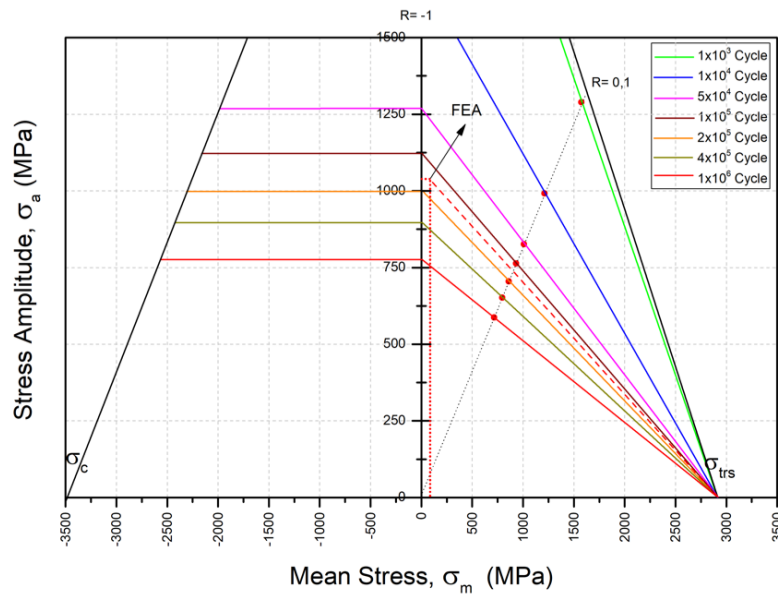
Figure 10. *Fatigue life estimation by using FEA data.*

$$\sigma_{m,R} = \frac{\sigma_{a,R}}{\sigma_{a,FEA}} \cdot (\sigma_{m,FEA} - 2900) + 2900 \tag{2}$$

$$\sigma_{a,R} = 0.8184\,(\sigma_{m,R}) \tag{3}$$

$$\sigma_{a,R} = \frac{2373.36 \cdot \sigma_{a,FEA}}{\sigma_{a,FEA} - 0.8184 \cdot (\sigma_{m,FEA} - 2900)} \tag{4}$$

$$\log N_f = 30.34 - 8.79\left[\log \sigma_{a,R}\right] \tag{5}$$

$$N_f = 10^{30.34 - 8.79 \cdot \left[\log\left(\frac{2373.36 \cdot \sigma_{a,FEA}}{\sigma_{a,FEA} - 0.8184 \cdot (\sigma_{m,FEA} - 2900)}\right)\right]} \tag{6}$$

Where; $\sigma_{a,FEA}$ and $\sigma_{m,FEA}$ are the stress amplitude and the mean stress calculated from the finite element analysis, respectively. $\sigma_{a,R}$ and $\sigma_{m,R}$ denote the stress amplitude and the mean stress values at R=0.1, respectively. R is the stress ratio and N_f is the number of cycles until failure. With the obtained correlation, it is possible to estimate the approximate life span by knowing σ_a and σ_m stress values of the die. An approximate life estimation system was obtained according to the stress values of WC-Co 20% dies that contain shrink fitting rings. Approximate life estimation of the forging die is obtained by placing FEA results in Equation 6. Accordingly, it is expected that the die that is simulated under current conditions will fail approximately in 136,719 cycles (Table 6). Table 7 shows the estimated fatigue lives of the forging die comparing with the values obtained from the production lines. Results shows a great accuracy with a difference around 5.60 %.

Table 6. *Mean stress, stress amplitude obtained from FEM and predicted fatigue life values.*

Mean Stress obtained from FEA (σ_m)	Stress Amplitude obtained from FEA (σ_a)	Fatigue life prediction through analytical formulation (N_f)
84 MPa	1038 MPa	136,719 Cycle

Considering that the loading curve (R=0.1) is the Wöhler curve obtained by the experimental results, the fatigue life equation can be obtained through the Basquin equation. With the examination of the Log-Log graph given in Figure 5, it is concluded that the fatigue life relation for the current loading condition can be described with Equation 2. To be able to use σ_a and σ_m stresses obtained from numerical simulations for fatigue estimation using fatigue life maps, it was determined that the FEA results should be adapted to the existing log-log equation obtained from the experimental study. In this context, mathematical equations are solved from the combination of the linear equation of the point obtained by numerical simulations and linear equation of the R= 0.1 curve and the following relations are obtained:

Table 7. *Estimated and measured fatigue life values.*

Forging die	Estimated cycle through FEA and analytical formulation	Production cycle until failure Die 1	Production cycle until failure Die 2	Production cycle until failure Die 3	Average die life (cycle)	Difference %
Die Life	136,719	124,854	132,735	130,798	129,462	5,60

Fractographical examination was also conducted on the fractured specimens by using SEM. Figure 11 (a) and (b) shows clearly the crack path on the specimens. It is also clearly identified that failure is in intergranular mode and Tungsten particles were also fractured during fatigue loading conditions.
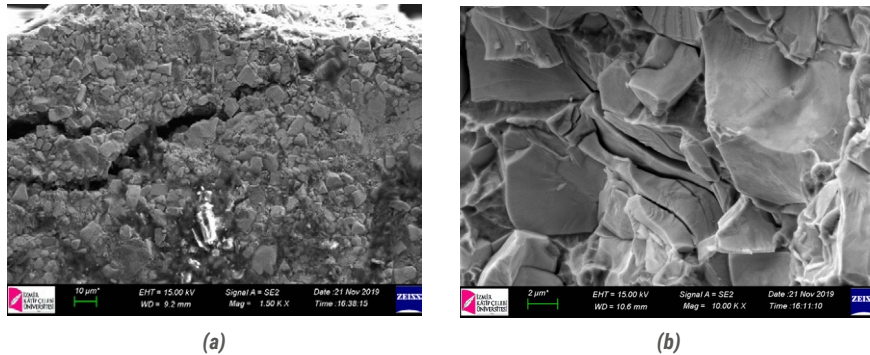

(a)   *(b)*

Figure 11. *SEM analyses on fractured coarse grain WC-Co 20% specimens (a) 1.50 KX (b) 10.00 KX.*

4. Conclusions

Within the scope of the study, an analytical formulation was obtained for predicting the service life of WC-Co 20% dies which contain shrink fitting process with the help of finite element analysis. For obtaining the analytical formulation, three point bending fatigue test values were used and it was found that experimentally obtained fatigue test results showed good agreement with the literature [28]. In order to determine the accuracy of the study, the dies were simulated numerically and life predictions made from analytical formulation were compared with the results obtained from the production line. The comparison shows that very close findings were obtained. According to the findings, the die life of the analytical formulation used with the FEA results was around 5.60% higher than that of the production line. These findings show that the analytical formulation based on the experimental data obtained from the three point bending test can be used for die life prediction. For a better reliability and precise prediction of the analytical formulation, different type forging dies has to be investigated and die life comparison should be made.
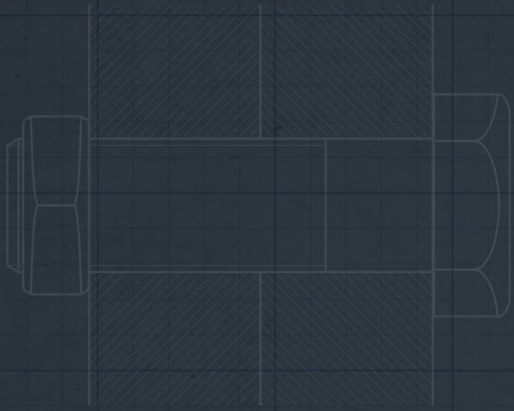
Acknowledgements

References

[1]   J.A.M. Ferreira, M.A.P. Amaral, F.V. Antunes, J.D.M. Costa, A study on the mechanical behaviour of WC/Co hardmetals, Int. J. Refract. Met. Hard Mater. 27 (2009) 1–8. doi:10.1016/j.ijrmhm.2008.01.013.

[2]   L. Llanes, Y. Torres, M. Anglada, On the fatigue crack growth behavior of WC–Co cemented carbides: kinetics description, microstructural effects and fatigue sensitivity, Acta Mater. 50 (2002) 2381–2393. doi:10.1016/S1359-6454(02)00071-X.

[3]   Y. Torres, M. Anglada, L. Llanes, Fatigue mechanics of WC–Co cemented carbides, Int. J. Refract. Met. Hard Mater. 19 (2001) 341–348. doi:10.1016/S0263-4368(01)00032-4.

[4]   U. Schleinkofer, H.-G. Sockel, K. Go¨rting, W. Heinrich, Fatigue of hard metals and cermets, Mater. Sci. Eng. A. 209 (1996) 313–317. doi:10.1016/0921-5093(95)10106-3.

[5]   U. Schleinkofer, H.-G. Sockel, K. Go¨rting, W. Heinrich, Microstructural processes during subcritical crack growth in hard metals and cermets under cyclic loads, Mater. Sci. Eng. A. 209 (1996) 103–110. doi:10.1016/0921-5093(95)10098-9.

[6]   T. Klünsner, S. Marsoner, R. Ebner, R. Pippan, J. Glätzle, A. Püschel, Effect of microstructure on fatigue properties of WC-Co hard metals, Procedia Eng. 2 (2010) 2001–2010. doi:10.1016/j.proeng.2010.03.215.

[7]   S. Okamoto, Y. Nakazono, K. Otsuka, Y. Shimoitani, J. Takada, Mechanical properties of WC/Co cemented carbide with larger WC grain size, Mater. Charact. 55 (2005) 281–287. doi:10.1016/j.matchar.2005.06.001.

[8]   ISO 3327:2009-Hardmetals - Determination of transverse rupture strength, 2009.

[9]   ASTM B406 - 96(2015)-Standard test method for transverse rupture strength of cemented carbides, 2015.

[10] A. Li, J. Zhao, D. Wang, X. Gao, H. Tang, Three-point bending fatigue behavior of WC–Co cemented carbides, Mater. Des. 45 (2013) 271–278. doi:10.1016/j. matdes.2012.08.075.

[11] J. Yang, M. Odén, M.P.P. Johansson-Jõesaar, L. Llanes, Grinding Effects on Surfac Integrity and Mechanical Strength of WC-Co Cemented Carbides, Procedia CIRP. 13 (2014) 257–263. doi:10.1016/j.procir.2014.04.044.

[12] J. Kawahara, S. Mori, K. Osakada, Surface finishing process and fatigue life of carbide tools, in: 46th Int. Cold Forg. Gr. Plenary Meet. Int. Cold Forg. Gr., 2013.

[13] D. Kanagarajan, P. Sivaraj, M. Seeman, R. Seetharaman, Evaluation of the reliability on WC-40%Co composites through Weibull analysis, Mater. Today Proc. 22 (2020) 519–524. doi:10.1016/j.matpr.2019.08.124.

[14] M.B. Toparli, S. Yurtdas, C. Kılıçaslan, White layer formation during edm cutting and fatigue performance of WC / CO cermet materials, (2019) 4–6.

[15] B. Tanrıkulu, Fatigue life of tungsten cobalt carbide used as a core material in cold forging dies, Dokuz Eylül University, 2016.

[16] M. Knoerr, K. Lange, T. Altan, Fatigue failure of cold forging tooling: causes and possible solutions through fatigue analysis, J. Mater. Process. Technol. 46 (1994) 57–71. doi:10.1016/0924-0136(94)90102-3.

[17] M.B. Toparli, Determination of effective failure mechanism to improve tool life of cold forging dies, Uludağ Univ. J. Fac. Eng. 24 (2019) 157–172. doi:10.17482/ uumfd.507586.

[18] S. Yurtdas, M.B. Toparli, B. Tanrikulu, T. Yavuzbarut, Numerical modeling coupled design studies to increase forging die & tool life of m8x21 . 5 hexagonal headed special bolts, in: Int. Conf. Mater. Sci. Mech. Automot. Eng. Technol. Cappadocia, 2019: pp. 23–25.

[19] T. Ørts Pedersen, Numerical modelling of cyclic plasticity and fatigue damage in cold-forging tools, Int. J. Mech. Sci. 42 (2000) 799–818. doi:10.1016/S0020-7403(99)00019-3.

[20] H.C. Lee, M.A. Saroosh, J.H. Song, Y.T. Im, The effect of shrink fitting ratios on tool life in bolt forming processes, J. Mater. Process. Technol. 209 (2009) 3766–3775. doi:10.1016/j.jmatprotec.2008.08.032.

[21] C. Wang, H. Kam, X. Wang, Determination of optimal shrink fitting ratio for 2-layer compound forging die by ımproving fatigue life in backward extrusion, Procedia Eng. 207 (2017) 2215–2220. doi:10.1016/j.proeng.2017.10.984.

[22] C. Wang, H. Kam, X. Wang, Determination of shrink fitting ratio to improve fatigue life of 2-layer compound forging die by considering elasto-plastic deformation of outer ring, Procedia Manuf. 15 (2018) 481–487. doi:10.1016/j.promfg.2018.07.256.

[23] S. Yurtdaş, U. İnce, C. Kılıçaslan, H. Yıldız, A case study for improving tool life in cold forging: Carbon fiber composite reinforced dies, Res. Eng. Struct. Mater. 3 (2016) 64–75. doi:10.17515/resm2016.24me2902.

[24] M.A. Saroosh, H.-C. Lee, Y.-T. Im, S.-W. Choi, D.-L. Lee, High cycle fatigue life prediction of cold forging tools based on workpiece material property, J. Mater. Process. Technol. 191 (2007) 178–181. doi:10.1016/j.jmatprotec.2007.03.015.

[25] B. Falk, U. Engel, M. Geiger, Fundamental aspects for the evaluation of the fatigue behaviour of cold forging tools, J. Mater. Process. Technol. 119 (2001) 158–164. doi:10.1016/S0924-0136(01)00934-7.

[26] Ceratizit, Hard material solutions by ceratizit, (2015) 16–20. https://www.ceratizit.com/en/products/wear-protection/list/detail/product-detail/forging-technology/ (accessed March 8, 2020).

[27] DIN EN 10263-4 Steel rod, bars and wire for cold heading and cold extrusion - Part 4: Technical delivery conditions for steels for quenching and tempering, (2002).

[28] A.B. Kotas, H. Danninger, B. Weiss, K. Mingard, J. Sanchez, L. Llanes, Fatigue testing and properties of hardmetals in the gigacycle range, Int. J. Refract. Met. Hard Mater. 62 (2017) 183–191. doi:10.1016/j.ijrmhm.2016.07.004.
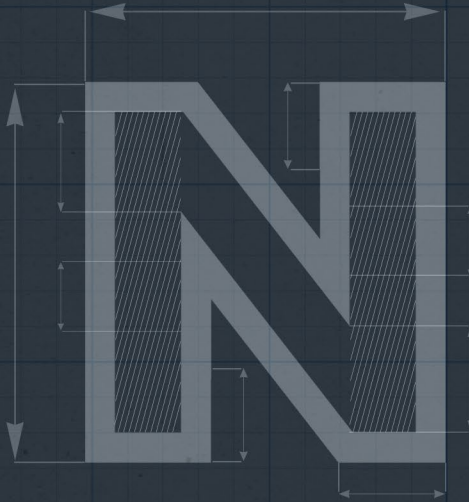
A NEW ANALYTICAL MODEL TO ESTIMATE MAXIMUM INTERNAL SOCKET DEPTH OF NON-REDUCED STRENGTH BOLTS

Fatih KOCATÜRK

M. Burak TOPARLI

Barış TANRIKULU

Umut İNCE

Cenk KILIÇASLAN
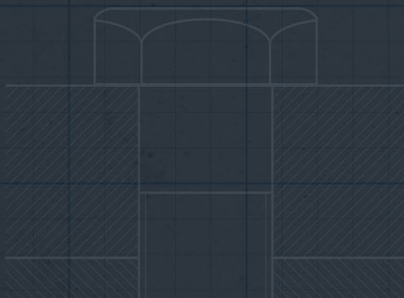
A NEW ANALYTICAL MODEL TO ESTIMATE MAXIMUM INTERNAL SOCKET DEPTH OF NON-REDUCED STRENGTH BOLTS

Fatih Kocatürk (a,b), M. Burak Toparli (a), Barış Tanrıkulu (a,c), Umut İnce (a), Cenk Kılıçaslan(a),

(a) *Norm Cıvata R&D Center, Norm Cıvata San. ve Tic. A.Ş., A.O.S.B., Çiğli, İzmir, Turkey*
(b) *Graduate School, Applied Mathematics and Statistics, İzmir University of Economics, İzmir, Turkey*
(c) *The Graduate School of Natural and Applied Sciences, Dokuz Eylül University, İzmir, Turkey*

Abstract

In this study, an analytical model for calculation of the maximum socket depth of bolts having shaft diameter smaller than socket diameter was introduced. A representative bolt was chosen and maximum socket depth satisfying the minimum ultimate tensile strength was calculated by the developed analytical model. The analytical findings were also compared with numerical simulations for validation. Numerical studies were carried out by using Simufact.forming finite element software. The maximum socket depth estimated by using the developed analytical model was in good agreement with the numerical results. The obtained critical socket depth through the analytical model was 1.4% safer compared to numerical simulation results. Therefore, it was concluded that the developed analytical model could be used to estimate the critical socket depths of bolts having shaft diameter smaller than socket diameter.

Keywords: Fracture (mathematical); Failure criterion; Structural integrity; Mechanical testing; Finite element modelling; Metal forming; Industrial applications

1. Introduction

Bolts, or fasteners, are one of most widely used engineering products used to assemble two or more components. Depending on the application, bolts are produced in various size, shape and grade which are effective on the mechanical behaviour. Considering service conditions, the factors that have to be considered in evaluating the strength of a threaded fastener were explained in (Bickford, 1998). Tensile loading, shear loading, torsional loading as well as combined loading were analysed in detail for threaded fasteners.

Nomenclature

α	the angle under the line passing through the end of socket and tip of socket
φ	the angle formed between the fracture pattern and the vertical line passing from point p
τ_B	the torsional strength
A_S	the nominal cross sectional area of the bolt thread
A_{Sch}	the surface area of the fracture cone formed in the head
d_m	the minimum socket diameter
d_{Sch}	the shaft diameter
f	difference between d_{Sch} and d_m
l_i	the equation of the ith line
m	slope of a line
m_i	the slope of the i'th line
R	the radius of the head
R_m	the tensile strength
R_{mred}	the resultant of the tensile stress ($R_m.\sin \varphi$) and the shear stress ($\tau_B.\cos \varphi$) acting on the fracture cone
t	sum of d_{Sch} and d_m
x	apsis of the fracture point p
x^*	the strength ratio
y	ordinate of the fracture point p
y^*	sum of y_{min} and the radius R
y_{min}	the minimum distance between the end of the socket and the bottom of the head

In addition to loading conditions, there are different features of fasteners having strong impact on failure mechanism and service life. For instance, the effect of socket depth on failure types of fasteners was investigated in (Tanrıkulu et al., 2018). In this study, experimental studies on cold forged bolts having various socket depths were carried out and torque-tension tests were conducted to reveal the effects of critical socket depth under different loading types. It was observed that the socket depth has significant influence on failure mechanism of fasteners. M8x1.25x50 Full Thread (FT) bolts with 10.9 and 8.8 grade were examined to determine the effect of socket depth for the purpose of weight reduction in (Tanrıkulu et al., 2019), as a continuation of the study of (Tanrıkulu et al., 2018). In order to determine the critical socket depth; i.e. the highest weight reduction, Finite Element (FE) simulations and experimental torque-tension tests were performed for the type of fastener being investigated. One of the analytical models used to estimate socket depth introduced in the literature by (Thomala and Kloos, 2007) was also used to compare the results obtained from numerical and empirical studies.

There exist studies concerning the failure modes of bolt and nut assemblies in the literature. The failure modes of bolt and nut assemblies under tension can be divided into three groups: bolt fracture, bolt thread failure, and nut thread failure. Using partially threaded bolt rather than fully threaded in connections could increase the possibility of thread failure (Grimsmo et al., 2016). Thread failure of the bolt-nut assemblies subjected to tension is generally undesirable since it is a less ductile failure mode than the bolt fracture (fracture of the threaded shaft of the bolt). Therefore, investigation of the causes of thread failure is important and the effect of the length of the threaded bolt shaft located within the grip was examined in (Grimsmo et al., 2016). The fatigue damage assessments of the M10 bolted joint made of 42CrMo4 heat treatable steel and grade 10.9 were performed in (Novoselac et al., 2014) for variable preload forces and variable amplitude eccentric forces for high reliability. Preload forces of 0%, 50%, 70% and 90% of force at bolt yield point were used to make assessments. In order to define the material cyclic scatter band having Gaussian normal distribution in logarithmic scales, range of dispersion was used. The multiaxial fatigue stress criterion based on a critical plane theory for fatigue damage assessment was applied to obtain the multiaxial stress field with high notch effect in thread root. The critical plane approach was used to estimate fatigue damage and fatigue fracture plane position. The fatigue life of the bolts is usually calculated using the nominal approach applied under normal loads, but this method is

insufficient for multiaxial loads. To this end, an effective method for calculating fatigue-induced damage to bolts was developed by improving the Schneider's method (Sorg et al., 2017).

Experimental studies to investigate the mechanical performance of high-strength 8.8 grade bolts under tensile load were conducted in (Hu et al., 2016). As a result of tests, it was observed that the failure of structural bolts occurred in two different ways: stripping on the thread and necking in the threaded portion of the bolt shaft. The fracture behaviour of 42CrMo ultrahigh strength steel-based bolt was investigated experimentally in (Hongfei et al., 2019) by performing macroscopic and microscopic fracture observation, metallographic test, mechanical property test and energy spectrum analysis. The results showed that a large amount of structural defect, such as sulphur inclusions, band and carbon depletion, appears in the fracture origin region and matrix of the bolt. Such defects reduced the fatigue strength of materials and led to fatigue failures. In the study performed by (Hedayat et al., 2017) for the prediction of bolt fracture in shear when threads are excluded from the shear plane, finite element methods were divided into two main categories in order to determine the appropriate failure criteria: i) Monitoring the level of stress and strain at the critical elements of the bolt shaft, ii) Describing crack initiation and crack formation.

The tensile state of bolts and nuts with ISO metric thread design was examined and optimized in (Pedersen, 2013). The maximum tension in the bolt was located in the fillet under the head, at the beginning of the thread or at the thread root. To minimize the stress concentration, shape optimization was applied. In this context, first the fillet under the head, nut thread design and the fillet in the shaft and thread transition region were optimized and 25.3%, 15.8% and 34% stress reductions were achieved, respectively. These design improvements, which lead to the reduction of stress in the bolt, was also observed to reduce the hardness of the bolt. Threaded fasteners are expected to fracture from the thread region under service loads. (ISO 898-1, 2004) standard dictates certain tensile strengths and bolts are expected to fracture from the thread region. The depth of the internal socket form at head of bolts is very crucial since it is one of the most important design parameters affecting the structural integrity of bolts, i.e. depending on the depth, the failure mode of bolts can mitigate from thread root to under head region. However, in some cases, it is known that the bolts are also fractured from the head region due to the bolt design required for specific applications, and this type of bolts must satisfy the minimum ultimate tensile strength given in (ISO 898-1, 2004) under tension loading.

Considering failure mechanisms of the bolts, the fracture cone formed under the bottom of the socket and the under head region was analysed in (Thomala and Kloos, 2007) for the bolts having shaft diameter larger than socket diameter. An analytical model was introduced to calculate the minimum height between the bottom of the socket and the head, i.e. the socket depth. The proposed model is valid for the case shaft diameter is greater than or equal to the socket diameter of the bolts with internal socket form.
Eq. (1) was derived by (Thomala and Kloos, 2007) and referenced in VDI 2230 standard to estimate critical socket depth for bolts having shaft diameter greater than the socket diameter:

$$y_{min} = \frac{\sqrt{16A_S^2 - \pi^2 (d_{Sch}^2 - d_m^2)^2}}{2.x^*.\pi.(d_{Sch} + d_m)} \tag{1}$$

where A_S is the nominal shaft cross-sectional area, d_{Sch} is the shaft diameter, d_m is the average socket diameter, $x^* = \frac{\tau_B}{R_m}$ is the strength ratio and τ_B is the torsional strength, R_m is the tensile strength (see Fig. 1).

In addition to bolt type investigated in Eq. (1), bolts having shaft diameter smaller than socket diameter are also preferred for certain applications, and there was no study in the literature on this type of bolts. In this study, analytical and numerical works were carried out on bolts having shaft diameter smaller than socket diameter. An analytical model was developed to estimate the maximum socket depth of bolts having shaft diameter smaller than socket diameter. For the sake of validation, a representative bolt geometry was chosen and FE model was constructed to compare the critical socket depth estimated by the analytical model.
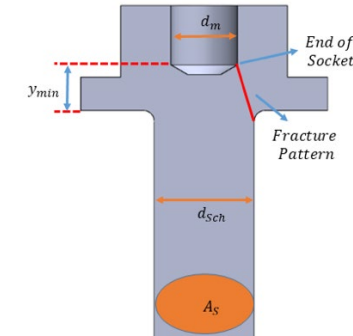
Figure 1. *Schematic of bolt having shaft diameter greater than the socket diameter.*

2. Sample specification

In this study, M8 bolt with 1.25 thread pitch and 23 mm shaft length was chosen as the representative sample. Bolt with N10 socket form and satisfying the mechanical requirements for 8.8 grade as given in (ISO 898-1, 2004) was modelled by using Simufact.forming finite element software. The material was 23MnB4, i.e. one of the most widely preferred low alloy steel in cold forging.

3. Socket depth estimation for bolts having shaft diameter smaller than socket diameter

3.1. Analytical modelling

Analytical Modelling studies were initiated by investigating Eq. (1) in detail, which is valid for the case of bolts having shaft diameter greater than the socket diameter. The minimum distance between the end of the socket and the bottom of the head, y_min, can be found in Eq. (1). The y_{min} value is called as the residual floor thickness and measured with the relation y_{min}=k-s for an inbus bolt where the head height is k and the socket depth is s shown in Fig. 2.

When the shaft diameter is greater than the socket diameter, the fracture pattern is expected to be formed between the bottom of head and the end of the socket (see Fig. 1). However, when the shaft diameter is smaller than the socket diameter, the fracture pattern was formed between the bottom of head and a point p, which is located between the end of the socket and the tip of the socket based on the experiences in production (see Fig. 2).

The two-dimensional bolt cross section is shown in Fig. 3 to locate the break point, p_1, required to calculate the surface area of the fracture cone. The local origin of the cross sectional area, (0,0) is selected as shown in Fig. 4. Then, p_1=(x,y) is obtained as follows:

Let us call the line passing through p_1 and p_2 as l_1 and the line passing through p_1 and p_3 as l_2.

• First, the equation of the line l_1 is found by using the slope of the line, m_1=tanα, and the point p_2= ($\frac{d_m}{2}$, y_{min}+R) in Eq. (3). The equation of a line can be found given that a point, A=(x_0,y_0), on the line and its slope, m, is known by using Eq. (2).

$$y - y_0 = m.(x - x_0) \tag{2}$$

If m=m_1 and A=p_2 are put in Eq. (3), the equation of the line l_1 in Eq. (4) is obtained.

$$y = \tan\alpha.\left(x - \frac{d_m}{2}\right) + (y_{min} + R) \tag{3}$$
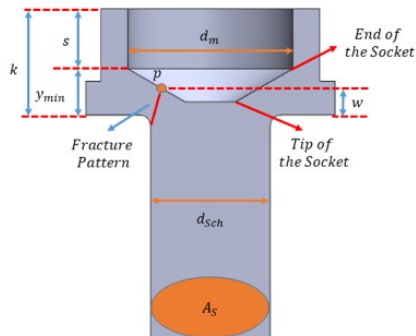
Figure 2. Schematic of bolt having shaft diameter smaller than the socket diameter.
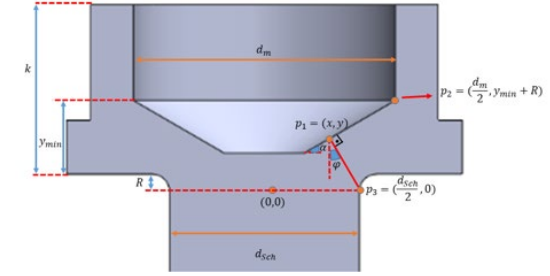
Figure 3. Bolt cross section in the coordinate system.

• Then, the equation of the line l_2 is found by using the slope of the line, and the point p_3=($\frac{d_{Sch}}{2}$,0) in Eq. (4). The slope of the line l_2 can be found by using the fact that the slopes of perpendicular lines are opposite reciprocals, i.e., if the slopes of two perpendicular lines (l_1 and l_2) are multiplied, the value -1 is obtained.

$$y = -\cot\alpha.\left(x - \frac{d_{Sch}}{2}\right) \tag{4}$$

• Finally, the intersection point, p_1=(x,y), of the lines l_1 and l_2 can be found by substituting Eq. (4) in Eq. (3) as follows:

$$-\cot\alpha.\left(x - \frac{d_{Sch}}{2}\right) = \tan\alpha.\left(x - \frac{d_m}{2}\right) + (y_{min} + R)$$

$$x.(\tan\alpha + \cot\alpha) = \frac{\cot\alpha.d_{Sch}}{2} + \frac{\tan\alpha.d_m}{2} - (y_{min} + R)$$

If tanα=$\frac{sin\alpha}{cos\alpha}$ and cotα=$\frac{cos\alpha}{sin\alpha}$ are substituted in the above equation, the x coordinate of the point p_1 is obtained. From now on, the equations t=d_{Sch}+d_m, f=d_{Sch}-d_m and y*=y_{min}+R will be used to simplify notation, where d_m is the minimum socket diameter, d_{Sch} is the shaft diameter, R is the radius of the head, and y_{min} is the min residual floor thickness.

$$x = \frac{\cos\alpha^2.f - \sin 2\alpha.y^* + d_m}{2} \tag{5}$$

If x given in Eq. (5) is substituted into the equation of the line l_1, y coordinate of the point p_1 is obtained.

$$y = \frac{\tan\alpha}{2}.(\cos\alpha^2 f - \sin 2\alpha.y^*) + y^* \tag{6}$$

When the fracture pattern is rotated by 360 degrees around the shaft, the fracture cone is obtained (see Fig. 4). In order to find the minimum residual floor thickness, the maximum stress acting on the fracture cone in the head and the maximum tensile stress acting on the thread are compared. When the following condition is met, the head of the bolt assumed to satisfy the minimum ultimate tensile load defined in (ISO 898-1, 2004).

$$R_{mred}.A_{Sch} > R_m.A_S \tag{7}$$

where R_{mred} is the resultant of the tensile stress ($R_m.\sin\varphi$) and the shear stress ($\tau_B.\cos\varphi$), A_{Sch} is the surface area of the fracture cone formed in the head, R_m is the tensile stress acting on the thread and A_S is the nominal cross sectional area of the bolt thread (Fig. 2). The strength ratio of the bolts, x*, is represented in the literature as $x* = \frac{T_B}{R_m}$ and this coefficient varies according to the grade of the bolt given in (ISO 898-1, 2004). The total stress acting on the fracture cone is calculated as follows (Thomala and Kloos, 2007).

$$R_{mred} = \sqrt{(R_m.\sin\varphi)^2 + (\tau_B.\cos\varphi)^2} \tag{8}$$

By substituting $\tau_B = x*.R_m$ into the Eq. (8), the following equation is obtained.

$$R_{mred} = R_m.\sqrt{\sin\varphi^2 + x*^2 \cos\varphi^2} \tag{9}$$

If the fracture cone surface area given in Fig. 4(a), A_{Sch}, is cut straight along a certain fracture line to make it two-dimensional, a trapezoid is obtained. The resulting trapezoid is given in Fig. 4 (b).

When the values given in the formula of the trapezoid area are fulfilled, the following equation that calculates the surface area of the fracture cone is obtained:

$$A_{Sch} = \pi.(x + \frac{d_{Sch}}{2}).\frac{y}{\cos\varphi} \tag{10}$$

If x and y in Eq. (10) are substituted, the following equation is obtained:

$$A_{Sch} = \pi.(\frac{\cos\alpha^2.f - \sin 2\alpha.y*+d_m}{2} + \frac{d_{Sch}}{2}).\frac{\frac{\tan\alpha}{2}.(\cos\alpha^2.f - \sin 2\alpha.y*)+y*}{\cos\varphi} \tag{11}$$

If Eq. (9) and (11) are substituted in Eq. (7), the following equation is obtained:

$$R_m.\sqrt{\sin\varphi^2 + x*^2 \cos\varphi^2}.\pi.(\frac{\cos\alpha^2.f - \sin 2\alpha.y*+d_m}{2} + \frac{d_{Sch}}{2}).\frac{\frac{\tan\alpha}{2}.(\cos\alpha^2.f - \sin 2\alpha.y*)+y*}{\cos\varphi} > R_m.A_S$$

The following equation is obtained after some simplifications:

$$(\cos\alpha^2.f - \sin 2\alpha.y*+t) > \frac{2.A_S.\cos\varphi}{\pi.\sqrt{\sin\varphi^2+x*^2\cos\varphi^2}.(\frac{\tan\alpha}{2}.(\cos\alpha^2.f - \sin 2\alpha.y*)+y*)} \tag{12}$$
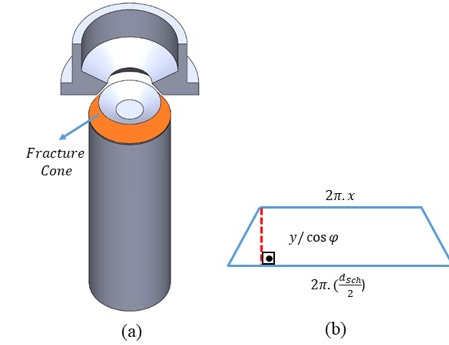
Figure 4. *(a) Schematic representation of fracture cone and (b) two-dimensional fracture cone surface area.*

Here, if the dividend and denominator of the right-hand side of the Eq. (12) are simplified by taking parenthesis of $\frac{1}{x.\cos\varphi}$ on the right hand side of the equation, Eq. (13) is obtained:

$$(\cos\alpha^2.f - \sin 2\alpha.y*+t) > \frac{2.A_S}{x*.\pi.\sqrt{(\frac{\tan\varphi}{x*})^2+1}.(\frac{\tan\alpha}{2}.(\cos\alpha^2.f - \sin 2\alpha.y*)+y*)} \tag{13}$$

$$\tan\varphi = \frac{\frac{d_{Sch}}{2}-x}{y} = \frac{\frac{d_{Sch}}{2} - \frac{\cos\alpha^2.f - \sin 2\alpha.y*+d_m}{2}}{\frac{\tan\alpha}{2}.(\cos\alpha^2.f - \sin 2\alpha.y*)+y*} = \frac{\sin\alpha^2.f+\sin 2\alpha.y*}{\sin\alpha.\cos\alpha.f+2\cos\alpha^2.y*} \tag{14}$$

$\tan\varphi$ defined in Eq. (14) is substituted in Eq. (13) and the mathematical formula Eq. (15) is obtained after the mathematical operations such as cross-multiplication and square root.

$$y_{min} = \frac{-\sqrt{\frac{1}{\pi}.\cos\alpha^4(\pi.f^2-16.A_S.\sqrt{\frac{1-\cos\alpha^2}{x*^2.\cos\alpha^2-\cos\alpha^2+1}}+\pi.t^2+2.\pi.t.f)-\cos\alpha^2.f+2.\cos\alpha^4.f+\cos\alpha^2.t}}{4.\cos\alpha^3.\sin\alpha} - R \tag{15}$$

The resulting Eq. (15) also takes into account the radius of the head to shaft transition region to calculate the maximum socket depth. In order to test the model derived in Eq. (15), the sample specified in Section 2 was used with the following parameters: d_{Sch}=7.10 mm; d_m=8.31 mm; R=0.63 mm; x*=0.65; A_S=36.60. Socket diameter, d_m, was selected as the minimum diameter corresponding to N10 socket form.

3.2. Numerical modelling

Numerical analyses were carried out by using Simufact.forming software. Initially, a FE model was prepared based on the analytical formulation derived in the previous section. In this model, stresses were intended to be compared between head region and thread region, as compared in Eq. (8). To determine the critical socket depth, a linear and full-elastic model was created as shown in Fig. 5. Loading was applied by a rigid plate attached from the bottom of the bolt. Bolts were loaded in tension so that the stresses at the thread root or under head region reaches to around 640 MPa, the plastic deformation limit of 8.8 grade bolts as defined in (ISO 898-1, 2004). The critical socket depth was estimated for the case in which the stresses at the thread root and under head region were similar. The elastic constants, Elastic Modulus (E) and Poisson's ratio (v), were taken as 210 GPa and 0.292, respectively. The element size of 0.5 mm for tetrahedral element type were used for numerical analysis. The numerical model used in this study was given in Fig. 5.
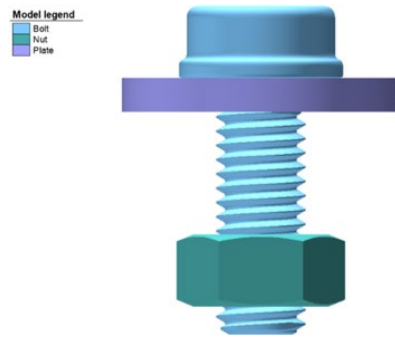
Figure 5. *FE Model to find y$_{min}$.*

4. Results and discussion

Numerical analysis were repeated for different socket depths and the results were presented in Fig. 6. Effective (Von-Mises) stresses were compared at the thread region and at the fracture cone region to assess the crack initiation site i.e. failure location. Higher stresses were expected at the thread region for standard bolts, since failure from the thread implies that the design of the investigated bolt is suitable for the tested assembly conditions. Similar approach was employed in this study to assess the critical socket depth of the investigated bolt. For a detailed statistical study, 10 measurements were recorded from under head and thread root regions for the bolts with y values of 2.10 to 3.10 mm. The maximum, minimum and average effective stress results were plotted in Fig. 6. The rectangular boxes in the plots represents measurements falling in one standard deviation. Based on the effective stresses presented Fig. 6, stresses were observed to be higher at the thread region for the y values higher than 3.10 mm. Likewise, the stresses were higher at the head radius compared to thread region for the y values lower than 2.45 mm. According to FE modelling, the y_min was found as around 2,78 mm considering the box plots given in Fig. 6.
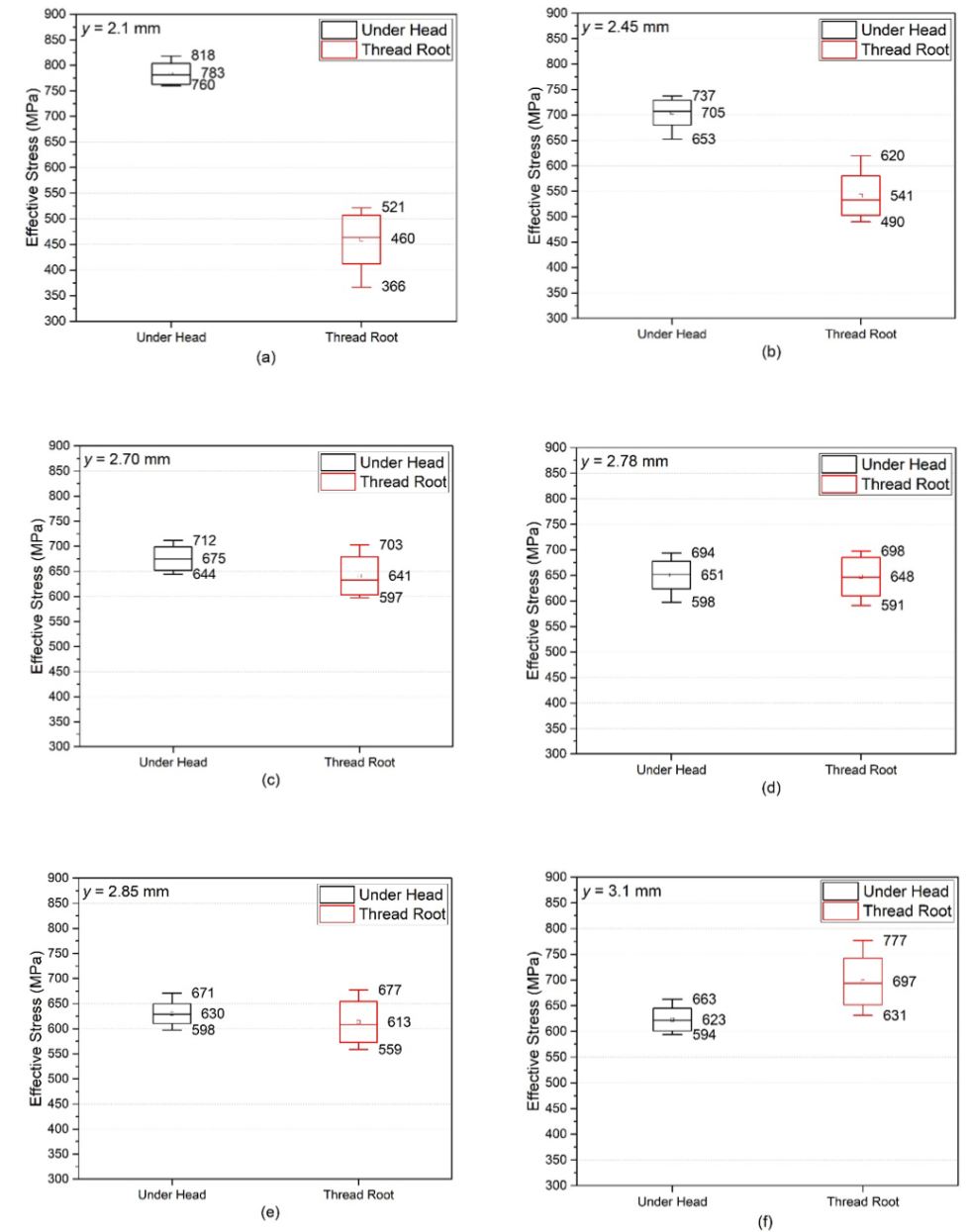
Figure 6. *Effective stress obtained from the under head and thread root region for bolts having y values (a) 2.10, (b) 2.45, (c) 2.70, (d) 2.78, (e) 2.85 and (f) 3.10.*

The y_{min} value of the investigated bolt was found as 2.82 mm and y value of point p_1 given in Fig. 3 was calculated as 2.33 mm by employing the analytical model developed in this study. The y_{min} value was found as around 2.78 mm from the numerical modelling. Analytical model estimated the socket depth on the safe side, i.e. socket depth value estimated by analytical model was higher compared to numerical modelling results. When analytical and FE modelling results were considered, the analytical model estimated the y_{min} value about 1.4% safer compared to FE modelling results. Therefore, the agreement between analytical and numerical modelling approaches can be considered as very good.

5. Conclusions

In this study, an analytical model was developed to estimate maximum socket depth of the bolts having smaller shaft diameter than socket diameter. The results of the model were validated through FE modelling studies. The critical socket depth i.e. y_{min} value obtained by analytical model was 1.4% safer compared to numerical studies. Therefore, it can be concluded that the analytical model developed in this study can be used to estimate the critical socket depth of the bolts having shaft diameter smaller than socket diameter. Maximum weight reduction for the bolts having smaller shaft diameter than socket diameter can be achieved by increasing the socket depth i.e. decreasing the y value of the investigated bolt by using the analytical model developed in this study. Analytical model developed in the scope of this study will also be verified with experimental studies by producing cold forged bolts with various socket depths and conducting tensile test for these bolts.
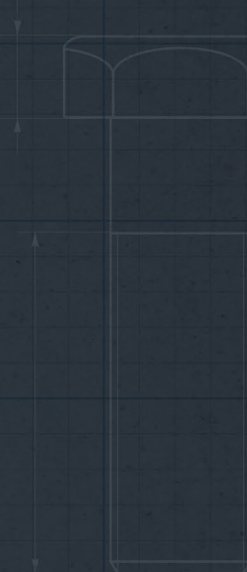
References

[1]   Bickford, J., 1998. Handbook of Bolts and Bolted Joints, 1st ed, Handbook of Bolts and Bolted Joints. CRC Press, Boca Raton. https://doi.org/10.1201/9781482273786

[2]   Grimsmo, E.L., Aalberg, A., Langseth, M., Clausen, A.H., 2016. Failure modes of bolt and nut assemblies under tensile loading. J. Constr. Steel Res. 126, 15–25. https://doi.org/10.1016/j.jcsr.2016.06.023

[3]   Hedayat, A.A., Afzadi, E.A., Iranpour, A., 2017. Prediction of the Bolt Fracture in Shear Using Finite Element Method. Structures 12, 188–210. https://doi.org/10.1016/j. istruc.2017.09.005

[4]   Hongfei, G., Yan, J., Zhang, R., He, Z., Zhao, Z., Qu, T., Wan, M., Liu, J., Li, C., 2019. Failure Analysis on 42CrMo Steel Bolt Fracture. Adv. Mater. Sci. Eng. 2019, 1–8. https://doi. org/10.1155/2019/2382759

[5]   Hu, Y., Shen, L., Nie, S., Yang, B., Sha, W., 2016. FE simulation and experimental tests of high-strength structural bolts under tension. J. Constr. Steel Res. 126, 174–186. https://doi.org/10.1016/j.jcsr.2016.07.021

[6]   ISO 898-1, 2004. Mechanical Properties of Fasteners Made of Carbon Steel and Alloy Steel.

[7]   Novoselac, S., Kozak, D., Ergić, T., Damjanović, D., 2014. Fatigue damage assessment of bolted joint under different preload. Struct. Integr. Life 14, 93–109.

[8]   Pedersen, N.L., 2013. Overall bolt stress optimization. J. Strain Anal. Eng. Des. 48, 155–165. https://doi.org/10.1177/0309324712470233

[9]   Sorg, A., Utzinger, J., Seufert, B., Oechsner, M., 2017. Fatigue life estimation of screws under multiaxial loading using a local approach. Int. J. Fatigue 104, 43–51. https://doi.org/10.1016/j.ijfatigue.2017.06.034

[10]   Tanrıkulu, B., Toparli, M.B., Kılınçdemir, E., Yurtdaş, S., İnce, U., 2019. Determination of the critical socket depths of 10.9 and 8.8 grade M8 bolts with hexagonal socket form. Eng. Fail. Anal. 104, 568–577. https://doi.org/10.1016/j.engfailanal.2019.06.064

[11]   Tanrıkulu, B., Toparli, M.B., Kılınçdemir, E., Yurtdaş, S., İnce, U., 2018. Effect of socket depth on failure type of fasteners. Procedia Struct. Integr. 13, 1840–1844. https://doi.org/10.1016/j.prostr.2018.12.331

[12]   Thomala, W., Kloos, K.-H. (Eds.), 2007. Tragfähigkeit von Schraubenverbindungen bei mechanischer Beanspruchung, in: Schraubenverbindungen. Springer Berlin Heidelberg, Berlin, Heidelberg, pp. 135–208. https://doi.org/10.1007/978-3-540-68470-1_5

LOOSENING BEHAVIOR OF RIPPED NUTS BASED ON THE FASTENER TIGHTENING STRATEGY AND PLATE HARDNESS

Barış TANRIKULU
Sezgin YURTDAŞ
M. Burak TOPARLI
Cenk KILIÇASLAN
Umut İNCE

LOOSENING BEHAVIOR OF RIPPED NUTS BASED ON THE FASTENER TIGHTENING STRATEGY AND PLATE HARDNESS

Barış Tanrıkulu (a,b)*, Sezgin Yurtdaş (a,c), M. Burak Toparli (a), Cenk Kılıçaslan (a), Umut İnce (a),

(a) *Norm Cıvata R&D Center, Norm Cıvata San. ve Tic. A.Ş., A.O.S.B., Çiğli, İzmir, Turkey*
(b) *The Graduate School of Natural and Applied Science, Dokuz Eylul University, Izmir, Turkey*
(c) *Mechanical Engineering Department, Katip Çelebi University Izmır,Turkey*

Abstract

Within the scope of this study, loosening behavior under vibration was investigated depending on the plate hardness, clamp length and tightening strategy of M8x1.25 10.9 quality nuts with rip form under flange. Two different plate hardness were used and two different types of tightening strategy, i.e. application of torque to either from bolt head or nut, were carried out by using bolts with 29 mm and 40 mm clamp length. During tightening, the effects created by rips on the plate were examined. A parametric study was also carried out to understand loosening behavior of fasteners depending on the plate hardness. Based on the experimental study, it was shown that plate hardness, clamp length and tightening strategy played a key role on the loosening behavior of fasteners. To decrease the loosening rate of the assembly on softer plate, nut with rip form should be tightened from the bolt element. However, for harder plates the selection of tightening strategy was less significant compared to that of softer plate.

Keywords: Fastener; Loosening; Vibration; Ripped Nut; Tightening strategy

1. Introduction

Fasteners are often preferred in many areas due to their easy-use and practicality. However, as a result of vibration loads acting on fasteners due to environmental conditions, the problem of loosening is often encountered. In particular, depending on the vibration load to which the fasteners are exposed, a decrease in the locking loads took place over time. The identification of the loosening mechanism and the development of the experimental test system which was known as "Junker test bench" was carried out by Junker in 1969. According to Junker, one of the most important causes of loosening problem in fasteners was vibration which acts in the lateral direction (Junker, 1969). With the emergence of the loosening effect, studies mostly focused on finding the factors affecting the loosening mechanism. A parametric study was conducted by Sanclamente and Hess (Sanclemente and Hess, 2007) which mainly focused on factors such as locking load, thread pitch, elasticity module and lubrication. According to the results obtained from the Junker test bench, the most important factor was found as locking load in case of exposure to vibration in the lateral direction. As a result of theoretical and experimental studies carried out, a mathematical model of the loosening phenomena was developed. The findings obtained as a result of the verification of the mathematical model revealed that the locking load and the thread-under head friction coefficients directly affects the loosening mechanism (Nassar and Yang, 2009). Studies in this area have

increased for investigating the effect of local slips on the loosening performance. Especially in the studies carried out to determine the critical local slip threshold, a numerical simulation model was established and supported by experimental studies (Dinger and Friedrich, 2011). The findings showed that the head geometry of the fastener had also an effect on the loosening behavior. The effect of the head angle was examined by investigating the loosening behavior of the countersunk head bolts (Yang et al., 2011).

Due to the detrimental effects of loosening mechanism and its difficulty to predict, some of the studies were focused on solutions that would directly prevent loosening. Especially, by using different types of fasteners, it has been tried to minimize the loosening effect. In one of the studies conducted in this area, the effects of different washer combinations on the loosening rate were investigated. The findings showed that chemical locking and plastic patch solutions provided more vibration resistance than different washer types (Bhattacharya et al., 2010). Some studies based on the secondary locking feature also showed that Heli-Coil with Loctite application had the ability to maintain the preload loss in a desired average value (Cheatham et al., 2009). Double Nut tightening and spring washer effects on loosening evaluation was investigated with the use of numerical methods. Results showed that with the correct preload application, double nut combination performed better vibration resistance compared to spring washer combination (Izumi et al., 2009). Another study carried out in this area was the design of bolts with a special thread profile providing loosening resistance (Sase et al., 1998).

Studies based on finding the critical slippage values were also conducted. It has been determined that if the fasteners are subjected to a displacement below the critical slippage value, loosening phenomena did not occur (Nishimura et al., 2007).

Especially in the studies carried out to prevent the loosening event, many different additional elements were used to slow down or prevent the loosening evaluation. In our study, the effects of DIN 6923 nuts on loosening process assembled with plates having appropriate combination and hardness values were investigated without the need for an additional element. Thus, it was revealed that the loosening behavior can be seriously affected depending on the tightening strategy and the hardness of the assembled area.

Studies have also been conducted to compare the vibration performances of locking washer combinations frequently used in aviation industry. Accordingly, it has been determined that plain washers give the worst performance. It was also determined that the hardness values of the washer affects the loosening resistance (Hess et al., 2014).

Nomenclature

HV   Hardness Vickers
B   position of
C   further nomenclature continues down the page inside the text box

2. Material and Methods

2.1. Test sample specifications

In this study conducted to compare the loosening behavior of fasteners, M8 x 1.25 x 50 8.8 DIN 933 bolts and M8x1.25 8 grade DIN 6923 with rip form and without rip nuts were used. Images of all 3 fasteners are given in Figure 1. 23MnB4 material was chosen as the material of bolts and nuts and all the fasteners were heat treated for 8.8 and 8 grade, respectively. All nuts and bolts were covered with Delta Protect KL100 VH301GZ coating, and the friction coefficient values, one of the important factor affecting loosening, were kept as around 0.12. Assembly plates preferred in this experimental study were used in two different hardness values, i.e. 175 HV and 300 HV. Thus, the effects of the nut rip form on the plate surface depending on hardness values were examined. Drawing and image of one of the plates are given in Figure 3.

Figure 1. Technical drawings of DIN 933 bolt and DIN 6923 Nuts with and without rip form.

Figure 2. Technical drawing and sample photo of plates used in junker vibration test.

2.2. Experimental procedure and setups

Within the scope of the experimental study, tests were carried out to examine the effect of tightening strategy, clamp length and plate hardness. During the tests, two different strategies were used as tightening the fastener from the nut or bolt head. The test plan given in Table 1 was created by combining plate hardness, tightening strategies and clamp length values for the Junker vibration tests. Results were averaged by performing 5 repetitions for each test combination so that total of 45 experimental tests were performed. The schematic representation of the Junker test device where loosening tests were performed is given in Figure 3.

Table 1. *Experimental test combinations.*

Experimental test	Plate Hardness	Nut Type	Tightening Strategy	Clamp Length
Set 1	175 HV	Rip Nut	Bolt Head	29 mm
Set 2	175 HV	Rip Nut	Nut Head	29 mm
Set 3	175 HV	Plain Nut	Nut Head	29 mm
Set 4	175 HV	Rip Nut	Bolt Head	40 mm
Set 5	175 HV	Rip Nut	Nut Head	40 mm
Set 6	175 HV	Plain Nut	Nut Head	40 mm
Set 7	300 HV	Rip Nut	Bolt Head	40 mm
Set 8	300 HV	Rip Nut	Nut Head	40 mm
Set 9	300 HV	Plain Nut	Nut Head	40 mm

Figure 3. *Representation of the Junker test machine.*

3. Results and Discussion

As a result of the performed Junker vibration tests, clamp load-cycle graphs of each combination were drawn and a comparison was made between loosening rates. Accordingly, for 29 mm clamp length, it was found that the loosening rate of the flat nut was the highest among the other two combination. The effect of tightening strategies was revealed in DIN 6923 nuts with a rip form under the flange. Accordingly, it was found that fastening from bolt head provides better vibration resistance compared to fastening from nut side. The reason for this behavior was explained by the rip form of the nut as deforming the plate. The results and comparisons of the tests performed for combinations with 29 mm locking length and 175 HV plate hardness are given in Figure 5.
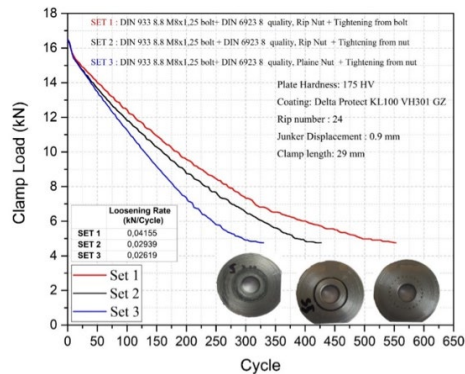

Figure 5. Junker test result of 175 HV plate with 29 mm clamp length.

One of the most important factors affecting the loosening resistance of fasteners is the clamp length. For this reason, tests were repeated with bolts having 40 mm clamp length and plates with 175 HV hardness. In this way, the loosening resistance between tightening strategies could be revealed based on the clamp length. Accordingly, the experimental studies showed that the order of the loosening rate of different tightening strategies was the same. However, the effect of the tightening strategies was more obvious, i.e. the difference in loosening rates were higher (Figure 6).
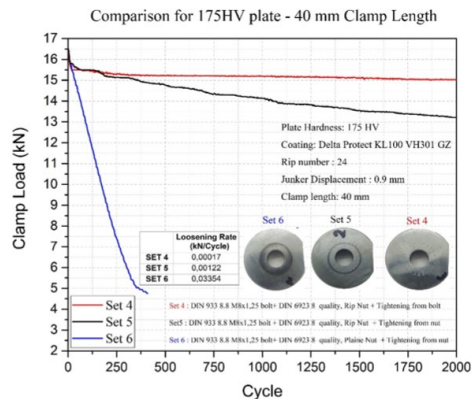

Figure 6. Junker test result of 175 HV plate with 40 mm clamp length.

In the third set of the experimental study, tests were carried out by using plates with 300 HV hardness and bolts with 40 mm clamp length. Results on 300 HV hardness values showed that loosening resistance decreases with the increase of the hardness value (Figure 7). Accordingly, with the comparison of the test results performed with plates having 300 HV and 175 HV hardness for 40 mm clamp length, it was determined that the loosening resistance decreased with the increase of plate hardness (Figure 8). This situation was determined to be due to the reduction of the deformation created by the rip form on the plate surface. Tightening method had a direct effect on the amount of deformation on the plate. Images containing the deformation shapes on the plate surface as a result of the tests are given in Figure 9. It was revealed that when the connection is tightened from the bolt head, the rip form under the flange deformed the plates and contributed to increase in vibration resistance, since the nut was directly exposed to axial load.
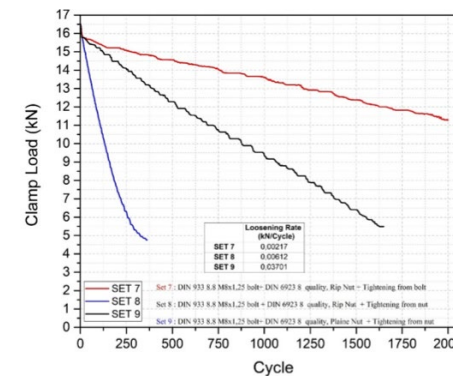

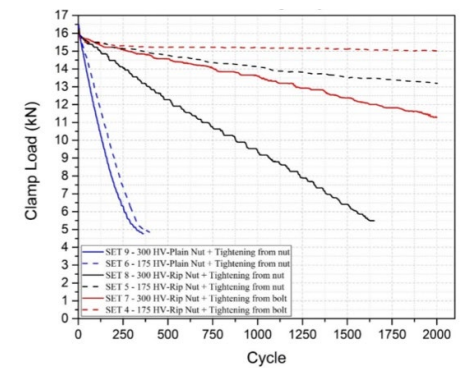**Figure 7.** Junker test result of 300 HV plate with 40 mm clamp length.

Figure 8. Comparison of Junker test result of 175 HV and 300 HV plate with 40 mm clamp length.

Figure 9. Plate deformation caused by rip form during different tightening strategies.

Loosening rate values given in Table 2 were obtained by linear fitting the loosening curves. With the use of loosening rate values, loosening behaviours can be easily compared among each sets. It was revealed that when the torque process was performed from the nut with rip form, the rip form caused deformation on the material surface in the form of a channel due to the axial load effect combined with the rotation of the nut. This feature prevented the nut from giving the actual vibration performance, although it provided resistance to vibration compared to the plain nut. As the plate hardness was increased, it was observed that the nut rip forms could not cause enough deformation on the plate surface, and there was a loss of vibration resistance. However, even if a reduction in vibration resistance is observed, the effect of the tightening strategy had the similar effect on the loosening resistance.

Table 2. Loosening Rate values of test combinations.

Experimental test	Plate Hardness	Nut Type	Tightening Strategy	Clamp Length	Loosening rates (kN / Cycle)
Set 1	175 HV	Rip Nut	Bolt Head	29 mm	0.04155
Set 2	175 HV	Rip Nut	Nut Head	29 mm	0.02939
Set 3	175 HV	Plain Nut	Nut Head	29 mm	0.02619
Set 4	175 HV	Rip Nut	Bolt Head	40 mm	0.00017
Set 5	175 HV	Rip Nut	Nut Head	40 mm	0.00122
Set 6	175 HV	Plain Nut	Nut Head	40 mm	0.03354
Set 7	300 HV	Rip Nut	Bolt Head	40 mm	0.00217
Set 8	300 HV	Rip Nut	Nut Head	40 mm	0.00612
Set 9	300 HV	Plain Nut	Nut Head	40 mm	0.03701

4. Conclusion

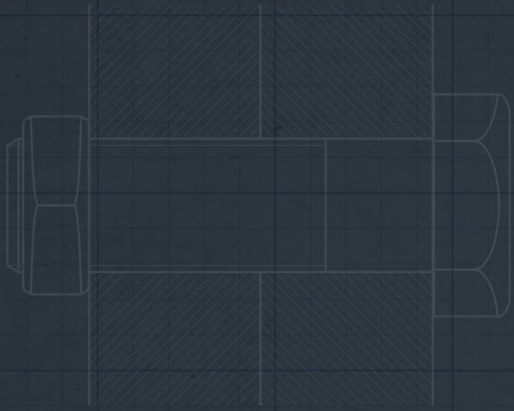Based on the experimental studies conducted in this study, following conclusions can be drawn:

1. Considering experimental test result, tightening strategy has a major effect on the loosening behavior of ripped nuts. Tightening from bolt side increases the loosening resistance of the assembly by causing plastic deformation on the plate with the rip form of the nut. However, when tightening is performed by the rip shaped nut, the deformation on the plate is in the form of a channel leading to decrease in the loosening resistance. Among the two tightening strategy and plain nut combination the best performance was obtained by tightening from bolt side, tightening from nut side, and plain nut respectively.

2. Although the tightening strategy has a major effect, the plate hardness and the clamp length also play a key role on the loosening performance. With the increase of hardness values of the plate, the ability of the rips to cause plastic deformation decrease. Thus situation decreases the loosening resistance. As the clamp length increases, loosening rate decreases, as observed in this experimental work.

3. Studies for a mathematical model based on different hardness values of nuts and plates for a loosening behavior prediction will be investigated.

References

[1] Bhattacharya, A., Sen, A., Das, S., 2010. An investigation on the anti-loosening characteristics of threaded fasteners under vibratory conditions. Mech. Mach. Theory. https://doi.org/10.1016/j.mechmachtheory.2008.08.004

[2] Cheatham, C.A., Acosta, C.F., Hess, D.P., 2009. Tests and analysis of secondary locking features in threaded inserts. Eng. Fail. Anal. https://doi.org/10.1016/j.engfailanal.2008.01.001

[3] Dinger, G., Friedrich, C., 2011. Avoiding self-loosening failure of bolted joints with numerical assessment of local contact state. Eng. Fail. Anal. https://doi.org/10.1016/j.engfailanal.2011.07.012

[4] Izumi, S., Yokoyama, T., Kimura, M., Sakai, S., 2009. Loosening-resistance evaluation of double-nut tightening method and spring washer by three-dimensional finite element analysis. Eng. Fail. Anal. https://doi.org/10.1016/j.engfailanal.2008.09.027

[5] Junker, G.H., 1969. New Criteria for Self-Loosening of Fasteners Under Vibration. https://doi.org/10.4271/690055

[6] Nassar, S.A., Yang, X., 2009. A Mathematical Model for Vibration-Induced Loosening of Preloaded Threaded Fasteners. J. Vib. Acoust. https://doi.org/10.1115/1.2981165

[7] Sanclemente, J.A.A., Hess, D.P.P., 2007. Parametric study of threaded fastener loosening due to cyclic transverse loads. Eng. Fail. Anal. 14, 239–249. https://doi.org/10.1016/j.engfailanal.2005.10.016

[8] Sase, N., Nishioka, K., Koga, S., Fujii, H., 1998. An anti-loosening screw-fastener innovation and its evaluation, Journal of Materials Processing Technology.

[9] Yang, X., Nassar, S.A., Wu, Z., 2011. Criterion for Preventing Self-Loosening of Preloaded Cap Screws Under Transverse Cyclic Excitation. J. Vib. Acoust. https://doi.org/10.1115/1.4003596
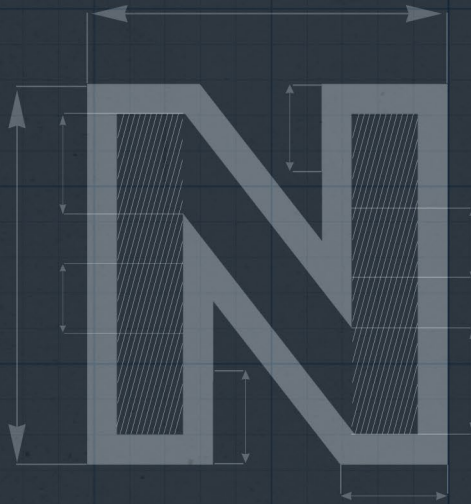
GEOMETRICAL OPTIMIZATION FOR A COLD EXTRUSION PROCESS

Sezgin YURTDAŞ
Levent AYDIN
Cenk KILIÇASLAN
H.İrem ERTEN

GEOMETRICAL OPTIMIZATION FOR A COLD EXTRUSION PROCESS

Sezgin Yurtdas (a), Levent Aydin (b), Cenk Kılıçaslan (c), H. Irem Erten (d)

(a) *Norm Cıvata San. ve Tic. A.Ş., A.O.S.B., İzmir, Turkey,* **sezgin.yurtdas@normcivata.com**
(b) *İzmir Katip Çelebi University, Department of Mechanical Engineering, İzmir, Turkey,* **leventaydinn@gmail.com**
(c) *Norm Cıvata San. ve Tic. A.Ş., A.O.S.B., İzmir, Turkey,* **cenk.kilicaslan@normcivata.com**
(d) *İzmir Katip Çelebi University, Department of Mechanical Engineering, İzmir, Turkey,* **erteniremm@gmail.com**

Abstract

In this chapter, extrusion die geometry prepared for bolt production is considered, and for this die, the die design conditions that provide minimum extrusion force requirement was determined. The primary objective is to obtain the minimum extrusion force by establishing the relationship between the inputs as three main parameters (extrusion angle, temperature and friction coefficient) and the output (extrusion force) in the extrusion die to form the workpiece. In light of these objectives, numerical analyzes were performed in simufact.forming a finite element software program for the determined parameters, and data were obtained. Then, different regression models were created through a commercial software Mathematica based on neuro-regression approach. Besides, the accuracy of the constructed models has been checked through $R^2_{training}$ and $R^2_{testing}$ values. After testing the reliability of the models, and to optimize the input parameters that minimize the output also, stochastic methods, which are Differential Evolution (DE), Random Search (RS) and Simulated Annealing(SA), and a deterministic one Nelder-Mead were used in Mathematica. As a result, it can be approached the optimum solution in a slight difference with the current sensitivity.

Keywords: *Cold Extrusion, Cold Forging, Stochastic Optimization, Extrusion Force, Neuro-Regression Modelling*

Introduction

In fastening applications, the majority of fasteners are produced by using the cold forming procedure. These fasteners are generally generated in multi-stage processes by cold forging, pressure forging, and reducing or a combination of all procedures [1-3].

Cold forging, which is a type of metal forming process used in a broad spectrum of applications, from electronics to automotive and medical devices manufacturing, permits high-speed mass production with excellent mechanical properties in several applications. It is also proper for pieces which have excellent concentricity, narrow geometrical tolerances, smooth surface finish, and near net shape [1-3].

In designing of the cold forging manufacturing processes, the forging process can be regarded as a complicated system which contains implicit interactions between the workpiece, forging force, temperature, forging die, tool and press influenced by environmental and tribological conditions. Therefore, it is a necessity to consider systematic design methods such as engineering optimization techniques. Engineering optimization is the matter which use optimization techniques to obtain the best design and performance evaluation in engineering systems as soon as possible. Hence, there are several optimization studies which are related to cold forging [1-3]. For instance, Han and Hua [4] studied on the contact pressure response in metal forming technology of cold rotary forging. They purposed to use finite element (FE) methods to find out the contact pressure response in a complex cold rotary forging. For cold rotary forging, a 3D FE model is improved, and then, the contact pressure is calculated. As a result, the process parameters' effect on the contact pressure response is revealed. Krusic et al. [5] investigated the stochastic nature for typical cold forging processes. They applied finite element computations on forwarding rod extrusion, closed-die forging, free upsetting, and retractile extrusion to examine the influence of Scatter's key process input parameters on the dimensional accuracy of products. The results show that for the four typical cold forging processes, stochastic interactions diverge and press stiffness has a significant effect on the stochastic relationships. Composite cold forging refers to the processing of hybrid raw parts at the same time by cold forging. Ossenkemper et al. [6] aimed to produce composite components by joining them with plastic deformation, and they manufactured composite shafts by forwarding rod extrusion of backward extruded steel cups. An analytical model has been improved to find the strength of the force of composite shafts which are generated by cold forging operation and push-out tests were done to identify the bond strength for the proposed model.

Finally, they decided that calculated bond strengths were appropriate in accordance with the experimental values. In the world, approximate twenty different tribological tests have been suggested for the friction coefficients' empirical definition in the cold forging processes. Groche et al. [7] compared six test principles by using identical tribological systems, and they observed large differences between the empirically determined friction coefficients. For process parameters design, Zhu et al. [8] proposed a multi-objective optimization method by using response surface methodology (RSM) approach and Latin hypercube design method in order to check product forming quality. As a result of this study, after conducting radial forging and experimental study, which is related to the mechanical property on the forming product, the feasibility of the multi-objective optimization method for product forming quality was validated. Francy et al. [9] studied on input process parameters (the shape of the workpiece; coefficient of friction, half die angle, logarithmic strain, die length and ram velocity) optimization in the extrusion process by Taguchi approach and DEFORM-3D software. The results showed that effective parameters have an important effect on decreasing the minimum extrusion force. Liang et al. [10] analyzed the serious earing defects in the initial extrusion process of an aluminum controller by using DEFORM-3D simulation. According to simulation results, the non-uniform velocity of metal flow is the basic cause of earing defects. Thus, a new process scheme which avoids the defects using a punch with a group of resistance ribs at the bottom was revealed. Results were compared with the initial process, and the earing defects have been saliently developed in the new process scheme. Forward and backward extrusion is important in the cold and hot forging industry and often use during the forging of complex parts.

Hu et al. [11] developed a new method depend on a steady combined forward and backward extrusion tests in order to specify the friction factor for the cold forging process of the complex parts. FE simulations optimized important parameters that define the deformation degree of the forward and backward extrusion and the punch geometry and die in order to develop the sensitivity to friction. As a result, according to simulation results, they constructed two groups of calibration curves for different ranges of friction factors. Jin et al. [12] proposed an optimization method for the cold orbital forging of the component with a deep and narrow groove. As a beginning, three types of metal flow mode are offered based on the preform and tool geometries, and then they analyzed the cold orbital forging processes for three types of metal flow mode using finite-element simulations and forging defects of underfilling, the folding and poor stress state of the tool are found out. Lilleby et al. [13] studied the cold pressure welding of seriously deformed aluminum. Firstly, pure aluminum is exposed to single-pass equal channel angular pressing and then assembled by divergent extrusion. The mechanical integrity of the spliced components is documented by using notch tensile testing and showed that the strength and the flow properties of the SPD processed base material are continued across the joint after cold welding.

In this chapter, extrusion die geometry which is prepared for bolt production is considered, and for this die, the die design conditions that provide minimum extrusion force requirement was determined. For this reason, the primary objective is to obtain the minimum extrusion force by establishing the relationship between the inputs as three main parameters (extrusion angle, temperature and friction coefficient) and the output (extrusion force) in the extrusion die to form the workpiece. In light of these objectives, numerical analyzes were performed in simufact.forming a finite element software program for the determined parameters, and data were obtained. Then, different regression models were created through a commercial software Mathematica based on neuro-regression approach. Besides, the accuracy of the constructed models has been checked through $R^2_{training}$ and $R^2_{testing}$ values. After testing the reliability of the models, and to optimize the input parameters that minimize the output also, stochastic methods, which are Differential Evolution (DE), Random Search (RS) and Simulated Annealing(SA), and a deterministic one Nelder-Mead were used in Mathematica.

Method

Numerical models of cold extrusion operation were prepared in simufact.forming finite element software. Mechanical models were also coupled with thermal analysis to consider temperature effects on the flow stress of the workpiece material. Schematic representation of numerical models is shown in Figure 13.1. Extrusion process was simulated with 2D models due to the axisymmetry. As shown in the figure, numerical models consist of stationary and moving dies and the workpiece. Dies were modeled as rigid. Workpiece material, medium carbon steel, was modeled as plastic material and true stress- true plastic strain curves between temperatures of 20-400°C and strain rates between 1 and 50 s^{-1} was defined to the software. In 2D models, 3444 quad elements were used in the mesh of the workpiece.

Problem description

In this study, the extrusion die has been taken into consideration for the bolts. Factors which affect the operation of the die are extrusion angle, temperature, and friction coefficient (see Fig. 13.2). Three steps have been performed for the design process: (i)the data for the determined parameters were obtained by performing numerical analyzes in simufact.forming software program (ii) the different regression models were created and (iii) optimization studies were carried out in Mathematica software.

a) before extrusion   b) after extrusion

■ moving die   ■ Stationary die (extrusion die)   ■ work-piece
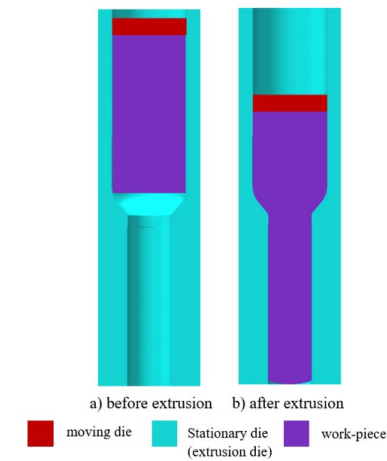
Figure 13.1. *Schematic representation of numerical model.*

1- extrusion angle (°)   2- T (°C)   X

3- μ friction coefficient
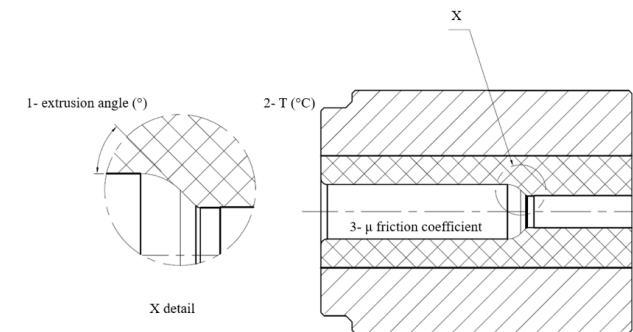
X detail

Figure 13.2. *Technical drawing of the extrusion die.*

Multiple nonlinear regression analysis was used in the modeling step. By neuro-regression approach, firstly, 30 simulation results were randomly divided into training and testing data for forging force. The training data consists of 80% of all data randomly selected, and it is necessary to check the accuracy of the constructed model while the testing data is obtained by 20% of all data (see Tables 13.1 and 13.2). After the separation of the data, five different regression models as the general functional form (see Table 13.3) have been introduced for the engineering parameters and $R^2_{training}$, and $R^2_{testing}$ values for each model have also been calculated by Mathematica (see Table 13.4). In these models, the input parameters X_1, X_2, and X_3 represent the extrusion angle, temperature, and friction coefficient, respectively.

Table 13.1. *Training Simulation Data.*

Case	Extrusion Angle X_1 [°]	Temperature X_2 [°C]	Friction Coefficient X_3	Extrusion Force [t]
1	40	100	0.09	116.481
2	35	25	0.18	263.745
3	40	25	0.18	265.189
4	35	100	0.12	15.465
5	40	25	0.05	803.995
6	45	25	0.09	126.291
7	45	100	0.12	158.635
8	25	250	0.12	150.349
9	30	100	0.18	249.746
10	25	250	0.18	242.671
11	30	25	0.18	263.603
12	45	100	0.05	783.371
13	30	250	0.12	148.395
14	30	25	0.05	767.811
15	35	250	0.12	151.231
16	45	100	0.18	252.247
17	25	100	0.05	743.887
18	40	100	0.12	155.502
19	25	25	0.05	780.922
20	30	100	0.12	150.971
21	40	25	0.12	164.658
22	25	25	0.09	118.979
23	35	25	0.05	799.821
24	35	25	0.09	115.575

Table 13.2. *Testing Simulation Data.*

Case	Extrusion Angle X_1 [°]	Temperature X_2 [°C]	Friction Coefficient X_3	Extrusion Force [t]
25	40	250	0.18	240.229
26	45	25	0.18	266.905
27	35	250	0.18	240.798
28	25	25	0.12	158.995
29	35	100	0.05	75.532
30	35	100	0.09	115.221

Table 13.3. *General Functional Form for Extrusion Force.*

Model No	Models
1	$$\sum_{n=0}^{3} a_n(1 + X_1 + X_2 + X_3)$$
2	$$\sum_{n=0}^{3} \frac{a_n(1 + X_1 + X_2 + X_3)^1}{b_n(1 + X_1 + X_2 + X_3)^1}$$
3	$$\sum_{n=0}^{3} a_n(1 + X_1 + X_2 + X_3)^2$$
4	$$\sum_{n=0}^{3} \frac{a_n(1 + X_1 + X_2 + X_3)^2}{b_n(1 + X_1 + X_2 + X_3)^2}$$
5	$$\sum_{n=1}^{3} 1 + Sin(X_1) + Sin(X_2) + Sin(X_3) + 1 + Cos(X_1) + Cos(X_2) + Cos(X_3)$$

Table 13.4. *Models for Extrusion Force.*

Model No	Models	R^2 Training	R^2 Testing
1	$0.65727 - 0.00490\,X_1 - 0.0095\,X_2 + 141.0383\,X_3$	0.9861	0.9832
2	$\dfrac{880.8394 + 11.0304\,X_1 + 0.4689\,X_2 + 23257.2733\,X_3}{333.4622 + 0.4202\,X_1 + 0.1041\,X_2 - 792.6936\,X_3}$	0.9984	0.9987
3	$5.4629 - 0.09870\,X_1 + 0.0020\,X_2^2 - 0.0035\,X_2 - 0.00006\,X_1X_2 + 0.00004\,X_2^2 + 55.5916\,X_3 - 0.1065\,X_1X_3 - 0.08841\,X_2X_3 + 402.62914\,X_3^2$	0.9994	0.9998
4	$(1153.551 - 271.8023X_1 + 5.4732\,X_1^2 + 16.008X_2 - 0.2322\,X_1\,X_2 + 0.0524X_2^2 + 76803.8248X_3 - 546.7535X_1X_3 + 544.9389X_2X_3 - 1664715.6592\,X_3^2)$ / $(2413.1719 - 16.4347X_1 + 0.3411X_1 + 7.5118X_2 - 0.0199X_1X_2 + 0.005X_2^2 - 28408.8632X_3 - 32.6094X_1X_3 - 21.8497X_2X_3 + 54583).$	0.9999	0.9488
5	$773.343 - 0.0664\,Cos(X_1) - 0.844Cos(X_2) - 767.7328\,Cos(X_3) + 0.2521\,Sin(X_1) + 2.2158\,Sin(X_2) + 51.6142\,Sin(X_3)$	0.9983	0.9930

Table 13.5. Maximum and Minimum values for Extrusion Force.

Model	Minimum Value [t]	Maximum Value [t]
1	50.955	256.823
2	73.757	262.626
3	73.442	263.221
4	72.538	The function is unbounded
5	77.589	298.866

Results and Discussion

In this part, the maximum and minimum values of each model were calculated, and then their compatibility with the maximum and minimum values in the actual data was checked (see Table 13.5). Among the five models introduced in Table 13.4, model 3, which have the highest testing value and the closest maximum and minimum values to actual data, was chosen as the candidate model for the optimization. Then, the selected engineering model is investigated by introducing three optimization problems which include minimizing extrusion force with appropriate constraints. The aim of problem 1 is to mathematically see the limitation of result values of the problem while design variables are chosen in continuous domains. In problem 2, while the extrusion angle and temperature are analyzed in the continuous domain, it has been taken available values given in the simulation data for friction coefficient. In this way, the dependence of the friction coefficient parameter on the selection domain was evaluated for optimization. In problem 3, all design variables have been created considering the actual working conditions in the industry. As shown in Table 13.6, for the problems, extrusion force is minimized based on the DE, RS, SA, and NM methods. When the first two problems were considered, the same optimum values were obtained regardless of whether they were stochastic or deterministic. So that, X_1 = 27.7653, X_2 = 116.1268, X_3 = 0.05, and forging force = 7.3422. In problem 3, the optimum results are X_1 = 30, X_2 = 100, X_3 = 0.05, and forging force = 7.3673. These values are higher than optimum values as expected. However, it was decided that there is approximately 0.31% tolerable difference for the industry conditions. This showed that it is not necessary to make the working conditions of the current process more sensitive. In other words, it can be approached the optimum solution in a slight difference with the current sensitivity.

*Table 13.6. Optimization Problems and Optimum Results.*

Problem No	Problem Definition	Method	Design Variables X_1 [°]	X_2 [°C]	X_3	Extrusion Force [t]
1	Minimize Extrusion Force (X_1, X_2, X_3) Subjected to $25<X_1<45$, $25<X_2<250$, $0.05<X_3<0.18$	DE	27.7653	116.1268	0.05	7.3442
		RS	27.7656	116.1258	0.05	7.3442
		SA	27.7655	116.1257	0.05	7.3442
		NM	27.7653	116.1256	0.05	7.3442
2	Minimize Extrusion Force (X_1,X_2,X_3) Subjected to $25<X_1<45$, $25<X_2<250$, $X_3 \in \{0.05, 0.09, 0.12, 0.18\}$	DE	27.7653	116.1256	0.05	7.3442
		RS	27.7653	116.1256	0.05	7.3442
		SA	27.7653	116.1256	0.05	7.3442
		NM	27.7653	116.1256	0.05	7.3442
3	Minimize Extrusion force (X_1,X_2,X_3) Subjected to $X_1 \in \{25,30,35,40,45\}$, $X_2 \in \{25,100,250\}$, $X_3 \in \{0.05,0.09,0.12,0.18\}$	DE	30	100	0.05	7.3673
		RS	30	100	0.05	7.3673
		SA	30	100	0.05	7.3673
		NM	30	100	0.05	7.3673

Conclusion

In the present study, simulation and optimization studies on the extrusion die geometry which is prepared for bolt production were carried out to investigate the effects of the input parameters (extrusion angle, temperature and friction coefficient) on the extrusion force (output). The main aim is to provide the minimum extrusion force with valid optimum parameters in the extrusion die to form the workpiece. Therefore, numerical analyzes were applied using simufact.forming a finite element software program and then data obtained each operating parameter and extrusion force. We consider the neuro-regression approach and developed five regression models by a commercial software Mathematica. According to the accuracy of the model, the most appropriate model was selected. In the optimization step for an appropriate model, the calculations have been performed based on DE, RS, SA, and NM to optimize the input parameters that minimize the extrusion force. As a conclusion, the optimum solution was achieved in a slight difference from industry condition with the current sensitivity thanks to constructed regression model for the problem.

References

[1]   Kroiß, T. and Engel U., Optimization of Tool and Process Design for the Cold Forging of Net-Shape Parts by Simulation, pp. 419-437. Process Machine Interactions.

[2]   Groche, P., 2018. Friction coefficients in cold forging: A global perspective. 261-264

[3]   Kılıçaslan, C. and Ince, U., 2017. Civata Soğuk Dövme İşleminde Kalıp Ömrünün Artırılması: Dövme Kademe Tasarımının Etkisi. SAUJS. 21: 961-967

[4]   Han, X. and Hua, L., 2013. 3D FE modelling of contact pressure response in cold rotary forging. Tribol. Int. 57: 115-123

[5]   Krusica, V., Masera, S., Pristovsek, A. and Rodica, T., 2009. Adjustment of stochastic response pf typical cold forging systems. J. Mater. Process. Technol. 209: 4983-4993

[6]   Ossenkemper, S., Dahnke, C. and Tekkaya, A.E., 2019. Analytical and experimental bond strength investigation of cold forged composite shafts. 264: 190-199

[7]   Groche, P., Kramer, P., Bay, N., Christiansen, P., Dubar, L., Hayakawa, K., Hue, C., Kitamura, K. and Moreau, P., 2018. CIRP annals-manufacturing technology. 67: 261-263

[8]   Zhu, F., Wang, Z. and Lv, M., 2016. Multi-objective optimization method of precision forging process parameters to control the forming quality. Int. J. Adv. Manuf. Tech. 83: 1763-1771

[9]   Francy, K.A., SrinivasaRao, D.C. and Gopalakrishnaiah, P., 2019. Optimization of direct extrusion process on 16MnCr5 and AISI1010 using DEFORM-3D. Procedia Manuf. 30: 498-505

[10]   Cheng-liang, H., Li-fen, M., Zhen, Z., Bing, G. and Bing, C., 2012. Optimization for extrusion process of aluminum controller housing. T. Nonferr. Metal. Soc. 22: 48-53

[11]   Hu, C., Yin, Q. and Zhao, Z. 2017. A novel method for determining friction in cold forging of complex parts using a steady combined forward and backward extrusion test. J. Mater. Process. Technol.

[12]   Jin, Q., Han, X., Hua, L., Zhuang, W. and Feng, W., 2018. Process optimization method for cold orbital forging of component with deep and narrow groove. J. Manuf. Process. 33: 161-174

[13]   Lilleby, A., Grong, Ø. And Hemmer, H., 2010. Cold pressure welding of severely plastically deformed aluminium by divergent extrusion. Mat. Sci. Eng. A-Struct. 527: 1351-1360
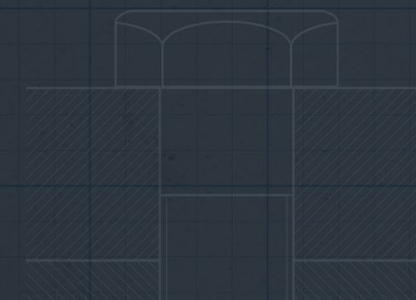
APPLICATION OF COLD EXPANSION ON DIFFERENT MATERIALS: A REVIEW

Tayfun DAMLA
Muhammed Burak TOPARLI
Pınar DEMİRCİOĞLU

APPLICATION OF COLD EXPANSION ON DIFFERENT MATERIALS: A REVIEW

Tayfun Damla (a,b), M. Burak Toparlı (a)*, Pınar Demircioğlu (b)

(a) *R&D Center, Norm Fasteners, AOSB, İzmir – TURKEY*
(b) *Mechanical Engineering Department, Engineering Faculty, Aydın Adnan Menderes University,*
Central Campus 09010 Aydın – TURKEY
* Corresponding author, burak.toparli@norm-fasteners.com.tr

Abstract

Cold expansion or cold-hole expansion is one of the mechanical surface treatment methods applied to circular holes of engineering structures for improved service performance. The main mechanism is to induce non-homogenous plastic deformation by oversized mandrels or balls leading to beneficial compressive residual stress fields and hardness increase around the applied holes. Cold expansion is an important method to enhance fatigue life of particularly lightweight materials and components in aviation industry. In addition to aluminium and titanium alloys, different materials such as steels were also treated via cold expansion for fatigue life improvement. In this study, characteristics of different methods used in cold expansion were introduced in detail. In addition, the review was presented according to application of cold expansion to different materials. Readers can navigate to materials of interest and find previous studies conducted on the same and/or similar materials. Therefore, this review shows a new direction along with an established process that has not been investigated before.

Keywords: *Cold expansion; hole edge expansion; direct mandrel expansion; ball expansion; split sleeve expansion; residual stress; fatigue.*

1. Introduction

Service performance of engineering components is very critical in terms of structural integrity. Parameters such as design, operating conditions and microstructural characteristics have an impact on final service life. Due to demanding performance requirements in industries such as aerospace and automotive, special surface treatments are applied to improve surface characteristics of materials for better performance. As a result of inducing compressive residual stress fields, hardness increase and microstructural modifications, resistance to failure mechanisms such as fatigue, stress corrosion cracking and wear can be improved. Mechanical surface treatments such as cold expansion, shot peening, laser peening and flapper peening are widely preferred methods to enhance service life of engineering components in aerospace and automotive industry.

Fatigue has detrimental effects on structural integrity of engineering components and is the main failure mechanism of engineering structures such as aircrafts [1]. Mechanical surface treatment methods such as cold expansion, shot peening and laser peening can be used to improve service performance of engineering components without any change in material type or design [2]. Owing to application of these surface treatments to susceptible-to-failure locations, local fatigue resistance can be improved significantly. One of the widely used mechanical surface treatment methods, shot peening employs ceramic or steel medium impacting on surface with a certain selected velocity [3]. Compressive residual stresses near surface layer and increase in hardness of applied materials can be achieved. However, surface roughness is also increased after shot peening, leading to increase in crack initiation sites. Laser peening introduces deeper compressive residual stresses with better surface profile compared to shot peening. However, application of laser peening to inside of cylindrical parts or deep holes with small diameter is challenging.

Cold expansion, widely used in aerospace industry, is a mechanical surface treatment method applied to circular holes for fatigue life improvement [4]. The main mechanism of this method is based on non-homogenous plastic deformation of hole edges to induce beneficial compressive residual stresses. Owing to beneficial residual stress fields, fatigue crack initiation and propagation can be delayed or even suppressed by application of this method. Compared to other mechanical surface treatment techniques such as shot peening and laser peening, this method is well-suited for edges or inside of the circular deep holes.

Due to higher stress intensity factor under loading, hole edges and adjacent regions are more susceptible to crack initiation and propagation leading to premature failures. For instance, fastener holes, which are geometrical discontinuities in structure of airplanes, can act as a stress concentrator under load and fatigue cracking can be observed initiating around fastener holes. Fatigue failures arising around the fastener holes are responsible for 50-90% of fractures of aging planes [5], as in the case of Aloha Airlines, Flight 243 [6], was one of the shocking incident in the aviation history.

In this review, cold expansion process was investigated in details. Different approaches used in the open literature were studied. In addition, the review was conducted based on the applied material. Readers can navigate to materials of interest and find previous studies conducted on the same and/or similar materials. Therefore, this review shows a new direction along with an established process that has not been investigated before.

2. Methods of Cold Expansion

There are different techniques for cold expansion used over the last decades such as mandrel expansion, split sleeve expansion and sleeveless expansion. [7,8]. All the methods are designed to induce plastic deformation of circular holes of components by using a harder tool compared to material to be processed. During removal of tool from circular hole, circumferential compressive residual stresses are generated [7]. Due to production history, there can be pre-cold expansion residual stresses either tensile or compressive. After the application of mandrel or ball, the hole is expanded leading to hoop stresses or tangential stresses will be close to yield stresses of the material but in tension. After the tool is removed, compressive residual stresses are formed owing to plastic deformation and spring-back effect [8]. A typical hoop stresses or tangential stress distribution after cold expansion can be seen in Figure 1. A significant compressive residual stress field, acting against crack initiation and propagation, is introduced after non-homogenous plastic deformation.

Balancing tensile residual stresses are also inherently formed through the radial direction. Residual stress profiles after cold expansion, measured by employing Sach's Method can be seen in Figure 2. Compressive residual stresses around the holes can delay initiation and also propagation of fatigue cracks by reducing the stress intensity factor around holes. Owing to residual stress profiles obtained in Figure 2, significant fatigue life improvement was observed particularly at low and intermediate stress levels for 7050 aluminium alloy as can be seen Figure 3.

Although the main mechanism for fatigue life improvement is the same, there are different methods of cold expansion technique. According to literature review most preferred methods for cold expansion are: hole edge expansion, direct mandrel expansion, ball expansion and split sleeve expansion processes [8,9]. Different methods of cold expansion surface treatment are summarised in Table 1.

Table 1. *Comparison of cold expansion methods.*

| Cold Expansion Techniques	Application Area	Advantage	Disadvantage
Hole Expansion	Hole edges	Simple and relatively fast	Smaller region is affected
Direct Mandrel	Whole inner surface	Better fatigue life improvement than ball expansion method	Misalignment of mandrel can disturb residual stress distribution
Ball Expansion	Whole inner surface	Applicable on hard materials	Weak points at the entrance and exit of specimen
Split Sleeve Expansion	Whole inner surface	Very limited surface damage	More process time is required
Sleeveless Split Mandrel	Whole inner surface	Faster process than split sleeve method	Appropriate lubrication is needed
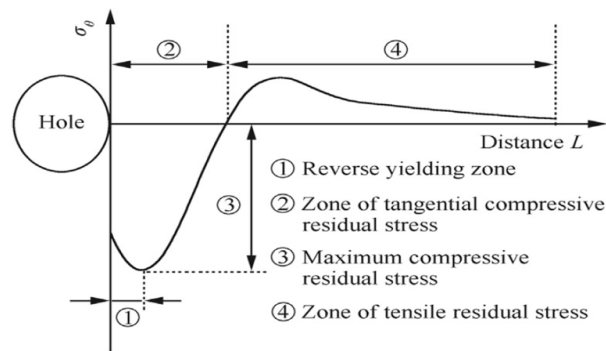
Figure 1. *A schematic of compressive residual stress generation during cold expansion for tangential or hoop stress [8].*
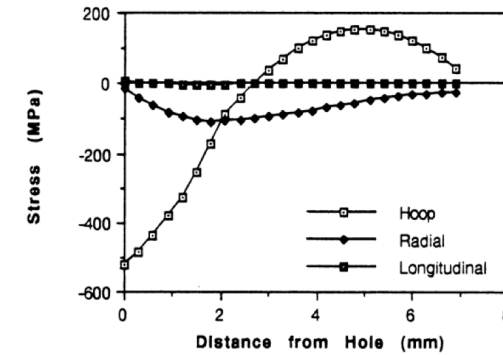

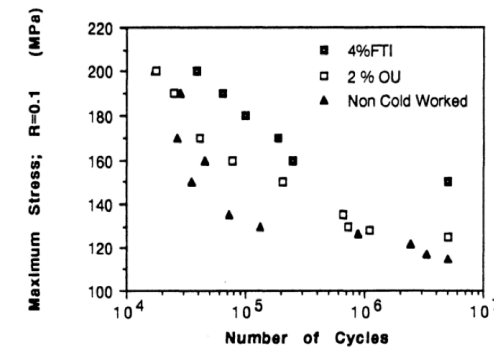**Figure 2.** *Measured residual stress profiles after cold expansion [7].*

Figure 3. *Fatigue life improvement after cold expansion owing to compressive residual stresses in hoop direction as given in Figure 2 [7].*

2.1. Hole edge expansion

Hole edge expansion is performed by hardened percussion tool with tapered indenter (Figure 4). In this method, only edges of holes are treated so that very limit area is plastically deformed. Therefore, the effective region is smaller compared to the other cold expansion methods. On the other hand, application of hole edge expansion method is simple and can be applied consecutive times to obtain desired performance improvement. In literature, this method is also called as hammer peening [8]. According to study of Liu et al., fivefold fatigue life enhancement was achieved by use of this method for 2A12-T4 aluminium sheets [10].
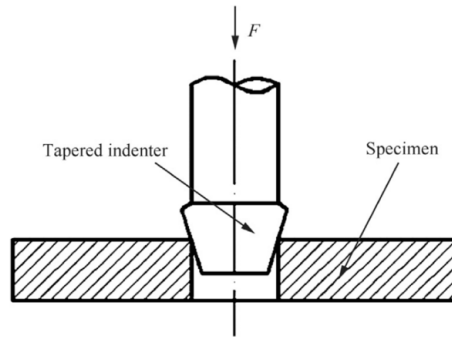
Figure 4. A schematic of hole edge expansion method [8].

2.2. Direct mandrel expansion

Direct mandrel expansion is performed by conical pin as shown in Figure 5. Compared to hole edge expansion method, oversized lubricated mandrel is pushed inside the hole so that through-thickness surface alteration can be obtained. There are many parameters affecting the efficiency of hole expansion, such as lubrication, expansion degree, mandrel speed, hole size [11-13]. In addition, orientation of mandrel has significant effect on the uniformity of the hardness increase and residual stress generation. If the axis of the alignment of mandrel is not fully vertical with respect to hole, distribution of residual stresses around hole will be non-axisymmetric after cold expansion [14]. This situation can generate weak points which allow fatigue cracks to initiate and grow. In order to eliminate this problem, double cold expansion is suggested to be applied [15]. However, depending on the orientation of mandrel, non-axisymmetric residual stress fields can be observed despite application of double cold expansion.
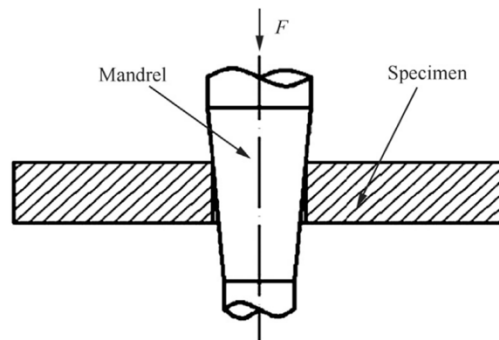

Figure 5. A schematic of direct mandrel expansion method [8].

2.3. Ball expansion

In ball expansion, an oversized ball goes through the hole to obtain plastic deformation leading to residual stress generation and hardness increase [16]. Compared to Direct Mandrel Expansion, harder materials can be processes by this method owing to lower friction forces between contact surfaces (Figure 6). In addition, there is no indents on the material because of formation of a natural hydrodynamic wedge between workpiece and tool. Thus, this method can be used in steel plates [8,17].
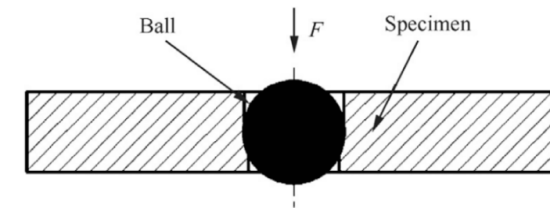

Figure 6. A schematic of ball expansion [8].

Compared to mandrel expansion methods, ball expansion leads to limited improvement on fatigue life. In the literature, it was stated that after ball expansion, tensile stresses were obtained at the entrance and exit face of hole. On the other hand, it was claimed that tensile stress was only observed on exit of hole in mandrel methods [15]. As a result, depending on the process parameters, limited improvement or even reduction in fatigue life can be observed if the balancing tensile residual stresses are obtained at critical locations.

2.4. Split sleeve expansion

Split sleeve cold expansion technique was developed by Boeing in early 1970s [18]. In this method, residual stresses are generated by pulling oversized mandrel through split sleeve (Figure 7). Split sleeve is used to avoid damaging surface of holes due to high friction caused by high interference [19]. On the other hand, cracking can occur during expansion process because of geometry of sleeve [20].
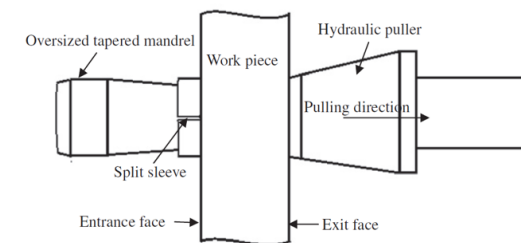

Figure 7. A schematic of split sleeve expansion [19].

In split sleeve process, mandrel with sleeve is pushed into the hole. Mandrel is drawn back through the sleeve and sleeve expands the hole [21]. After that, sleeve is removed from the hole (Figure 8).
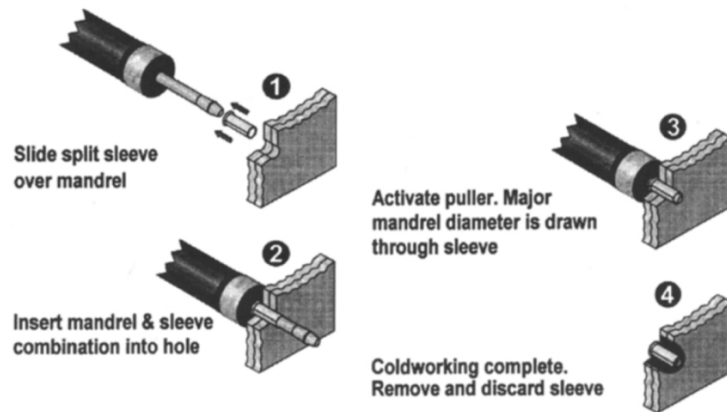

Figure 8. Process of split sleeve expansion with sleeve [21].

Due to process time of sleeve application, Boeing developed sleeveless split mandrel method in 1980 [21]. Instead of split sleeve, mandrel with longitudinally slot is used as can be seen in Figure 9. Longitudinally slot allows mandrel to collapse during pulling process into hole. However, this method requires appropriate lubrication because of lack of sleeve [22]. Otherwise, soft materials can be damaged during the application of sleeveless split mandrel method.
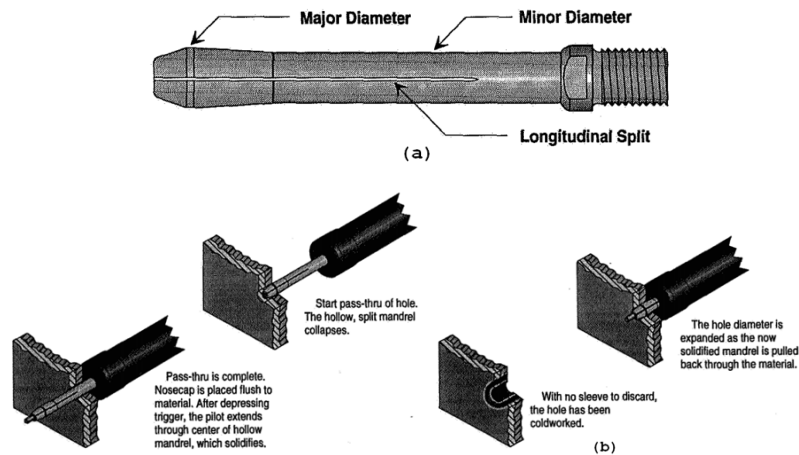

Figure 9. A schematic of the Side-view of mandrel in (a) and the schematic of Split Mandrel Expansion without sleeve in (b) [22].

In the open literature, there are also studies comparing two methods such as ball expansion and split sleeve expansion. According to study of Gopalakrishna et al. tapered pin is compared with mandrel with ball end in terms of improving fatigue life [23]. It was found that taper method led to higher fatigue life improvement compared to ball expansion.

Regardless of the applied method, the cold expansion was suggested to be applied twice to achieve more homogenous compressive stress distribution [24]. It was revealed that, application of cold expansion in opposite directions resulted in better fatigue life improvement since entrance regions were susceptible to have lower residual stresses and after double cold expansion these regions were treated in different orientation to have more homogeneous residual stress distribution [25,26].

3. Applications in Different Materials

Cold expansion method is used mostly in aviation industry [8,18]. The main reason is to increase fatigue resistance of holes, particularly rivet holes, number of which is very high in aircrafts. Therefore, many examples of application on light metals including aluminium alloys can be found in literature [8]. On the other hand, studies related to harder materials are limited in the open literature. There are very few articles on the investigation of fatigue behaviour of titanium alloys and steels after cold expansion. There are also studies about developing of a new model for analytical prediction and simulate the different conditions [27-30]. As a result of experimental studies, simple and realistic models were developed to predict fatigue crack growth [31]. Effects of cold expansion on different materials was summarized in Table 2.

Table 2. Effect of cold expansion to fatigue performance of different materials.

Material	Cold Expansion Method	Improvement of Fatigue life	Reference
Al- 2024-T3	Split sleeve with taper pin	5.3x	[23]
	Split sleeve with ball	1.8x	
Al- 6061-T6	Ball expansion	2x	[4]
Al- 7085-T7651	SWCW	2.2-47x	[33]
Al- 7475-T7351	Split sleeve	1.5-3.2x	[39]
Ti- TC4	Split sleeve	1.5-3x	[19]
Ti-6Al-4V	Split sleeve	3-6x	[24]
Ti- TC4	Split sleeve	1.7-2.2x	[41]
St-30CrMnSiNi2A	Direct Mandrel	1,21x	[43]
St-1020	Split sleeve	1.5-7x	[45]
Mg- AZ31B	Split sleeve	3x	[47]

3.1. Aluminium alloys

Considering cold expansion studies in the open literature, aluminium alloys are the most widely investigated material. Owing to use in aerospace and automotive industry, aluminium alloys were preferred in the studies. Mostefa et al. performed ball expansion on 6082-T6 aluminium alloys to compare results of tests with stress model calculated by Miner's rule under changing load sequence. It was found that experimental service life was lower compared to prediction of Miner's rule and it was argued that load sequence had a minor effect on crack initiation [32]. Edwards and Ozdemir analysed fatigue life of 5.0 mm-thick 7050 plate with sleeveless cold expansion and compared with commercial split sleeve method [7]. They found that although both methods led to improvement, fatigue life after split sleeve process was higher, which was incorporated with higher compressive residual stress fields. In another study, Easterbrook and Landy developed a new process called Stress Wave Cold Working (SWCW) and compared with split sleeve cold expansion [33]. It was claimed that the new process generated beneficial residual compressive stresses around the hole and through thickness of the part before hole drilling. According to test results of 7085-T7651 and 7050-T7451 plates, SWCW led to fatigue life improvement greater than split sleeve cold working ranging from over 1.5 to 12 times. Viveros et al. investigated fatigue crack growth in welds of 6061-T6 samples after cold expansion [4]. According to experimental results, cold expansion with 4.1% expansion rate increased fatigue life of 6061-T6 aluminium alloy, but it was ineffective for weld metal and heat affected zone specimens. Kawdi and Shanmukh performed a stress analysis for 7050 during split sleeve process with FEM [34]. This analysis showed that a significant fatigue life improvement could be obtained with split sleeve cold expansion after a period of constant amplitude. Shahriary and Chakherlou studied the effect of cold expansion on fretting fatigue life of 2024-T3 plates [35]. According to their results, high expansion rates of cold expansion process had no significant effect on fretting fatigue life. In addition, it was discussed that geometrical distortion could be observed due to high expansion rate. It was also stated to fully benefit from bolt clamping and cold expansion, the plate deformation should be reduced during the cold expansion process by using sleeve. Liu et al. investigated residual stress distribution of 2A12T4 [14]. After series of fatigue tests, it was found that fatigue life increases six times with direct cold expansion technique. Baltach et al. performed numerical study to analyse the effect of mandrel shape on residual stress around the hole of 7075-T6 plate [15]. In this study, ball and conical mandrel were modelled with different taper angle. It was found that conical mandrel was more suitable for the cold expansion, especially for thick plates while ball mandrel generates tensile stress around the hole edge. Moreover, lower taper degree has a positive effect on compressive residual stress at the entrance face of hole. Su et al. presented both experimental and numerical studies to investigate the effect of the single and double expansion on 6082-T6 [25]. Result of studies showed that double expansion provided better fatigue life and especially double expansion in opposite direction was highly beneficial, because it generated more compressive residual stress at the entrance of the hole. Kumar et al. investigated effect of cold expansion with rotating mandrel [36]. A 3D thermo-mechanical finite element model was developed to analyse residual stress fields. It was found that the effectiveness of the method relied on friction and plastic deformation between workpiece and mandrel. It was concluded that by employing the optimised parameters, this method could prevent damage in the entry and exit of hole and allow higher degree of cold expansion with nanopowder lubricating. Gopalakrishna et al. presented experimental results of residual stresses of Al 2024-T3 after split sleeve with taper

and ball cold expansion methods [23]. According to this comparative study, split sleeve with taper pin method achieved 200 % higher fatigue life enhancement compared to ball method. It was also found that, residual stresses raised up to 5%-hole expansion rate and decreased for further rate of expansion rate. Kumar and Babu found out by finite element simulations that fatigue life of 7075-T651 plate could be improved up to 6.6 times with 2% expansion rate [11]. Nigrelli and Pasta performed cold expansion simulation of 5083-H321 aluminium plate by using DEFORM [37]. They found that residual stress could change through the thickness and their analyses showed that the compressive residual stresses increases with increasing plate thickness, because thicker plate provided distributed compressive hoop residual stresses. Lacarac et al. compared fatigue life of 2024 and 2650 samples before and after cold expansion [38]. They found that cold expanded hole had better fatigue life. However, cold expansion had a slightly effect on fatigue life in surface cracks less than about 1 mm. Burlat et al. applied cold expansion on the 7475-T7351 samples in different degrees. They found that crack grows rate was higher at the entry face because of low residual stress and at cold expansion degree of 5,58% fatigue life improvement factor is 3,2 [39].

3.2. Titanium Alloys

Titanium alloys are one of the most-widely used materials in aircrafts because of lightweight and better mechanical properties compared to aluminium alloys. Yan et al. investigated fatigue behaviour of TC4 titanium alloy by using split sleeve cold expansion method [19]. It was found that fatigue life of the materials was increased 1.5 – 3.0 times after cold expansion. In other study, fatigue behaviour of Ti-6Al-4V was investigated [24]. In this study, single split sleeve and double cold expansion methods were compared. It was shown that both methods improved fatigue life of the work-piece, but double cold expansion in different direction led to better life improvement. Accard et al. [40] investigated fatigue performance of Ti-6Al-4V under various expansion rates. It was concluded that titanium alloys could withstand up to 8% expansion rates. At 8% expansion rates, tension stresses increased significantly and it was argued that they might cause crack initiation. Yuan et al. compared Smith-Watson-Topper method with Wang- Brown method to predict fatigue life of TC4 [41]. Based on the results of experimental studies, it was found that Wang – Brown method was more realistic.

3.3. Steels

Maximov et al. studied hardening behaviour of medium carbon steel after cold expansion process [42]. They developed a finite element model to analyse residual stress concentration. Experimental tests were performed to optimize the model. Su et al. developed a simplified model to estimate fatigue growth behaviour of high strength steel, 30CrMnSiNi2A [43]. By using oversized mandrel fatigue endurance limit was increased 1.21 times. It was seen that there was a good agreement between S-N curves of the model and the experimental results. In another study, Hacini et al. investigated hammer peening process of 304L plates to optimize process parameters [44]. It was found that surface compressive residual stresses were generated during the first three hammering process. Moreover, hammer peening did not initiate any cracks at the surface of sample. Stack and Stephens studied fatigue behaviour of 1020 steel by using split sleeve method [45]. They found an improvement in fatigue life. Rather than crack initiation, there was a significant improvement in crack growth stage of the fatigue life.

Furthermore, it was concluded that the split-sleeve cold-expansion process had compressive residual stress relaxation under higher stress values, therefore, it had limited advantages for low alloy steels. Caron et al. performed neutron diffraction experiments to analyse residual stress of A42 ferritic steels after ball expansion [46]. Neutron diffraction experiments showed the effectiveness of cold expansion in improving fatigue life of component.

3.4. Other materials

Sasan Faghih analysed fatigue behaviour of magnesium sheets after cold expansion [47]. It was shown that split sleeve cold expansion increased the fatigue life of magnesium sheets by delaying crack initiation. Experimental studies were carried out to verify the numerical model. It was found that optimum cold expansion rate for 3.18 mm magnesium sheet was 6%. Higher rate of expansions was claimed to cause micro cracks so that decrease in fatigue life could be expected. Fatigue Technologies developed GromEx system to improve fatigue life of fastener hole of Carbon Fiber Reinforced Plastics without causing localized damage [48]. During removal of the mandrel, the grommet was expanded radially leading to an increase in fatigue life and protection against lightning strike measured based on sparks observed during testing. Additionally, there was no fastener installation and removal damage on composite.

4. Conclusıons

Cold expansion is one of the mechanical surface treatment methods preferred mainly to enhance fatigue life of lightweight material in aerospace industry. Depending on the application and requirements, different approaches can be applied to achieve service life improvements. In addition, various materials were processes by the cold expansion method to increase mainly fatigue performance. Based on the open literature, it was found that cold expansion method is mostly applied to aluminium alloys owing to wide usage in aerospace. Application to titanium alloys, steels and other materials were very limited. Depending on service conditions, about 5% expansion rate was declared as the optimum rate to achieve maximum compressive residual stress [49,50]. It was discussed that increase in expansion rate would start to induce micro-cracking leading to decrease in service life. Fatigue life enhancement was declared as 6-28 times depending on the application configuration [8,11,51,52]. In titanium alloys, fatigue life improvement can be reached up to 3 times [17]. Therefore, it can be concluded that service performance of various materials can be improved by employing cold expansion method. However, numerical and experimental investigations are required to optimize process parameters to maximize performance enhancement.

References

[1]   Meguid, S. A., and Papanikos, P. Mechanics of the Cold Hole Expansion of Aerospace Components. International Conference on Experimental Mechanics (1998).

[2]   Kim, C., Kim, D.J., Seok, C.S., and Yang WH. Finite element analysis of the residual stress by cold expansion method under the influence of adjacent holes. Journal of Materials Processing Technology 153–154 (2004), 986–991.

[3]   Toparli, M.B. Effect of Shot Peening on Ballistic Limit of Al6061-T651 Aluminium Alloy Plates. Experimental Techniques (2019), 1-11.

[4]   Viveros, K.C., Ambriz, R.R., Amrouche, A., Talha, A., García, C., and Jaramillo, D. Cold hole expansion effect on the fatigue crack growth in welds of a 6061-T6 aluminum alloy. Journal of Materials Processing Technology 214 (2014), 2606-2616.

[5]   Yongshou, L., Shao, X., Liu, J., and Yue, Z. Finite element method and experimental investigation on the residual stress fields and fatigue performance of cold expansion hole. Materials and Design 31 (2010), 1208–1215.

[6]   Aloha Airlines, Flight 243, Boeing 737-200, N73711 Accident Report, The National Transportation Safety Board (NTSB), (1989).

[7]   Edwards, L., and Ozdemir, A.T. Effect of residual stress on fatigue life of cold expanded fastener holes. Transactions on Engineering Sciences 2 (1993).

[8]   Fu, Y., Ge, E., Su, H., Xu, J., and Li, R. Cold expansion technology of connection holes in aircraft structures: A review and prospect. Chinese Journal of Aeronautics 28 (2015), 961-973.

[9]   Chakherlou, T.N., and Vogwell, J. The effect of cold expansion on improving the fatigue life of fastener holes. Engineering Failure Analysis 10 (2003), 13–24.

[10] Liu, J., Gou, W.X., Liu, W., and Yue, Z.F. Effect of hammer peening on fatigue life of aluminum alloy 2A12-T4. Materials & Design 30 (2009), 1944-1949.

[11] Kumar, A. R., and Babu, M. The Effect of Cold Expansion on Fatigue Life of Closely Spaced Adjacent Fastener Holes. SasTech Journal 16 (2017).

[12] Farhangdoost, K., and Hosseini, A. The Effect of Mandrel Speed upon the Residual Stress Distribution around Cold Expanded Hole. Procedia Engineering 10 (2011), 2184–2189.

[13] Amrouche, A., Mesmacque, G., Garcia, S., and Talha A. Cold expansion effect on the initiation and the propagation of the fatigue crack. International Journal of Fatigue 25 (2003), 949–954.

[14] Liu, J., Shao, X.J., Liu, Y.S., and Yue, Z.F. Effect of cold expansion on fatigue performance of open holes. Materials Science and Engineering: A 477 (2008), 271-276

[15] Baltach, A., Abdelkader, D., Mostefa, B., and Besseghier, E. Numerical analysis and optimization of the residual stresses distribution induced by cold expansion technique. Frattura ed Integrità Strutturale 12 (2018), 252-265.

[16] Semari, Z., Aid, A., Benhamena, A., Amrouche, A., Benguediab, M., Sadok, A., and Benseddiq, N. Effect of residual stresses induced by cold expansion on the crack growth in 6082 aluminum alloy. Engineering Fracture Mechanics 99 (2013), 159–168.

[17] Maximov, J.T., and Duncheva, G.V. A new 3D finite element model of the spherical mandrelling process. Finite Elements in Analysis and Design 44 (2008), 372 – 382.

[18] Phillips, J. L. Sleeve coldworking fastener hole. Manufacturing Technology Division, Air Force Materials Laboratory 1 (1974).

[19] Yan, W.Z., Wang, X.S., Gao, H.S., and Yue, Z.F. Effect of split sleeve cold expansion on cracking behaviors of titanium alloy TC4 holes. Engineering Fracture Mechanics 88 (2012), 79-89.

[20] Karabin, M.E., Barlat F., and Schultz R.W. Numerical and experimental study of the cold expansion process in 7085 plate using a modified split sleeve. Journal of Materials Processing Technology 189 (2007), 45–57.

[21] Leon, A. Benefits of split mandrel coldworking. Internal Journal of Fatigue 20 (1998), 1-8.

[22] Rodman, G. A., and Matthew C. Split mandrel vs split sleeve coldworking: Dual methods for extending the fatigue life of metal structures. NASA International Symposium on Advanced Structural Integrity Methods for Airframe Durability and Damage Tolerance 2 (1994), 1077-1086.

[23] Gopalakrishna, H.D., Narasimha Murthy, H.N., Krishna M., Vinod M.S., and Suresh A.V. Cold expansion of holes and resulting fatigue life enhancement and residual stresses in Al 2024 T3 alloy – An experimental study. Engineering Failure Analysis 17 (2010), 361-368.

[24] Elajrami, M., Miloud, R., Melouki, H., and Boukhoulda, F. Numerical study of the effect of double cold expansion of rivet hole on the residual stresses distribution, Journal of Engineering Manufacture 227 (2013), 621–626.

[25] Su, M., Amrouche, A., Mesmacque, G., and Benseddiq, N. Numerical study of double cold expansion of the hole at crack tip and the influence on the residual stresses field. Computational Materials Science 41 (2008), 350-355.

[26] Achard, V., Daidié, A., Paredes, M., and Chirol, C. Optimization of the Cold Expansion Process for Titanium Holes. Advanced Engineering Materials 19 (2016), 1-13.

[27] Zhang, Y., Fitzpatrick, M. E., and Edwards, L. Analysis of the Residual Stress around a Cold-expanded Fastener Hole in a Finite Plate. Strain 41(2005), 59–70.

[28] Chakherlou, T. N., Taghizadeh, H., and Aghdam, A. B. Experimental and numerical comparison of cold expansion and interference fit methods in improving fatigue life of holed plate in double shear lap joints. Aerospace Science and Technology 29 (2013), 351–362.

[29] Stuart, D. H., Hill, M. R., and Newman, J. C. Correlation of one-dimensional fatigue crack growth at cold-expanded holes using linear fracture mechanics and superposition. Engineering Fracture Mechanics 78 (2011), 1389–1406.

[30] Newman, J. C., and Daniewicz, S. R. Predicting crack growth in specimens with overloads and cold-worked holes with residual stresses. Engineering Fracture Mechanics 127 (2014), 252–266.

[31] Wu, H. On the prediction of initiation life for fatigue crack emanating from small cold expanded holes. Journal of Materials Processing Technology 212 (2012), 1819–1824.

[32] Mostefa, B., Aid, A., Benhamena, A., and Mohamed B. Effect of Hardening Induced by Cold Expansion on Damage Fatigue Accumulation and Life Assessment of Aluminum Alloy 6082 T6. Materials Research 15 (2012), 981-985.

[33] Easterbrook, E.T., and Landy, M.A. Evaluation of the StressWave Cold Working (SWCW) Process on High-Strength Aluminum Alloys for Aerospace. Air Force Research Laboratory (2009).

[34] Kawdi, B., and Shanmukh, N. Cold Hole Expansion Process for Stress Analysis and Evaluation of Fatigue Properties. Journal of Mechanical and Civil Engineering (2013), 21-27.

[35] Shahriary, and P., Chakherlou, T.N. Investigating the effect of cold expansion on frictional force evolution during fretting fatigue tests of AL2024-T3 plates. International Journal of Mechanical Sciences 135 (2018), 146-157.

[36] Kumar, B.M., Panaskar, N.J., and Sharma, A. A fundamental investigation on rotating tool cold expansion: numerical and experimental perspectives. The International Journal of Advanced Manufacturing Technology 73 (2014), 1189-1200.

[37] Nigrelli, V., and Pasta, S. Finite-element simulation of residual stress induced by split-sleeve cold-expansion process of holes. Journal of Materials Processing Technology 205 (2008), 290–296.

[38] Lacarac VD, Smith DJ, Pavier MJ, and Priest M. Fatigue crack growth from plain and cold expanded holes in aluminium alloys. International Journal of Fatigue 22 (2000), 189–203.

[39] Burlat, M., Julien, D., Lévesque, M., Bui-Quoc, T., and Bernard, M. Effect of local cold working on the fatigue life of 7475-T7351 aluminium alloy hole specimens. Engineering Fracture Mechanics 75 (2008), 2042–2061.

[40] Achard, V., Daidié, A., Paredes, M., and Chirol, C. Cold expansion process on hard alloy holes-experimental and numerical evaluation. Mechanics & Industry 17 (2016), 303-319.

[41] Yuan, X., Yue, Z.F., Wen, S.F., Li, L., and Feng T. Numerical and experimental investigation of the cold expansion process with split sleeve in titanium alloy TC4. International Journal of Fatigue 77 (2015), 78-85.

[42] Maximov, J., Duncheva, G.V., and Kuzmanov, T. Modelling of hardening behaviour of cold expanded holes in medium-carbon steel. Journal of Constructional Steel Research 64 (2008), 261-267.

[43] Su, X., Gu, M., and Yan, M. A simplified residual stress model for predicting fatigue crack growth behavior at coldworked fastener holes. Fatigue & Fracture of Engineering Materials & Structures 9 (1986), 57-64.

[44] Hacini, L., Van Lê, N., and Bocher, P. Effect of impact energy on residual stresses induced by hammer peening of 304L plates. Journal of Materials Processing Technology 208 (2008), 542-548.

[45] Stack, C.P., and Stephens, R.I. Effect of split-sleeve cold-expansion on the fatigue resistance of hot-rolled 1020 steel. International Journal of Fatigue 11(1989), 327-334.

[46] Caron, I., Fiori, F., Mesmacque, G., Pirling, T., and Su, M. Expanded hole method for arresting crack propagation: residual stress determination using neutron diffraction. Physica B 350 (2004), 503–505.

[47] Faghih, S., Shaha, S. K., Behravesh, S. B., and Jahed, H. Split sleeve cold expansion of AZ31B sheet: Microstructure, texture and residual stress. Materials & Design (2019).

[48] Reid, L., Ransom, J., and Wehrmeister, M. Grommet. Hole Reinforcement and Lightning Strike Protection in Composite Structural Assembly. SAE International Journal of Aerospace 4 (2011), 988-997.

[49] Amrouche, A., Su, M., Aid, A., and Mesmacque, G. Numerical study of the optimum degree of cold expansion: Application for the pre-cracked specimen with the expanded hole at the crack tip. Journal of Materials Processing Technology 197 (2008), 250–254.

[50] Pasta, S. Fatigue crack propagation from a cold-worked hole. Engineering Fracture Mechanics 74 (2007), 1525–1538.

[51] P.F.P., McEvily, A.J., Moreira, P.M.G.P., and Castro, P.M.S.T. Analysis of the effect of cold-working of rivet holes on the fatigue life of an aluminum alloy. International Journal of Fatigue 29 (2007), 575–586.

[52] De Matos, P. F. P., Moreira, P. M. G. P., Camanho, P. P., and de Castro, P. M. S. T. Numerical simulation of cold working of rivet holes. Finite Elements in Analysis and Design, 41 (2005), 989–1007.
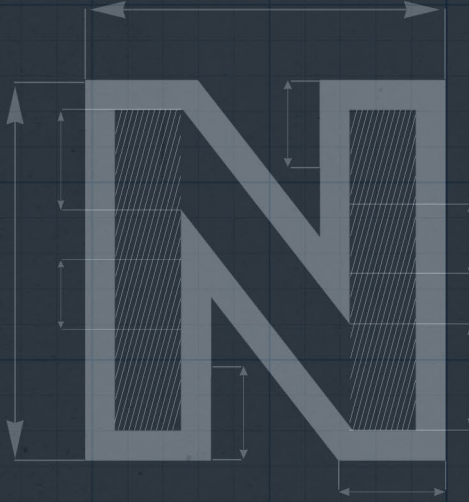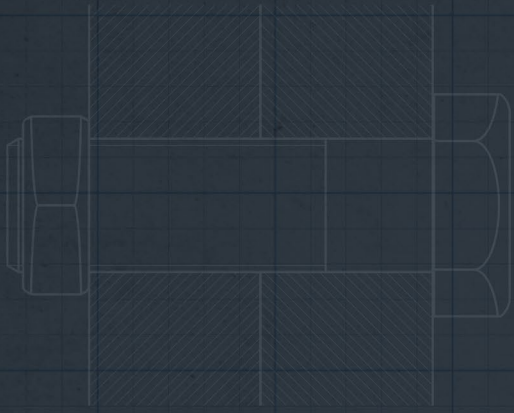
SOĞUK DÖVMEDE KULLANILAN YÜZEY İŞLEM METOTLARI

SURFACE PREPARATION METHODS USED IN COLD FORGING

Fatih KOCATÜRK
Doğuş ZEREN
Sezgin YURTDAŞ
M. Burak TOPARLI
Cenk KILIÇASLAN

SOĞUK DÖVMEDE KULLANILAN YÜZEY İŞLEM METOTLARI

Fatih Kocatürk, Doğuş Zeren, Sezgin Yurtdaş, M. Burak Toparlı, Cenk Kılıçaslan

Öz

Hammadde yüzey işlem ve yüzey kaplama aşamaları soğuk dövme için elzem uygulamalardır. Yüzey işlemin kalitesi, kaplamanın yüzeye yapışma derecesini ve korozyon direncini etkilemektedir. Buna bağlı olarak malzemenin dövme sırasındaki akışı da doğrudan etkilenmektedir. Soğuk dövme işleminin başarılı bir şekilde uygulanması verimli bir hammadde kaplama sistemi ile yakından ilgilidir ve en yaygın kaplama sistemi çinko-fosfat kaplamasıdır. Son zamanlarda çinko-fosfat kaplama çevreye zarar veren bir kaplama türü olarak kabul edilmektedir. Çinko-fosfat kaplama performansına en yakın alternatif kaplama tipi polimer kaplamadır. Polimer kaplama, daha yalın üretimi teşvik edebilen, işletme maliyetlerini ve stokları azaltabilen ve karlılığı artırabilen çevre dostu bir kaplama yöntemidir. Bu çalışmada soğuk dövmede kullanılan çevreye daha az zararlı, yüzey temizleme ve kaplama yöntemleri incelenmiştir. Ayrıca, kumlama işlemi sonrası polimer kaplanmış hammaddeler ile asitle temizlenmiş ve çinko-fosfat kaplanmış hammaddeler ile üretilen cıvata örneklerinin yüzey kaliteleri incelenmiştir. Çevreye daha duyarlı bir yöntem olan polimer kaplamaya ait dövme performansının geleneksel yöntem olan çinko-fosfat kaplama ile benzer olduğu görülmüştür.

Anahtar Kelimeler: *Kumlama, asit temizleme, polimer kaplama, çinko-fosfat kaplama, soğuk dövme*

SURFACE PREPARATION METHODS USED IN COLD FORGING

Fatih Kocatürk, Doğuş Zeren, Sezgin Yurtdaş, M. Burak Toparlı, Cenk Kılıçaslan

Abstract

Pre-treatment and coating stages of raw material are essential applications for cold forging. The quality of the pre-treatment affects the adhesion, appearance, and corrosion resistance of the coating. Accordingly, the material flow during forging is also highly affected. Successful cold forging operation is closely related to an efficient raw material coating operation and the most common coating system is zinc-phosphate coating. Recently, zinc-phosphate coating has been accepted as an environmentally dangerous coating type. The most promising alternative of zinc-phosphate coating is polymer coating. Polymer coating is an environment-friendly coating method that can promote lean production, low operating costs and stocks and higher profitability. In this study, raw material pre-treatment and coating methods used in cold forging were examined. Moreover, the surface qualities of bolt samples produced with polymer coated after sandblasting raw materials and zinc-phosphate coated after acid cleaning raw materials were studied. The forging performance of the polymer coating, which is a more environmental-friendly method, has been found to be similar to that of the conventional method, the zinc-phosphate coating.

Keywords: *Sandblasting, acid cleaning, polymer coating, zinc-phosphate coating, cold forging*

1. Giriş

Soğuk dövme otomotiv parçalarının üretiminde sıklıkla kullanılan bir yöntemdir. Hammadde sarfiyatının düşük hacimde olması, üstün malzeme özellikleri ve dar geometrik toleranslar sunması, soğuk dövmeyle üretilen parçalara maliyet kazancı sağlamaktadır. Soğuk dövme işleminde malzeme akışını, dövme kuvvetini ve buna bağlı olarak kalıp ömrünü etkileyen en önemli faktör dövülen malzeme ile kalıplar arasındaki tribolojik durumdur. Neredeyse tüm çelik soğuk dövme işlemlerinde çinko fosfat kaplama üzerine sabun yağlama sistemi kullanılmaktadır. Bununla birlikte, bu yağlama sistemine ait kimyasal yan ürünlerin imha edilmesi zordur ve zararlı çevresel etkileri bulunmaktadır [1]. Literatüre bakıldığında kaplamalar üzerine önemli çalışmaların olduğu görülmektedir. Gariety ve diğerleri [1] çalışmasında çinko fosfat bazlı yağlama sistemine alternatif olacak üç yağlayıcı geliştirilmiştir: EC Homat, Daido AquaLub ve MCI Z-Coat. Bu yağlayıcıların performans değerlendirmesi geriye ikili bardak ekstrüzyon (İng. double cup backward extrusion) testi kullanılarak yapılmıştır. DEFORM sonlu elemanlar yazılımı kullanılarak farklı sürtünme faktörü değerleri için sürtünme faktörü kalibrasyon eğrileri yani zımba strokuna karşı bardak yükseklik oranı oluşturulmuştur. Geliştirilen üç yağlayıcının çinko fosfat kaplama ile karşılaştırılabilir veya ondan daha iyi performans gösterdiği bulunmuştur. Ngaile ve diğerleri [2] tarafından gerçekleştirilen çalışmada polimerik malzemelerden oluşan yeni bir metal şekillendirme yağlayıcısı geliştirilmiştir. Yağlayıcı, emülsiyon kopolimerizasyonu yoluyla geliştirilmiştir. Stearil metakrilat ve 2-hidroksietil metakrilat asit fosfatın ortak bileşimine sahip kopolimerler üç ikincil polimerle yapılmıştır: metil metakrilat, butil akrilat ve 2-hidroksietil metakrilat. Geliştirilen yağlayıcının performansı halka basma (İng. ring-compression) ve burma basma (İng. twist-compression) testleri kullanılarak gerçekleştirilmiş ve geliştirilen polimerik yağlayıcının performansı, dövme işleminde yaygın olarak kullanılan çinko-fosfat kaplama ve diğer üç ticari yağlayıcı ile karşılaştırılmıştır. Polimerik yağlayıcı, oda sıcaklığında yapılan tüm testlerde diğer yağlayıcılar ile yakın sonuçlar vermiştir. Gerçekleştirilen test sonuçlarına göre, geliştirilen yağlayıcının düşük deformasyon oranlı kafa şişirme ve ekstrüzyon işlemleri gibi soğuk dövme işlemleri için etkili bir şekilde kullanılabileceği gösterilmiştir.

Yağlayıcılar (kaplama), iş parçası ile kalıplar arasındaki sürtünme katsayısını düşürmek ve malzemenin kalıp üzerine yapışmasını önlemek amacıyla kullanılmaktadır. Soğuk dövme işleminde kullanılan kaplama iki işlevi yerine getirmelidir; i) düşük sürtünme katsayısı ve ii) kaplamanın yüzeyden kalkmasını önlemek için ana metale yüksek yapışma mukavemeti. Wang ve diğerleri [3] tarafından gerçekleştirilen çalışmada, iki işlevi ayırarak kaplama performansını değerlendirmek için bir test yöntemi önerilmektedir. Geliştirilen test yöntemi kullanılarak çok istasyonlu soğuk dövme işleminde yerinde kuru kaplamanın (İng. dry in-place coating) performansı çinko fosfat kaplama ile düşük karbonlu çelik numuneler kullanılarak gerçekleştirilen deneylerle karşılaştırılmıştır. Su bazlı yağlayıcıdan suyun buharlaştırılması ile uygulanan ve numune yüzeyinde tipik reaktif olmayan bir tip kaplama oluşturma işlemi yerinde kuru kaplama olarak adlandırılmıştır. Bu yöntemin "yerinde kuru kaplama" olarak isimlendirilme-

sinin sebebi kaplamanın bir dövme hattında yapılabilmesidir [4]. Yerinde kuru kaplamanın yapısı çinko fosfat kaplamasının yapısına benzemektedir, yani kaplama filmi iki katmandan oluşmaktadır: üst katman, kalıp yüzeyi ile sürtünmeyi azaltmakta ve alt katman, kalıp yüzeyinin doğrudan numune yüzeyi ile temasını engellemektedir. Alt tabakanın ana bileşeni suda çözünen bir alkali metal tuzudur. Alkali metal tuzu, çelik numune yüzeyi ile yüksek birleşme eğilimine sahiptir ve yüksek temas basıncı ve sıcaklığa karşı direnç göstererek numune yüzeyini fiziksel olarak korumaktadır. Üst tabaka, başlangıçta suda dağılan inorganik veya organik yağlama bileşenlerinden oluşmaktadır. İnorganik bileşenler için grafit, molibden disülfür ve çinko fosfat kullanılmaktadır. İnorganik bileşenler sıcaklık artışına ve temas basıncına karşı yüksek dirence sahiptir ve bu nedenle kapalı kalıp dövme gibi ağır çalışma koşullarında kullanılabilmektedir. Wang ve diğerleri [3] çalışmasında gerçekleştirilen tek aşamalı sürtünme testinde, yerinde kuru kaplamanın çinko fosfat kaplama ile aynı sürtünme eğilimi ortaya koyduğu gözlemlenmiştir. Geliştirilen çok aşamalı testle, çok aşamalı proseste kuru yerinde kaplamanın yüzeye yapışma kabiliyetinin çinko fosfat kaplamasından daha düşük olduğu şişirme adımında kaplamanın yüzeyden ayrılmasıyla ortaya çıkmıştır. Yerinde kuru kaplamanın yüzeye yapışma kabiliyeti, numune yüzeyinin ıslak kumlama kullanılarak ön işlemden geçirilmesi ile büyük ölçüde geliştirilmiş ve çinko fosfat kaplamasından daha iyi bir seviyeye getirilmiştir. Çok istasyonlu soğuk dövme işleminde numune yan yüzeyindeki kaplamanın performansını araştırmak için Wang ve diğerleri [5] çalışmasında yeni bir sıkma-ekstrüzyon tipi tribometre geliştirilmiştir. Çinko fosfat kaplama ve yerinde kuru kaplama kullanılarak yapılan deneysel sonuçlar, takımın yüzey pürüzlülüğünün yüzeyden kaplama ayrılması üzerindeki etkisini ifade etmek için azaltılmış tepe yüksekliği olan Rpk değerinin maksimum yükseklik değeri Rz'den daha uygun olduğunu göstermiştir. Yerinde kuru tip kaplamanın yüzeye yapışma kabiliyeti, kaplamadan önce iki aşamalı bir kumlama ile büyük ölçüde geliştirilmiş ve çinko fosfat kaplamanın tutunma kabiliyetinden daha iyi bir seviyeye ulaşmıştır. 23MnB4 dövme çeliği çinko fosfat üzerine sabun kaplama ve polimer bazlı yağlayıcı ile kaplanarak akış davranışları Tanrıkulu ve diğerleri [6] tarafından ileri yönde soğuk ekstrüzyon testleri yapılarak karşılaştırılmıştır. İş parçası ve kalıp arasındaki sürtünme katsayısını belirlemek için, simufact.forming sonlu elemanlar yazılımı kullanılarak ekstrüzyon test modelleri hazırlanmıştır. Sonuçlar, polimer bazlı kaplamanın tribolojik performansının geleneksel çinko fosfat üzerine sabun kaplamasına çok yakın olduğunu göstermiştir. Bay ve diğerleri [7] tarafından yayınlanan çalışmada da soğuk, ılık ve sıcak dövme işlemlerinin yanı sıra sac şekillendirme ve delme gibi operasyonlarında da kullanılan çevreye zararlı yağlayıcıların yerine geçebilecek çevreye daha az zararlı yağlayıcıların olduğundan bahsedilmiştir.

Farklı yağlayıcıların sürtünme kuvvetine olan etkisi yaygın olarak uygulanan üç yağlayıcı (molibden disülfid, polimer, vaks ve inorganik tuz bileşimi) için ikili-bardak-ekstrüzyon (İBE, İng. double-cup-extrusion) testleri gerçekleştirerek incelenmiştir [8]. Klasik yağlama yöntemi olan fosfat kaplamanın sürtünme faktörü üzerindeki etkisi de araştırılmış, ancak bu kaplamanın araştırılan yağlama sistemlerinin yağlama özellikleri için önemli bir gelişme sağlamadığı bulunmuştur. İBE testleri sonucuna göre molibden disülfid bazlı yağlayıcı en yüksek sürtünme koşullarını ortaya çıkarırken vaks ve polimer esaslı yağlayıcılar çok daha düşük sürtünme kaybı oluşmasını sağlamıştır. Lorenz ve diğerleri [8] İBE test sonuçlarına en yakın tribolojik koşullar için ZWEZ-Lube PD 470 gibi polimer bazlı yağlayıcıları önermişlerdir. Polimer kaplı metal ekstrüzyonunu başarıyla gerçekleştirmek için gerekli olan işlem parametrelerini analiz etmek için üst sınır yöntemini uygulayan yeni bir matematiksel model Wang ve diğerleri [9]

çalışmasında geliştirilmiştir. Soğuk dövme işleminde kullanılan sert kaplamalı kalıplara uygulanan mikro tekstürlerin kalıp ömrüne olan etkisi Geiger ve diğerleri [10] tarafından araştırılmıştır. Yapışma mukavemeti testlerinin sonuçları nedeniyle, kalıplar önce kaplanmış ve daha sonra tekstüre edilmiştir. Basma testi ve genel tasarım kriterleri ile yapılan deneylerin sonuçlarına dayanarak, soğuk dövme zımbalarına tekstürler uygulanmış ve endüstriyel seri üretim koşulları altında bir test merkezinde testler gerçekleştirilmiştir. Test sonuçlarına göre kalıp ömrünün mikro tekstür etkisi ile arttırıldığı gösterilmiştir. Soğuk dövme işlemlerinde kaplamalı kalıplara uygulanan doğrudan lazer tekstüre (İng. direct laser texturing) yönteminin triboloji üzerindeki etkisi Popp ve Engel [11] çalışmasında araştırılmıştır. Gerçekleştirilen saha testlerinde kalıp ömrünün bazı durumlarda %300'ün üzerine çıkabileceğini kanıtlamışlardır. Soğuk dövme işlemleri için sıcaklığın çevreye duyarlı tribolojik yağlayıcılar üzerindeki etkisi Groche ve diğerleri [12] tarafından araştırılmıştır. İncelenen tuz vaks kaplamanın ve polimerin performansının sıcaklıktan büyük ölçüde etkilendiği gözlemlenmiştir. Her iki yağlayıcı için de sürtünme katsayısı 100 °C yüzey sıcaklığına ulaşıldığında %30 azalmıştır. Tuz vaks yağlayıcısı için 25 °C yüzey sıcaklığına kıyasla %50 oranında bir azalma ile 200 °C yüzey sıcaklığında en düşük sürtünme katsayısı gözlemlenmiştir, ancak üçüncü numuneden sonra yapışma oluşmuştur. Yapılan çalışmada kayganlaştırıcıdan bağımsız olarak kayar plakada veya numunede 125 °C'nin altındaki sıcaklıklarda aşınma tespit edilmemiştir. Bu nedenle, tek banyo ile uygulanabilen her iki yağlayıcının düşük konsantrasyonda ve düşük yağlayıcı miktarında bile düşük sıcaklıklarda iyi bir performans gösterdiği gözlemlenmiştir. 150 °C'nin üzerindeki sıcaklıkların kaplama performansının kritik olduğu kanıtlanmıştır. Kalıp-iş parçası yüzeyindeki gerçek sıcaklık bilgisi ve kontrolünün, uygulanan yağlayıcı ve tribolojik yük için ideal bir sıcaklık ayarlanabilmesini sağlayarak soğuk dövme işlemlerini iyileştirebileceği belirtilmiştir. İş parçası üzerinde kalan yağlayıcı miktarının sürtünme katsayısı üzerindeki yüksek etkisi bir soğuk dövme tribometresi olan kayma basma testi (İng. sliding compression test) kullanılarak Müller ve diğerleri [13] tarafından gösterilmiştir. Ayrıca, önceden yağlanmış takımlarla yapılan testlerin sürtünmeyi azalttığı gösterilmiş ve kaba takım yüzeyleriyle yapılan testlerin sonuçları sunulmuştur. Kaba yüzeylerle sürtünme katsayısı araştırması yapılabilmesi için önceden yağlanmış takımların kullanılması gerektiği aksi takdirde yapışma görüleceği belirtilmiştir. Bununla birlikte, literatürdeki söz konusu araştırmaların aksine, kumlanmış takım yüzeyleri ile sürtünme katsayısının optimizasyonu mümkün olmamıştır. Yanlış bir yağlama işlemi sonrası numune üzerindeki kaplama çok ince ise ya da numuneye uzun kayma mesafesi uygulanmış ise kaba yüzeyli bir takım pürüzsüz olandan daha fazla yağlayıcı sağlayabilmektedir [13]. Sürtünme katsayısının belirli değerlerde olması işlem performansını etkilemektedir. İş parçası ile kalıplar arasındaki kritik sürtünme katsayısı hammaddenin dövme işleminden önce özel operasyonlarla temizlenmesi ve kaplanması ile istenilen değerlere getirilmektedir. Bu işlem bütününe yüzey işlem adı verilmektedir. Yüzey işlem iki adımda gerçekleştirilmektedir: i) yüzey temizleme işlemi ile hammadde yüzeyindeki tüm pas ve kir giderilmektedir, ii) temizleme işleminden sonra hammadde yüzeyi fosfat ya da polimer gibi kimyasallarla kaplanmaktadır. Yüzey temizleme işlemi genellikle hammadde (kangal olarak da adlandırılmaktadır) asit ve su dolu havuzlara sırasıyla daldırılması şeklinde gerçekleştirilmektedir. Diğer bir metotta ise küçük çelik bilyelerin yüksek hızlarda hammadde yüzeyine püskürtülmesiyle uygulanan (kumlama adı verilmektedir) yüzey temizleme işlemi gerçekleştirilmektedir. Kaplama işlemi hammaddenin sırasıyla kaplama kimyasalının bulunduğu havuzlara daldırılmasıyla uygulanmaktadır. Bu işlem sayesinde hammaddenin oksijen ile teması kesilerek paslanma önlenmektedir. Çinko-fosfat kaplama yöntemi daldırma metoduyla gerçekleştirilmekte, hammadde

kangalları her bir banyonun içine daldırılarak belli sürelerde bekletilmektedir. Klasik bir çinko-fosfat kaplama prosesi şu şekilde sıralanabilir: asitle yüzey temizleme (hidroklorik ya da sülfürik asit), durulama, aktivasyon, çinko-fosfat kaplama, nötralizasyon, reaktif sabun banyosu ve kurutma. Çinko fosfat kaplama işlemi yüksek seviyelerde atık su, enerji tüketimi ve fosfor bileşiği oluşmasına sebep olmaktadır [14]. Polimer kaplama reaktif olmayan, su bazlı ve sürdürülebilir bir yüzey işlem yöntemidir. Tek adımlı bir işlem olarak, polimer kaplama tüm durulama adımlarını ortadan kaldırdığı için su tasarrufu sağlamakta ve aynı zamanda suyu ısıtmaya gerek kalmadığı için daha az enerji kullanmakta ve CO2 salınımını azaltmaktadır. Kaplama, herhangi bir reaksiyon olmadan fiziksel olarak yüzeye yapıştığından kaplamadan sonraki kurutma aşamasında ortaya çıkan su buharıdır. Ayrıca, soğuk şekillendirilmiş cıvatalar son ısıl işlem için defosfatlama işlemine alındığında, polimer kaplamanın çıkarılması daha kolay olduğundan daha düşük konsantrasyonda defosfatlama kimyasalı kullanılır ve maliyet kazancı sağlanmış olur [15]. Hammadde ön işlem ve kaplama aşamaları soğuk dövme için elzem uygulamalardır. Ön işlem aşaması, kaplama öncesi ham madde yüzeyine uygulanan işlemlere verilen isimdir. Ön işlemin kalitesi, kaplamanın yapışmasını, görünümünü, nem ve korozyon direncini etkiler. İyi bir ön işleme sahip kaplama ömrü basit hammadde temizliği (asitle yıkama) sonrası yapılanla karşılaştırıldığında, 4-5 kat daha uzun ömre sahiptir.

Bu makale, soğuk dövme uygulamalarında önem arz eden yüzey işlem prosesi hakkında detaylı bilgiler içeren ve çevre dostu yağlayıcılar hakkında literatürde yapılan çalışmaları özetleyen bir derlemedir. Çalışma kapsamında, soğuk dövmede kullanılan hammadde yüzey işlemi sırasında uygulanan asitle ve kumlama yöntemiyle yüzey temizleme metotları ile çinko-fosfat ve polimer kaplama metotları incelenmiştir.

2. Yüzey İşlem Metotları

Bu bölümde soğuk dövme yönteminde kullanılan hammaddelere uygulanan yüzey işlem metodu iki ana başlık altında incelenmiştir: Yüzey temizleme yöntemleri ve yüzey kaplama yöntemleri. Yüzey kaplama yöntemi öncesinde uygulanan asitle temizleme ve kumlama yöntemiyle yüzey temizleme metotları açıklanmış, yüzey kaplama yöntemi olarak çinko-fosfat ve polimer kaplama yöntemleri açıklanmıştır.

2.1. Yüzey temizleme yöntemleri

Soğuk dövme işleminde kullanılacak olan kangalların ilk gördüğü işlem yüzey temizleme işlemidir. Yüzey temizleme işleminin amacı kangalların üzerinde zamanla oluşan Şekil 1'de görülen yağ, pas ve tufallerin temizlenerek kaplamaya hazır hale getirilmesidir. Yüzeyi iyi temizlenmiş hammadde kullanımı kaplama havuzlarında oluşan kirlenmeyi engellemektedir ve bu sayede kullanılan kaplama sıvıları daha uzun süre kullanılabilir. Bilinen en yaygın yüzey temizleme yöntemi asitle temizleme yöntemidir ve kullanılan asitler genellikle hidroklorik veya sülfürik asitlerdir. Asitle temizlemeye alternatif olarak kullanılan diğer yüzey temizleme metodu kumlama yöntemidir. Kumlama yönteminde asit kullanılmadığı için hem çevreye daha az zarar vermekte hem de su kullanımını ortadan kaldırarak su tasarrufu sağlamaktadır.

Şekil 1. Kangal yüzeyindeki pas ve tufaller.

2.1.1. Asitle temizleme

Asitle hammadde temizliği sıvı dolu havuzlara kangalların daldırılmasıyla gerçekleştirilmektedir. Temizleme işlemi belirli sıcaklıktaki su ve asit dolu havuzlara sırasıyla daldırılarak ve belirli süre bekletilerek yapılmaktadır. Tipik bir asitle temizleme işlemi şu şekildedir: Öncelikle basınçlı su ile hammadde yıkanarak üzerindeki pas ve tufaller kabaca temizlenmekte, daha sonra sıcaklığı 30°C - 70°C arasında olan su havuzunda durulama yapılmakta ve asit havuzuna alınarak belirli bir süre bekletilmektedir. Son olarak tekrar basınçlı suyla ve su havuzuna daldırılarak durulama yapılmaktadır. Hammadde yüzeyinin yeteri kadar temizlenmemesi halinde asit ve durulama havuzlarına tekrar daldırılarak işlem tekrarlanabilmektedir.

2.1.2. Kumlama yöntemiyle temizleme

Klasik ön işlem yöntemi olan asitle yıkama metodunun alternatifi kumlama yöntemidir. Kumlama yönteminde numune yüzeyine yüksek hızda püskürtülen kum parçacıkları yüzeydeki oksit tabakasını azaltır, yüzey salgısını ortadan kaldırır ve yüzey katmanda yerel plastik deformasyon oluşumunu sağlar. Ek olarak, yüzey altı bölgede bir sıkıştırılmış artık stres katmanı oluşur. Yapılan çalışmalarda östenitik çeliklerde kumlama kaynaklı mikro yapı değişikliklerinin de meydana geldiği gözlemlenmiştir [2].

Şekil 2. *Norm Cıvata tesislerinde kullanılan kumlama makinesi.*

Kumlama, yüksek hızlı kum akışının etkisiyle bir yüzeyi temizlemek ve pürüzlü hale getirmek için kullanılır [3]. Püskürtme malzemelerini (bakır cevheri, kuvars kumu, zımpara kumu, demir kumu, hainan kumu) işlenecek iş parçasının yüzeyine yüksek hızda püskürtmek için basınçlı hava kullanılır ve bu şekilde iş parçası yüzey formunda değişiklik meydana gelir. İş parçası yüzeyi üzerindeki aşındırıcı maddenin etkisi ve kesme hareketi nedeniyle, iş parçası yüzeyi temiz olmakla birlikte farklı pürüzlülükte gelebilmektedir. Kumlamayla iş parçası yüzeyinin mekanik özellikleri iyileştirilir, böylece iş parçasının yorulma direncini ve iş parçası ile kaplama arasındaki yapışmayı arttırırken kaplamanın akışını da kolaylaştırmaktadır. Hammaddeye kaplama işlemi öncesinde kumlama yapılırsa hammadde yüzeyindeki tüm kirleri vs. temizleyebilir ve iş parçası yüzeyinde pozitif özellikler sunan pürüzlü bir yüzey oluşturabilir. Hammadde kaplama kalitesini büyük ölçüde iyileştirmek ve kaplamanın yapışmasını daha güçlü ve kaliteli hale getirmek için farklı boyutlarda aşındırıcılar kullanılabilir. İş parçasının ısıl işlemden sonra kumlama işlemiyle temizlenmesi ve parlatılması iş parçası yüzeyindeki (oksit veya yağ kalıntıları vb.) tüm kirleri temizleyebilir. İş parçasının yüzey parlatma amacıyla kumlanması iş parçasının daha parlak görünmesini sağlayabilir. Kumlama çapak alma amacıyla kullanılırsa, iş parçası yüzeyindeki küçük talaşları temizleyebilir ve iş parçası yüzeyini daha düzgün hale getirebilir. Dahası, kumlama işlemi iş parçası yüzeyinin birleşme noktalarında oluşan küçük köşelere uygulanarak daha pürüzsüz bir yüzey elde edilebilir.

2.2. Yüzey kaplama yöntemleri

Karmaşık geometriler ve hassas ölçülerde üretim yapılması soğuk dövme prosesinde iş parçasına uygulanan kaplama işleminin sürtünmeyi azaltarak kalıp ömrünü uzatmak için daha yüksek mekanik ve ısıl gerilmelere dayanmasını gerekli kılmaktadır. Soğuk dövmedeki tribolojik koşullar son derece ağırdır. Yüksek sıcaklıklardaki kalıp yüzeyleri ve yüksek yüzey genleşme faktörleriyle birleşir. Bu nedenle, hammadde üzerindeki kaplama tribolojik olarak zor koşullara maruz kalır. Bu ağır koşullar altında iyi yüzey özelliklerine sahip olmayan hammadde, iş parçasının hatalı üretilmesine ya da kalıbın hasar görmesine sebep olur. Soğuk dövme prosesinin başarılı bir şekilde uygulanması verimli bir hammadde kaplama işlemiyle yakından ilgilidir. Yukarıda belirtilen tüm koşullara karşı etkinliği ile bilinen en yaygın kaplama sistemlerinden biri çinko-fosfat üzerine sabun kaplamasıdır.

2.2.1. Çinko-Fosfat kaplama

Çinko-fosfat kaplama en çok kullanılan yüzey işlem kaplama yöntemi olarak bilinmektedir. Çinko-fosfat kaplama, bir metal ile bir kimyasal çözeltinin reaksiyonu sonucunda oluşmaktadır. Kaplama esnasında sıcaklık, banyo konsantrasyonu, süre, pH, toplam ve serbest asit dikkat edilmesi gereken noktalardır [4]. Çinko-fosfat kaplama işlemi 35-98°C sıcaklıkta 5-10 dakika ve %3-20 konsantrasyonlarda yapılabilmektedir. Çinko-fosfat kaplamanın iyi şekilde yapılması için kangalların (hammaddelerin) pas, yağ ve tufallerden arındırılmış olması gerekmektedir. Bu nedenle çinko-fosfat kaplama öncesi kangalı pas ve tufalden arındırmak amacıyla yüzey temizleme işlemi uygulanmaktadır. Tel çekme işlemi için çinko-fosfat kaplama kalınlığı 7 - 15 g/m² arasında olması gerekmektedir [5]. Çinko-fosfat kaplama işleminden en iyi verimin alınabilmesi için yapılan kaplamanın ince ve homojen bir yapıda olması gerekmektedir. Tel üzerindeki kaplama ince kristalli veya homojen değil ise fosfat banyosu öncesinde aktivasyon kullanılmalıdır. Fosfat banyosu öncesi uygulanan aktivasyon, çinko fosfat çekirdek yapısını etkileyerek kaplamanın daha ince ve pürüzsüz olmasını sağlamaktadır. Ayrıca, alkali titanyum tuzları içeren aktivasyon banyosu ince ve yoğun bir çinko-fosfat kaplamasının oluşmasını sağlayarak kalın kristalli kaplamalarda görülen tozlanma problemini de ortadan kaldırmaktadır. Metal yüzeyin fosforik asit ile eritilmesi sonucu oluşan asit-baz etkileşimi çinko-fosfat kaplama reaksiyonu olarak kabul edilmektedir. Fosforik asit etkisi ile metal eridikçe asit havuzunun pH değerinde artış gözlemlenmektedir. Gerçekleşen kimyasal reaksiyon sonucu oluşan metalik fosfat metal üzerinde çözünmez bir tabaka oluşturur ve metalik renkli bir görünüm elde edilir. Teller çinko-fosfat kaplama işleminden sonra nötralizasyon banyosuna alınmaktadır. Buradaki amaç tellerin pastan korunması ve tel üzerinde tuz oluşumu sağlayarak reaktif sabunun daha iyi tutunmasını sağlamaktadır. Çinko-fosfat kaplamanın son aşamada teller reaktif sabun banyosuna alınarak çekime hazır hale getirilmektedirler. Çinko-fosfat kaplama daldırma metoduyla, kangallar her bir banyonun içine daldırılarak belli sürelerde bekletilerek gerçekleştirilmekte ve bu şekilde kaplama sağlanmaktadır (Şekil 3).

Klasik bir çinko-fosfat kaplama proses hattı sırası ile şu şekildedir:

* Pas, yağ ve tufal alma
* Durulama
* Aktivasyon

- Çinko-fosfat kaplama
- Nötralizasyon
- Reaktif sabun banyosu
- Kurutma

Şekil 3. *Çinko-fosfat kaplama tesisi.*

Fosfat banyosundaki demir yoğunluğunu azaltmak için hızlandırıcı veya serbest asit düzenleyici kullanılmaktadır. Fosfat banyolarında zamanla kangallar üzerinden temizlenen pas, yağ ve tufaller çamur oluşturur. Bu çamur belli zamanlarda temizlenmeli veya bir filtre sistemi ile sürekli dışarı alınmalıdır. Çinko-fosfat kaplanmış kangallar soğuk dövme öncesi tel çekme işlemine tabi tutulmaktadır. Hammadde yapısındaki karbon oranı çinko-fosfat kaplama kalınlığını belirlemektedir. Çinko-fosfat kaplı kangalların çekiminde uygun fosfat kalınlığının sağlanması gerekmektedir. Çinko-fosfat kaplama kalınlığının aşırı yüksek olması sürtünme katsayısını arttırırken, düşük kaplama kalınlığı da çoklu tel çekimlerinde kaplamanın tamamen kalkmasına ve başka sorunların oluşmasına neden olmaktadır. Çinko-fosfat kaplamanın amacı haddeden geçen telin haddeye zarar vermesini önlemek ve çekilen telin korozyon direncini yükseltmektir. Çinko-fosfat kaplama sayesinde tel çekim hızı da artmaktadır. Soğuk dövmede kullanılacak olan kangalların çinko-fosfat kaplanmasının en önemli tercih sebebi, çinko-fosfat kaplamanın metal yüzeye çok iyi tutunması ve çoklu çekim sonrasında dahi devamlılığını korumasıdır. Çinko-fosfat kaplamanın kristal yapısı film kırılmaları ve bozulmalarını engellemekte ve sonraki aşamalarda uygulanacak yağlayıcı ve sabunlar için mükemmel bir zemin oluşturmaktadır. Çinko-fosfat kaplanan kangalların kullanılması sayesinde tel çekim kalıplarının ve haddenin aşınımı azalmakta ve bu sayede hadde ve kalıp ömürleri uzamaktadır. Soğuk çekim sonrası yüzeydeki fosfat tabakası hem iyi bir yüzey kaplaması oluşturmakta hem de depolama ve nakliye sırasında yüksek bir korozyon direnci sağlamaktadır. Her ne kadar çinko-fosfat kaplamanın performansı zaman içinde kanıtlanmış olsa da, son zamanlarda hem işyeri hem de küresel çevre açısından çevreye zarar veren bir kaplama türü olarak kabul edilmektedir. Endüstriyel üretimin küreselleşmesi dövme endüstrisini daha iyi bir çözüm aramaya zorlamaktadır. Güçlü yapışma ve gelişmiş korozyon koruması gibi avantajları ile bilinmesine rağmen, çinko-fosfat kaplama birçok dezavantaja da sahiptir. Çinko-fosfat kaplama işleminin en büyük dezavantajı, tehlikeli atık oluşturan ve bu atığın işlenmesini ya da elden

çıkarılmasını gerektiren farklı kimyasallar içermeleridir. Kaplama işlemi sırasında kullanılan banyolar kurşun ve kadmiyum gibi ağır metallerle kirlenir. Hem banyo hem de atık sularda tehlikeli kirleticiler içeren çamur birikmektedir. Banyoların ve kullanılmış suların çoğu geri dönüştürülememekte ve tehlikeli atık olarak işlem görmektedir. Bu olumsuzluklara ek olarak, çinko-fosfat kaplama işlemi, yeni kaplama sistemlerden daha fazla miktarda su, enerji ve daha uzun işlem süresi gerektirmektedir. Şüphesiz, dövme öncesi yapılan çinko-fosfat kaplama işlemi soğuk dövme parçasının kalitesi için önemli olmasına rağmen beraberinde bir takım çevresel kaygı uyandırmaktadır. Bu nedenle lider şirketler alternatif süreçler üzerinde çalışmaya başlamışlardır. Çinko-fosfat kaplama sistemine alternatif olarak polimer bazlı kaplamalardan söz edilebilir.

2.2.2. Polimer kaplama

Basma ve ekstrüzyon testleri ile yeni bir kaplama sisteminin sürtünme katsayısının belirlenebilir. Kaplamanın iş parçası yüzeyine tutunmasının iyi olduğu ve kalıp aşınmasının yüksek olduğu soğuk dövme koşulları için yüksek kaliteli bir kaplama çözümü bulmak oldukça güçtür. Kaplama maddesinin kimyasal bileşimi, tribolojik koşullar üzerinde önemli bir etkiye sahiptir. Ayrıca, son yüzey çok önemlidir çünkü yüzey pürüzlülüğünün azalması sürtünmeyi önemli ölçüde azaltmaktadır. Polimer kaplama tek veya çok aşamalı soğuk dövme hatları için uygundur [6]. İş parçasının deformasyonu arttıkça, kontrol parametreleri daha hassas hale gelecektir. Bu nedenle, üretimde kapsamlı deneyime sahip nitelikli bir işgücü ile bu yeni kaplama türünden oldukça faydalanılabilir. Polimer kaplamanın faydaları şu şekilde sıralanabilir: i) Çevre dostu olması: Ağır metaller, çamurlar ve tehlikeli atıklar bulunmadığından, hem iş gücü hem de küresel çevre için oldukça emniyetli bir tribolojik sistemdir. ii) Maliyette düşüş sağlaması: Kaplama işleminin toplam maliyetini düşürür: Daha düşük enerji ve su tüketimi sağlamakla beraber atıkların masraflı arıtımına ihtiyaç bulunmamaktadır. iii) Devam eden işleri azaltır: Polimer kaplama, neme duyarlı kuru bir işlemdir. Bu nedenle, kaplamalı hammaddeler kesin olarak tanımlanmış bir süre içinde dövülmelidir ki bu da bekleyen işlerin artmasını engeller. iv) İşleme kolaylığı sağlar: Polimer kaplamanın sonraki işleme operasyonlarında işlenmesi çok daha kolaydır. Çinko-fosfat kaplama, tornalama gibi talaşlı imalat işlemlerinde fazla toz oluşumuna sebebiyet vermektedir. Soğuk dövme endüstrisi, daha iyi çözümler aramaya kendini yönlendirmiştir ve çinko-fosfat kaplama sistemi ve bu sistemin tehlikeli atıklarıyla ilgili sorunu en kısa sürede çözmeye zorlamıştır. Sonuç olarak, polimer kaplama, daha yalın üretimi teşvik edebilen, işletme maliyetlerini ve stokları azaltabilen ve karlılığı artırabilen çevre dostu bir kaplama yöntemi olmaya aday olduğu söylenebilir.

3. Örnek Uygulama

Bu bölümde Norm Cıvata Salihli fabrikasında uygulanmakta olan kumlama ve polimer kaplama süreçlerinden bahsedilmiş ve bu yöntemle üretilen cıvatalar ile çinko-fosfat kaplı cıvatalar karşılaştırılmıştır. Norm Cıvata Salihli fabrikasında Şekil 2'de verilen kumlama makinesi bulunmaktadır. Bu makinede işlenen kangallar iki kollu ve kendi ekseninde dönebilen tezgâha yerleştirilir ve değişmeli olarak çok sayıda metal kum tanesinin kangalın tüm yüzeyine yüksek hızda püskürtüldüğü kumlama odasına taşınır. Makine tezgâhının iki kollu olmasından dolayı aynı anda iki kangal hammadde kumlama işlemine alınabilir ve kangallar tezgâha açılarak yerleştirildiği için kumlama işlemi hammaddenin bütün yüzeylerinde eşit olarak uygulanabil-

mektedir. Şekil 4'de verilen tezgâhın kangal taşıyan kolundan iki adet bulunmaktadır. Görseldeki kolun simetriği tezgâhın içindedir. Kapı görseldeki eksende dönmekte olup kangal içeri alınmakta ve kapının arkasındaki simetrik kol dışarı çıkmaktadır. Bir kangal kumlanırken diğer koldaki kangal da değiştirilmektedir.

Şekil 4. Kumlama makinesi tezgâh kolu.

Kumlama bölmesinin içindeki kolun dönüşü, kangalın aşındırıcı etkiye en etkili şekilde maruz kalmasını sağlamak için programlanmıştır. Tezgâhın dışta kalan kolunun dönüşü operatör tarafından kontrol edilebilir. Tezgâh kollarının zıt pozisyonda olması aynı anda iki kangalın kumlanmasına ve bir kangal kumlanırken diğer tarafta kangal yükleme / boşaltma işleminin yapılabilmesine olanak sağlar. Kumlama işleminde kangallar açılarak kumlama tezgâhının kollarına yerleştirilmektedir (Şekil 5). Kumlama işlemi uygulanan kangalın kumlama öncesi ve sonrası görüntüleri Şekil 6'da verilmiştir. Kumlama işlemi sonrasında parlak ve hafif pürüzlü bir yüzeye sahip hammadde elde edilmiştir.
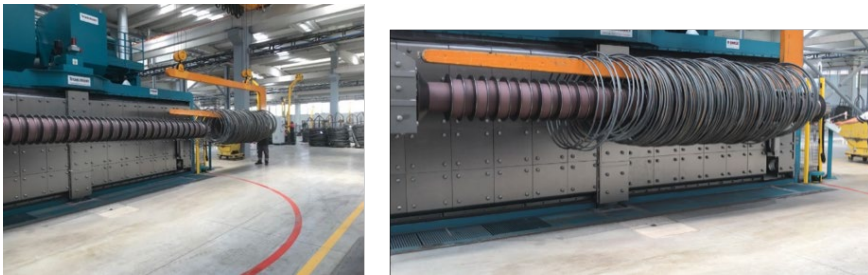
Şekil 5. Kangalların açılarak kumlama tezgâhının kollarına takılması.

Şekil 6. Kangal görünümü a) Kumlama öncesi, b) Kumlama sonrası.

Kumlama makinesinde makine hızı ve kumlama süresi olmak üzere iki ayar bulunmaktadır. Kumların püskürtüldüğü makinenin hız kapasitesi 1800–3000 dev/dk'dır. Kumlama süresi ise malzemenin tedarikçisine göre ve malzeme çapına göre ayarlanmaktadır. Hammadde çapı küçüldükçe kangal sarımının sıkılaşması sebebiyle kumlama süresi uzatılmaktadır. Bununla beraber, hammadde tonajı arttıkça da kumlama süresi artabilmektedir. Kumlama makinesinde hammadde temizlemek için kum olarak isimlendirilen düşük karbonlu çelik bilyeler kullanılmaktadır. Düşük karbonlu çelik bilyeler, başlangıçta 43-44 HRC sertliğinde iken çalışma sırasında ortalama 50 HRC sertlik değerine ulaşmaktadır. Bu nedenle temizleme performansı artmaktadır. Kumlama bilyeleri tezgâh çalıştıkça devir daim ettirilerek tekrar kullanılmaktadır, ancak bir süre sonra makine içindeki tamburdan geçebilecek kadar küçülen taneler tezgâh tarafından hurdaya ayrılmaktadır (Şekil 7).

Şekil 7. (a) Kullanılmamış bilye yüklemesi, (b) Tekrar kullanılabilen bilyeler, (c) Hurda bilyelerin biriktirilmesi.

Kumlama sonrası kangallar önce polimer havuzuna alınmaktadır. Polimer fırınından çıkan kangallar haddelenmektedir. Şekil 8'de fosfat ve polimer kaplı malzemeden üretilen cıvata numuneleri gösterilmektedir. Polimer kaplı malzemeden üretilen cıvatanın daha parlak ve pürüzsüz bir yüzeye sahip olduğu görülmektedir.

*Şekil 8. Dövme hattından alınan ürün formu (a) Çinko-fosfat kaplı, (b) Polimer kaplı.*

4. Sonuçlar

Soğuk dövmede kullanılacak olan hammaddeye uygulanan yüzey işlemin kalitesi soğuk dövmede kullanılan kalıpların ömrünü ve üretilen ürünün kalitesini doğrudan etkilemektedir. Bu çalışmada yüzey işlem metotları yüzey temizleme ve yüzey kaplama yöntemleri olmak üzere iki ana başlık altında incelenmiştir. Geleneksel asitle yüzey temizleme ve bu yöntemin alternatifi olarak ortaya çıkan kumlama yüzey temizleme yöntemleri incelenmiştir. Asitle yüzey temizleme sonucunda asit banyolarında oluşan kimyasal atıkların geri dönüştürme maliyetleri ve çevreye verdiği zararlar, yoğun su ve suyu belli derecelere kadar ısıtmak için enerji kullanılması global ölçekte ve firmalar nezdinde yeni yüzey temizleme yöntemi arayışının başlamasına neden olmuştur. Bu kapsamda su ve kimyasal madde kullanmadan bir kumlama odasında küçük metal bilyeleri hammadde yüzeyine yüksek hızlarda püskürterek hammadde yüzeyini temizleyen kumlama yöntemi ortaya çıkmıştır ve birçok endüstriyel uygulamada bu yöntem kullanılmaktadır.

Yüzey kaplama yöntemlerinden ilk olarak klasik çinko-fosfat kaplama yöntemi incelenmiştir. Çinko-fosfat kaplama soğuk dövmede kullanılacak olan kangalların metal yüzeyine çok iyi tutunduğu için ve çoklu çekim sonrasında dahi devamlılığını korumasından dolayı tercih edilmektedir. Çinko-fosfat kaplanan kangalların kullanılması sayesinde tel çekim kalıplarının ve hadde kalıbının aşınımı azalmakta ve bu sayede kalıp ömürleri uzamaktadır. Soğuk çekim sonrası yüzeydeki fosfat tabakası hem iyi bir yüzey kaplaması oluşturmakta hem de depolama ve nakliye sırasında yüksek bir korozyon direnci sağlamaktadır. Güçlü yapışma ve gelişmiş korozyon koruması gibi avantajları ile bilinmesine rağmen, çinko-fosfat kaplama birçok dezavantaja da sahiptir. Çinko-fosfat kaplama işleminin en büyük dezavantajı, tehlikeli atık oluşturan ve bu atığın işlenmesini ya da elden çıkarılmasını gerektiren farklı kimyasallar içermeleridir. Kaplama işlemi sırasında kullanılan banyolar kurşun ve kadmiyum gibi ağır metal-

lerle kirlenir. Hem banyo hem de atık sularda tehlikeli kirleticiler içeren çamur birikmektedir. Banyoların ve kullanılmış suların çoğu geri dönüştürülememekte ve tehlikeli atık olarak işlem görmektedir. Bu olumsuzluklara ek olarak, çinko-fosfat kaplama işlemi, yeni kaplama sistemlerden daha fazla miktarda su, enerji ve daha uzun işlem süresi gerektirmektedir. Çinko-fosfat kaplama sistemine alternatif olarak polimer bazlı kaplamalardan söz edilebilir. Polimer kaplama yöntemi makalede bahsedildiği üzere birçok avantaja sahiptir. Bu nedenle uygulanacak olan yüzey temizleme ve kaplama türü hassasiyetle seçilmedir.

Referanslar

[1] Gariety, M., Ngaile, G., Altan, T. 2007. "Evaluation of New Cold Forging Lubricants without Zinc Phosphate Precoat," Int. J. Mach. Tools Manuf., vol. 47, no. 3–4, p. 673–681.

[2] Ngaile, G., Cochran, J., Stark, D. 2007. "Formulation of Polymer-Based Lubricant for Metal Forming," Proc. Inst. Mech. Eng. Part B J. Eng. Manuf., vol. 221, no. 4, p. 559–568.

[3] Wang, Z. G., Komiyama, S., Yoshikawa, Y., Suzuki, T., Osakada, K. 2015. "Evaluation of Lubricants without Zinc Phosphate Precoat in Multi-Stage Cold Forging," CIRP Ann., vol. 64, no. 1, p. 285–288.

[4] Yamaguchi, H., Imai, Y., Yoshida, M. 2002. "Metallic Material for Plastic Working With Gradient Two-Layer Lubricant Coating Film and Process for Producing the Same," Patent no. WO2002072345A1.

[5] Wang, Z. G., Komiyama, S., Yoshikawa, Y. 2014. "Development of Upsetting-Extrusion Type Tribometer for Evaluating Lubrication Coating Performance in Cold Forging," Adv. Mater. Res., vol. 966–967, p. 281–289.

[6] Güneş, S., Tanrıkulu, B., Özuğurlu, D. C., Kılıçaslan, C., İnce, U. 2018. "A Comparative Study : Zinc Phosphate-Soap Coating Versus Polymer Based Coating in Cold Forward Extrusion," Manisa Celal Bayar University II. International University Industry Cooperation, R&D and Innovation Congress, p. 14–15.

[7] Bay, N., Azushima, A., Groche, P., Ishibashi, I., Merklein, M., Morishita, M., Nakamura, T., Schmid, S., Yoshida, M. 2010. "Environmentally Benign Tribo-Systems for Metal Forming," CIRP Ann., vol. 59, no. 2, p. 760–780.

[8] Lorenz, R., Hagenah, H., Merklein, M. 2018. "Experimental Evaluation of Cold Forging Lubricants Using Double-Cup-Extrusion-Tests," Mater. Sci. Forum, vol. 918, p. 65–70.

[9] Wang, J., Shah, R., Huang, Y.-H., Chang, D.-F. 2009. "An Analysis of Polymer Coated Metal Rod Extrusion," J. Manuf. Sci. Eng., vol. 131, no. 1, p. 0110121–0110129.

[10] Geiger, M., Popp, U., Engel, U. 2002. "Excimer Laser Micro Texturing of Cold Forging Tool Surfaces - Influence on Tool Life," CIRP Ann., vol. 51, no. 1, p. 231–234.

[11] Popp, U., Engel, U. 2006. "Microtexturing of Cold-Forging Tools - Influence on Tool Life," Proc. Inst. Mech. Eng. Part B J. Eng. Manuf., vol. 220, no. 1, p. 27–33.

[12] Groche, P., Zang, S., Müller, C., Bodenmüller, D.. 2015. "A Study on the Performance of Environmentally Benign Lubricants at Elevated Temperatures in Bulk Metal Forming," J. Manuf. Process., vol. 20, p. 425–430.

[13] Müller, C., Rudel, L., Yalcin, D., Groche, P. 2014. "Cold Forging with Lubricated Tools," Key Eng. Mater., vol. 611–612, p. 971–980.

[14] Bay, N. 1994. "The State of the Art in Cold Forging Lubrication," J. Mater. Process. Technol., vol. 46, no. 1–2, p. 19–40.

[15] Smyth, L. 2017. "New Polymeric Coatings for Cold Forming," https://www.engineerlive.com/content/new-polymeric-coatings-cold-forming.

[16] Wang, X. Y., Li, D. Y. 2003. "Mechanical, Electrochemical and Tribological Properties of Nano-Crystalline Surface of 304 Stainless Steel," Wear, vol. 255, no. 7–12) p. 836–845.

[17] Ningbo Hewcho Industrial Limited. "Sandblasting," http://www.hewcho.com/surface-treatment/sandblasting.html.

[18] İlve Kimya. "Tel Çekme Öncesi Çinko Fosfat Kaplama," http://cinko.fosfatkaplama.com/tel-cekme.html.

[19] İlve Kimya. 2019. "Tel Çekme Çinko Fosfat," http://www.ilve.com.tr/yislem/tel-cekme-cinko-fosfat.html.

[20] Peycheva, R. 2015. "Using Polymer Lubricants to Optimize Cold Forging," https://www.forgingmagazine.com/forming/using-polymer-lubricants-optimize-cold-forging.
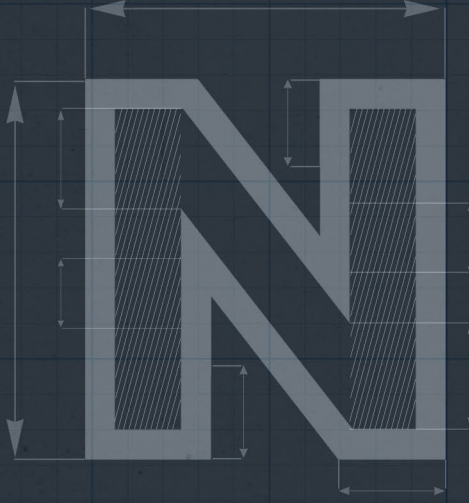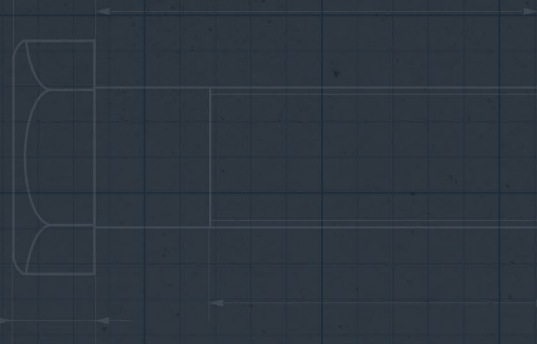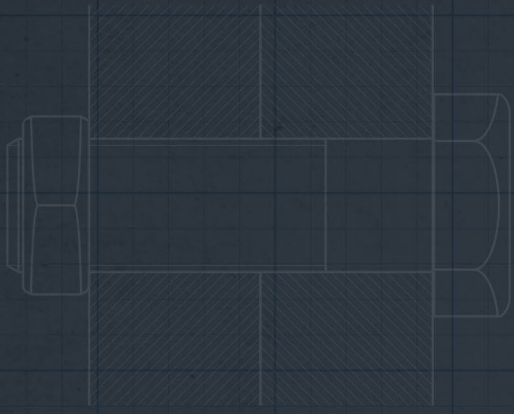
GELİŞTİRİLMİŞ DAYANIMA SAHİP BİR BAĞLANTI ELEMANI TASARIMI

Sezgin YURTDAŞ
Barış TANRIKULU
Özlem TOKER
Cenk KILIÇASLAN
Umut İNCE

GELİŞTİRİLMİŞ DAYANIMA SAHİP BİR BAĞLANTI ELEMANI TASARIMI

Sezgin Yurtdaş, Barış Tanrıkulu, Özlem Toker, Cenk Kılıçaslan, Umut İnce,

Norm Cıvata Ar-Ge Merkezi, İzmir, Türkiye
Email: sezgin.yurtdas@normcivata.com

Özet

Ağırlık azaltma çalışmaları otomotiv sektöründe son yılların en popüler çalışma konularından bir tanesidir. Özellikle elektrikli ve hibrit araçların kullanımında menzil mesafelerinin artırılması, CO_2 emisyon değerlerinin düşürülmesi ve daha düşük yakıt tüketiminin sağlanabilmesi amacıyla makine elemanlarında hafifletme çalışmaları önem kazanmış durumdadır. Çalışma kapsamında incelenen DIN EN ISO 7380-2 bağlantı elemanı, Karbon çeliği ve alaşımlı çeliklerden üretilen bağlantı elemanlarının mekanik özelliklerinin verildiği ISO 898-1 şartnamesinde tam dayanıma sahip olmayan bağlantı elemanı olarak ifade edilmektedir. İlgili şartnameye göre DIN EN ISO 7380-2 ürününün çekme dayanımı standart ürünlerin %80'ini sağlamaktadır. Yapılan çalışma ile DIN EN ISO 7380-2 grubunda yer alan M12x1.75x40 ürününün kafa geometrisinde tasarım revizesi sayesinde ürün gramajında bir değişime yol açmadan tam dayanıma sahip bağlantı elemanın mekanik özelliklerini göstermesi hedeflenmiştir. Revize edilen tasarımın 3 boyutlu modelleme çalışmaları Catia, soğuk şekillendirme malzeme akış analizleri ise Simufact Forming yazılımları ile gerçekleştirilmiştir. Numune üretimi tamamlanan revize bağlantı elemanı formu için çekme testleri gerçekleştirilmiş ve ISO 898-1'de istenen mekanik değerlerde tam dayanımı sağladığı tespit edilmiştir.

Anahtar Kelimeler: *Soğuk dövme, bağlantı elemanı, ağırlık azaltma, CO_2 emisyonu, çekme dayanımı.*

Giriş

Bağlantı elemanları uygulama alanlarına göre farklı standartlar altında derlenmiş olup metal endüstrisinde en yaygın kullanılan emniyet elemanlarından birisi olarak ifade edilmektedir. Artan küresel rekabet ortamı nedeniyle bağlantı elemanı üreticilerinden üstün mekanik dayanım ve ağırlık azaltma konularında ürün beklentisi oluşmaktadır. Çevreci uygulamaların artması ve 2020 yılı itibariyle uygulamaya alınan 95 gram CO_2/km emisyon değeri kısıtlamaları neticesinde hafifletilmiş makine elemanlarının kullanımı zorunluluk haline gelmiştir [1]. Bağlantı elemanları sektöründe ağırlık azaltma çalışmaları malzeme ve geometrinin değişiminin yanı sıra özel bağlantı elemanlarının kullanımı ile gerçekleştirilebilir [2]. Bu bağlamda üstün mekanik özelliklerde bağlantı elemanlarının tercih edilmesi ile kullanılması gereken toplam bağlantı elemanı sayısı azaltılabilir. Bunun yanı sıra malzeme değişkeni sabit tutularak tasarım çalışmalarıyla toplam ağırlıkta hafifletme sağlanabilir.

Ayrıca özel kilitleme sistemlerinin kullanımına yönelik uygulamaların devreye alınmasıyla da emniyet parçalarına olan ihtiyaç ortadan kaldırılabilir. Yapılan çalışmada M12x1.75x40 ürünün kafa formu tasarımında incelenen parametreler Şekil 1'de verilmiştir.

Detay Numarası	Tanımı
1	w ölçüsü
2	Konik açısı
3	Kafa kalınlığı
4	Flans çapı
5	Flans kalınlığı
6	Soket anahtarı

İzometrik Görünüm

Şekil 1. *Ürün dizaynında incelenen tasarım değişkenleri.*

Tasarım revizesinin yapılmasının ardından (Şekil 2) nümerik simülasyon çalışmaları gerçekleştirilerek ürün geometrisinin soğuk şekillendirilebilirliği incelenmiştir. Bu kapsamda Şekil 3'de simülasyondan alınan ara istasyon ürün formlarına yer verilmiştir. Elde edilen sonuçlar revize formun tamamen soğuk şekillendirme ile üretilebileceğini göstermektedir.


(a)   *(b)*
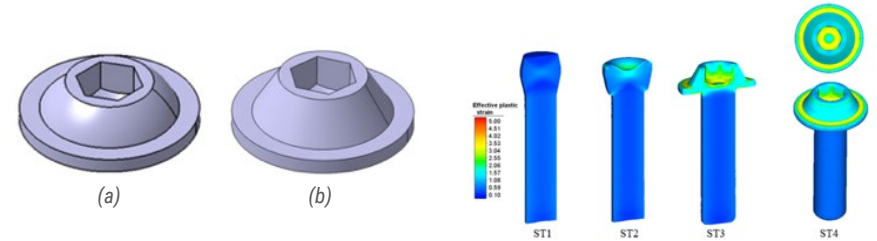
Şekil 2. *Bağlantı elemanı kafa formu;*
(a) DIN EN ISO 7380-2 (b) revize tasarım.

Şekil 3. *Revize tasarımın dövülebilirliğine yönelik simülasyondan alınan ara istasyon ürün formları.*

Nümerik çalışmalar sonucunda üretim hattı denemeleri gerçekleştirilmiştir. Soğuk şekillendirme prosesinin nümerik çalışmalara paralel olarak sorunsuz bir şekilde tamamlanmasının ardından elde edilen yarı mamuller sırasıyla ısıl işlem ve kaplama proseslerine tabi tutularak nihai ürün formu elde edilmiştir. Rastgele belirlenen 3 adet numune için çekme testleri gerçekleştirilmiş olup elde edilen mekanik veriler cıvatanın tam dayanıma sahip olduğunu doğrulamaktadır. Şekil 4'de tüm prosesleri tamamlanmış final ürün formuna, Şekil 5'de de çekme testlerinin sonuçlarına yer verilmiştir.

Şekil 4. *Revize M12x1.75x40 final formu.*
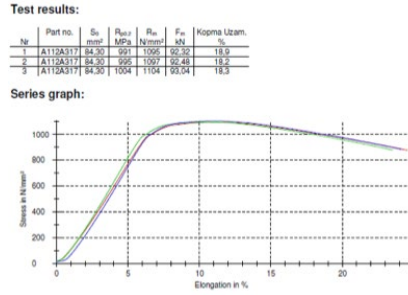
Şekil 5. *Çekme testi sonuçları.*

Sonuçlar

Yapılan çalışmada DIN EN ISO 7380-2 ürün grubunun kafa geometrisinde tasarım revizesi yapılarak ISO 898-1 şartnamesine göre gerekli çekme dayanım değerleri elde edilmiş ve nihai ürün formu tam dayanıma evirilmiştir. ISO 898-1 şartnamesine göre M12 10.9 kalite sınıfına sahip ürünün tam dayanım mekanik özelliklerini sağlayabilmesi için çekme testinde minimum 87,7 kN değere sahip olması gerekmekte iken bu değer revize ürün formunda minimum 92,3 kN olarak tespit edilmiştir. Belirlenen final kafa formu ile ürünün gramajında bir değişime yol açmadan mekanik özelliklerinde iyileşme sağlanmış ve yeni nesil bir bağlantı elemanı elde edilmiştir.

Referanslar

[1]   EU Parliament and Council (2009), "Regulation (EC) No 443/2009: Setting Emission Performance Standards for New Passenger Cars as Part of the Community's Integrated Approach to Reduce CO2 Emissions from Light-Duty Vehicles".

[2]   Toparli, M.B., Kılınçdemir, N. E., Yurtdaş, S., Tanrıkulu B. and İnce U. (2018). Otomotiv Sanayinde Kullanılan Bağlantı Elemanlarında Ağırlık Azaltma., 9th International Automotive Technologies Congress, OTEKON 2018.

SOĞUK EKSTRÜZYON PROSESİNDE MEYDANA GELEN SIVAMA PROBLEMİNİN İNCELENMESİ

Sezgin Yurtdaş
Sarper Doğan
Cenk Kılıçaslan
Doğuş Zeren

SOĞUK EKSTRÜZYON PROSESİNDE MEYDANA GELEN SIVAMA PROBLEMİNİN İNCELENMESİ

Sezgin Yurtdaş, Sarper Doğan*, Cenk Kılıçaslan, Doğuş Zeren,

*   İletişim yazarı: sarper.dogan@normcivata.com

Özet

Ekstrüzyon işlemi soğuk şekillendirme uygulamalarında yaygın olarak kullanılan bir prosestir. İşlem sırasında hammadde kesit çapında yaklaşık %30'un üzerinde bir kesit daralması meydana gelmekle birlikte, soğuk dövme kalıbı ile iş parçası arasındaki yüksek temas basıncı ve artan sürtünme kuvveti nedenleriyle malzeme akışında sıvama ve yapışma problemleri yaşanabilmektedir. Malzeme akışında yüksek pres kuvveti gereksinimlerine ihtiyaç duyulması, kalıp bileşenlerinde gerilme yığılmasına sebebiyet vermekte ve düşük çevrimlerde yorulma ve aşınma kaynaklı kalıp hasarlarına yol açmaktadır. Yapılan çalışmada soğuk şekillendirme işlemi sırasında ekstrüzyon istasyonuna uygulanan özel yağ püskürtme uygulaması ile malzeme akışının rahatlatılması ve soğuk dövme takım hasarlarının minimize edilmesi hedeflenmiştir. Bu kapsamda belirlenen bağlantı elemanı formu için üretim hattı denemeleri gerçekleştirilmiş ve ürünün kritik olarak belirlenen şaft yüzeyinde meydana gelen sıvama problemi %15 oranında indirgenmiştir.

Anahtar Kelimeler: *Soğuk dövme, bağlantı elemanı, ekstrüzyon, sürtünme, yağlama, sıvama*

Giriş

Soğuk şekillendirme prosesi ile bağlantı elemanı üretimi uygulamalarında karşılaşılan en büyük kısıtlardan bir tanesi de sürtünme faktörüdür. Dövme işlemi esnasında yarı mamul iş parçası, dövme kalıpları ile maksimum seviyede temas etmektedir. Özellikle kesit daralmasının olduğu ekstrüzyon ve redüksiyon proseslerinde malzeme akışında sıvama ve yapışma gibi kusurlar meydana gelebilmektedir. Sıvama, genellikle metal yüzeyler olmak üzere, iki hareketli yüzey arasındaki aşırı sürtünmeden kaynaklanan yaygın bir mekanik aşınma şeklidir [1]. İş parçasında kesit alanına göre yüksek daralma oranlarında artan sürtünme kuvvetinden dolayı, yarı mamul iş parçasının kalıba yapışarak malzeme akışının sağlanamaması ve bunun sonucunda da sıvama probleminin meydana gelmesi karşılaşılan önemli problemlerdendir. İş parçası ve kalıp formlarına uygun tribolojik çözümler devreye alınarak, malzeme akışının rahatlatılabileceği ve sıvama probleminin önüne geçilebileceği tespit edilmiştir [2]. Bu çerçevede yapılan çalışma ile ekstrüzyon prosesinde karşılaşılan malzeme akış kusurunun giderilmesi ve soğuk dövme kalıp ömürlerinin artırılması hedeflenmiştir.

Bu amaçla soğuk dövme sırasında yağ yarı mamul üzerine basınçla püskürtülmüş, yağ tabakasının iş parçası yüzeyine tutunması sağlanmıştır. Bu sayede iş parçasının şekillenmesinde ihtiyaç duyulan dövme yüklerinde düzensiz artışların önüne geçilerek malzeme akışı rahat bir şekilde gerçekleştirilebilmiştir. Şekil 1'de ek yağlama işlemi temsili olarak verilmiştir. Yapılan denemelerde ekstrüzyon prosesine göre kullanılması gereken nozül açısı, yağ basıncı ve debi miktarı parametreleri belirlenmiştir. Şekil 2'de pulverize yağ püskürtme uygulamasının öncesi ve sonrası soğuk şekillenme presinden alınan yarı mamul iş parçasının şaft formunda meydana gelen sıvama bölgesinin karşılaştırmasına yer verilmiştir. Yapılan incelemede yağ püskürtme işlemi ile şaft bölgesinde yer alan sıvama alanında %15'lik iyileşme (azalma) meydana gelmiştir.
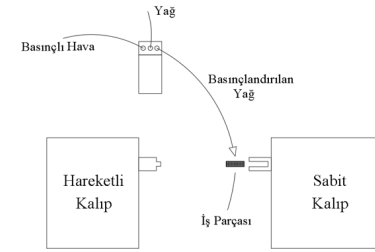
Şekil 1. *Yağlama işlemi temsili resmi.*
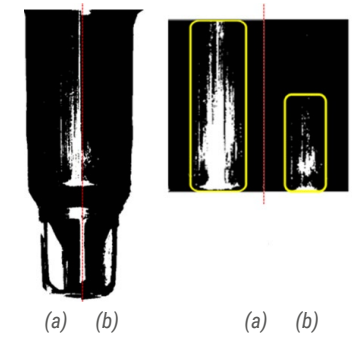
Şekil 2. *Üretim hattından alınan yarı mamul yüzeyi; (a) konvansiyonel (b) püskürtme yağlama.*

Sonuçlar

Yapılan çalışmada bağlantı elemanı üretiminde sıklıkla kullanılan ekstrüzyon proseslerinde meydana gelen sıvama ve yapışma problemlerinin giderilmesine yönelik inceleme yapılmış ve üretim hattı denemeleri gerçekleştirilmiştir. Yağ püskürtme yöntemi ile iş parçasında kritik olarak belirlenen lokal bölgede ince bir film tabakası oluşturularak malzeme akışı rahatlatılmış ve sıvamanın %15 oranında elimine edildiği tespit edilmiştir. Yarı mamul ürün formu ve kalıp formları arasında sağlanan tribolojik iyileşme, iş parçasında yer alan ve şekillenmeyi kolaylaştırıcı etkisi bulunan fosfat tabakasının yüzeyde daha uzun süre kalmasını sağlamıştır. Çalışma ile mikro ölçekli yağlamanın özellikle yüksek kesit daralmalarının tercih edildiği soğuk şekillendirme proseslerinde, sıvama ve yapışma kusurlarını gidermeye yönelik önemi ortaya çıkarılmıştır.

Referanslar

[1]   Söderman, A. And Törnquist, P.L. (2019). Galling is a serious issue in many industries that use stainless steel fasteners- but there are solutions. Metal Powder Report, Special Feature, 1-2.

[2]   Otter, C.D. And Maljaars, J. (2020). Preload loss of stainless steel bolts in aluminium plated slip resistant connections. Thin-Walled Structures, 157, 1-15.

NORM
FASTENERS